https://doi.org/10.35662/unine-thesis-2809

UNIVERSITÉ DE NEUCHÂTEL

TOWARDS COMPACT ULTRALOW PHASE NOISE LASERS AND MICROWAVE SIGNALS BASED ON NEW APPROACHES

Thesis presented to the *Faculty of Science* for the degree of

Doctor of Science

Pierre Brochard

M. Sc. In Physics

submitted on 06.09.2019 to the jury:

Prof. Thomas Südmeyer	Director
Prof. Pascal Ruello	Examiner
Dr. Rodolphe Le Targat	Examiner
Dr. Giorgio Santarelli	Examiner
Dr. Stéphane Schilt	Examiner

Neuchâtel, 2019

UNIVERSITÉ DE NEUCHÂTEL

Faculté des Sciences
Secrétariat-décanat de Faculté
Rue Emile-Argand 11
2000 Neuchâtel – Suisse
Tél : + 41 (0)32 718 21 00
E-mail : secretariat.sciences@unine.ch

IMPRIMATUR POUR THESE DE DOCTORAT

La Faculté des sciences de l'Université de Neuchâtel autorise l'impression de la présente thèse soutenue par

Monsieur Pierre BROCHARD

Titre:

"Towards compact ultralow phase noise lasers and microwave signals based on new approaches"

sur le rapport des membres du jury composé comme suit:

- Prof. Thomas Südmeyer, directeur de thèse, Université de Neuchâtel, Suisse
- Dr Stéphane Schilt, Université de Neuchâtel, Suisse
- Dr Rodolphe Le Targat, SYRTE, Observatoire de Paris, France
- Dr Giorgio Santarelli, Université de Bordeaux, France
- Prof. Pascal Ruello, Le Mans Université, France

Neuchâtel, le 30 octobre 2019

Le Doyen, Prof. P. Felber

P. Fel

Keywords – Mots-clés

Keywords

Oscillators, time and frequency metrology, frequency noise, phase noise, frequency stability, linewidth, laser, mode-locked laser, optical frequency combs, optical frequency division, carrier-envelope offset, radio-frequency, microwave, transfer oscillator.

Mots-clés

Oscillateurs, métrologie temps-fréquence, bruit de fréquence, bruit de phase, stabilité de fréquence, largeur de raie, laser, peignes de fréquence optique, division de fréquence optique, décalage de phase entre porteuse et enveloppe, fréquence radio, micro-onde, oscillateur de transfert.

Abstract

Today, the lowest phase noise microwave signals are generated optically by frequency division of an ultra-stable optical reference using a femtosecond frequency comb. In the commonly used approach, the ultra-stable optical reference is obtained by frequency-stabilizing a laser to a high-finesse ultra-low expansion optical cavity, and the frequency division is performed by optically locking a mode-locked laser to the ultra-stable laser. Both sub-systems are fairly complex and cumbersome, but have demonstrated state-of-the-art performance.

In this thesis, alternative approaches have been investigated for low-noise microwave generation based on a transfer oscillator scheme. In a first part, a novel method inspired by the transfer oscillator concept has been developed and validated to characterize the offset frequency of a comb spectrum without relying on the traditional self-referencing method and, thus, without requiring an octave-spanning spectrum that is challenging to be generated, especially with high repetition rate frequency combs. This method has then been successfully applied to characterize three different types of comb spectra from a semiconductor mode-locked laser, a diode-pumped solid-state laser with 25-GHz repetition rate, and a quantum cascade laser frequency comb emitting in the mid-infrared spectral region.

By modifying and improving this scheme, ultra-low phase noise microwave signal generation based on a transfer oscillator was demonstrated and characterized. The method was also implemented with a micro-resonator Kerr-comb for a first proof-of-principle demonstration of frequency division performed with a Kerr comb.

In addition, frequency stabilization of a mid-infrared quantum cascade laser to an optical delay-line is presented for the first time and led

to a sub-10-kHz linewidth using only a meter-scale free-space delay-line. The same approach can be applied in the near-infrared with a long fiber delay with the potential to achieve Hz-level linewidth.

The technologies developed in this thesis are attractive components for future compact ultra-low noise microwave generators.

Résumé

Aujourd'hui, les signaux micro-ondes à bruit de phase le plus faible sont générés optiquement par division de fréquence d'une référence optique ultra-stable utilisant un peigne de fréquence femtoseconde. Dans l'approche couramment utilisée, la référence optique ultra-stable est obtenue par stabilisation en fréquence d'un laser sur une cavité optique à très faible coefficient d'expansion thermique, et la division en fréquence est effectuée en stabilisant optiquement un laser à verrouillage de mode au laser ultra-stable. Ces deux sous-systèmes sont assez complexes et encombrants, mais ils ont démontré des performances de pointe.

Dans cette thèse, des approches alternatives ont été étudiées pour la génération de micro-ondes à faible bruit basées sur un schéma d'oscillateur de transfert. Dans une première partie, une nouvelle méthode inspirée du concept de l'oscillateur de transfert a été développée et validée pour caractériser la fréquence d'offset (décalage de phase entre la porteuse et l'enveloppe, *carrier-envelope offset* en anglais, CEO) d'un peigne de fréquence optique sans s'appuyer sur la méthode traditionnelle d'auto-référencement et donc sans le besoin d'un spectre optique couvrant une octave de fréquence, qui est difficile à générer notamment avec des peignes à fréquence de répétition élevée. Cette méthode a ensuite été appliquée avec succès pour caractériser trois différents types de peignes de fréquence optiques générés à partir d'un laser à semi-conducteur à verrouillage de mode, d'un laser à l'état solide pompé par diode avec un taux de répétition de 25 GHz et d'un laser à cascade quantique émettant dans la région spectrale de l'infrarouge moyen.

En modifiant et en améliorant cette technique, on a démontré et caractérisé la génération d'un signal hyperfréquence à bruit de phase ultra-faible basé sur un oscillateur de transfert. La méthode a également été mise

en œuvre à l'aide d'un micro-résonateur à peigne de Kerr pour une première démonstration de principe.

En outre, la stabilisation en fréquence d'un laser continu à cascade quantique émettant dans l'infrarouge moyen sur une ligne à retard optique est présentée pour la première fois et conduit à une largeur de raie inférieure à 10 kHz en utilisant un montage en espace libre. La même approche peut être appliquée dans le proche infrarouge avec un long délai utilisant des fibres optiques, donnant la possibilité d'atteindre une largeur de raie au niveau du hertz.

Les technologies développées dans cette thèse sont des composants attrayants pour les futurs générateurs de micro-ondes compacts à très faible bruit.

List of symbols and acronyms

Symbols

$*$	Convolution product
ν_{rms}	Integrated frequency noise (Hz)
$\sigma_y(\tau)$	Allan deviation
ϕ_{rms}	Integrated phase noise (rad)
$\langle . \rangle$	Ensemble average
Δ, δ	Fluctuations
D	Slope coefficient
$\mathcal{F}$	Fourier transform
f_{CEO}, f_0	Optical comb offset frequency (Hz)
$f_{\mathrm{rep}}, f_{\mathrm{FSR}}$	Optical comb repetition frequency or intermode frequency (Hz)
L	Length (m)
P	Power (W)
S	Power spectral density
V	Voltage signal (V)
Γ_Δ	Coherence factor
$E(t)$	Electrical signal (V)
R	Auto-correlation function

T, H, C	Transfer function
ν, f, Ω	Frequency (Hz)
τ, t	Time (s)
$\phi(t)$	Phase (rad, °)

Acronyms

AOM	Acousto-optic modulator
AN	Amplitude noise
BS	Beam splitter
(O)BPF	(Optical) bandpass filter
CEO	Carrier-envelope offset
CSO	Cryogenic sapphire oscillator
CW	Continuous wave
DBM	Double-balanced mixer
DC	Direct current
DDS	Direct digital synthesizer
DFB	Distributed feedback (laser)
DKS	Dissipative Kerr soliton
DPSSL	Diode-pumped solid-state laser
DRO	Dielectric resonator oscillator
DWDM	Dense wavelength division multiplexing
ECDL	External cavity diode laser

EDFA	Erbium-doped fiber amplifier
EO	Electro-optic
eOFD	Electro-optical frequency division
EOM	Electro-optic modulator
Er	Erbium
ERGO	Er:Yb:glass laser oscillator
ESA	Electrical spectrum analyzer
FACT	Future Atomic Clock Technologies
FBG	Fiber Bragg grating
FFT	Fast Fourier transform
FN	Frequency noise
FSR	Free spectral range
FWHM	Full width at half maximum
$FWHM_{\beta}$	Full width at half maximum using the β-separation line method
GVD	Group velocity dispersion
HWHM	Half width at half maximum
IR	Infrared
LNA	Low noise amplifier
MCT	Mercury-Cadmium Telluride
MI	Michelson interferometer
MIR	Mid-infrared

MIXSEL	Mode-locked integrated external-cavity surface-emitting laser
mQAM	Multi-level quadrature amplitude modulation
MZI	Mach-Zehnder interferometer
NIR	Near infrared
OCXO	Oven-controlled crystal oscillator
OEO	Opto-electronic oscillator
OFC	Optical frequency comb
OFD	Optical frequency division
OPLL	Optical phase locked loop
PD	Photodiode, Photo-detector
PDH	Pound-Drever-Hall
PID	Proportional-integral-derivative
PLL	Phase-locked loop
PN	Phase noise
PNA	Phase noise analyzer
PRRM	Pulse repetition rate multiplier
PSD	Power spectral density
PZT	Piezoelectric transducer
QCL	Quantum cascade laser
RBW	Resolution bandwidth
RF	Radio-frequency

RIN	Relative intensity noise
SC	Super-continuum
SESAM	Semiconductor saturable absorber mirror
SI	Supplementary information
SNR	Signal-to-noise ratio
Sr	Strontium
SSA	Signal source analyzer
SSB	Single-side band
TCXO	Temperature-compensated crystal oscillator
TO	Transfer oscillator
ULE	Ultralow expansion
USL	Ultra-stable laser
VECSEL	Vertical external-cavity surface-emitting laser
Yb	Ytterbium

Publications

Parts of this thesis are published or submitted in the following journal papers. The text and figures are printed as published, only the format of the text, the numbering and the size of figures were adapted to the thesis style. All papers are reprinted with permission from the corresponding publishers. The copyright of the original publications is held by the respective copyright holders.

Journal publications

1. **P. Brochard**, B. Rudin, F. Emaury, V. J. Wittwer, S. Schilt and T. Südmeyer, *Low-noise transfer of the spectral purity of an optical comb line using a feedforward scheme*, Submitted to Optics Express (2019).

2. E. Lucas*, **P. Brochard***, R. Bouchand, S. Schilt, T. Südmeyer, T. J. Kippenberg, *Ultralow-Noise Photonic Microwave Synthesis using a Soliton Microcomb-based Transfer Oscillator*, Accepted for publication in Nature Communications (2019)

3. A. Shehzad, **P. Brochard**, R. Matthey, T. Südmeyer, S. Schilt, *Sub-10-kHz-Linewidth Mid-Infrared Quantum Cascade Laser by Stabilization to an Optical Delay Line*, Optics Letters 44(14), 3470-3473 (2019)

4. **P. Brochard**, S. Schilt, T. Südmeyer, *Ultra-Low Noise Microwave Generation with a Free-Running Optical Frequency Comb Transfer Oscillator*, Optics Letters 43(19), 4651-4654 (2018)

5. **P. Brochard**, V.J. Wittwer, S. Bilicki, B. Resan, K.J. Weingarten, S. Schilt, T. Südmeyer, *Noise characterization of the carrier-envelope offset signal in a 25-GHz diode-pumped mode-locked laser*, IEEE Photonics Journal 10(1), 1-10 (2018)

6. A. Shehzad, **P. Brochard**, R. Matthey, S. Blaser, T. Gresch, R. Maulini, A. Muller, T. Südmeyer, S. Schilt, *Electrically-driven pure amplitude and frequency modulation in a quantum cascade laser*, Optics Express 26(9), 12306-12317 (2018)

7. N. Modsching, C. Paradis, **P. Brochard**, N. Jornod, K. Gürel, C. Kränkel, S. Schilt, V.J. Wittwer, T. Südmeyer, *Carrier-envelope offset frequency stabilization of a thin-disk laser oscillator operating in the strongly self-phase modulation broadened regime*, Opt. Express 26(22), 28461-28468 (2018)

8. S. Hakobyan, V.J. Wittwer, **P. Brochard**, K. Gürel, S. Schilt, A.S. Mayer, U. Keller, T. Südmeyer, *Full stabilization and characterization of an optical frequency comb from a diode-pumped solid-state laser with GHz repetition rate*, Optics Express 25(17), 20437-20453 (2017)

9. **P. Brochard**, S. Schilt, T. Südmeyer, *Power spectrum computation for an arbitrary phase noise using Middleton's convolution series: implementation guideline and experimental illustration*, IEEE Trans. Ultrason., Ferroelect., Freq. Control 64(11), 1766-1775 (2017)

10. N. Jornod, K. Gürel, V.J. Wittwer, **P. Brochard**, S. Hakobyan, S. Schilt, D. Waldburger, U. Keller, T. Südmeyer, *Carrier-envelope offset frequency stabilization of a gigahertz semiconductor disk laser*, Optica 4(12), 1482-1487 (2017)

11. K. Balskus, S. Schilt, V.J. Wittwer, **P. Brochard**, T. Ploetzing, N. Jornod, R.A. McCracken, Z. Zhang, A. Bartels, D.T. Reid, T. Südmeyer, *Frequency comb metrology with an optical parametric oscillator*, Optics Express 24(8), 8370-8381 (2016)

12. **P. Brochard**, N. Jornod, S. Schilt, V.J. Wittwer, S. Hakobyan, D. Waldburger, S.M. Link, C.G.E. Alfieri, M. Golling, L. Devenoges, J. Morel, U. Keller, T. Südmeyer, *First Investigation of the Noise and Modulation Properties of the Carrier Envelope Offset in a Mode-locked Semiconductor Laser*, Optics Letters 41(14), 3165-3168 (2016)

13. **P. Brochard**, S. Schilt, V.J. Wittwer, T. Südmeyer, *Characterizing the carrier-envelope offset in an optical frequency comb without traditional f-to-2f interferometry*, Optics Letters 40(23), 5522-5525 (2015)

Conference presentations

1. **P. Brochard**, N. Jornod, V.J. Wittwer, S. Schilt, T. Südmeyer, Gigahertz VECSEL frequency combs: characterization, stabilization, and applications, SPIE LASE Photonics West Conference, San Francisco, USA; January 27 - February 1, 2019

2. **P. Brochard**, E. Lucas, R. Bouchand, S. Schilt, T. Südmeyer, T. Kippenberg, Optical-to-Microwave Frequency Division with a Kerr-Frequency-Comb Transfer Oscillator, oral MoAT3.1, EFTF-IFCS, Orlando, USA; April 14-18, 2019

3. E. Lucas, **P. Brochard**, R. Bouchand, S. Schilt, T. Südmeyer, T. Kippenberg, Kerr Comb-based Transfer Oscillator for Ultralow Noise Photonic Microwave Synthesis, oral SW4G.5, CLEO US 2019, San Jose, USA, May 13-18, 2019

4. A. Shehzad, **P. Brochard**, R. Matthey, T. Südmeyer, S. Schilt, Frequency Noise Reduction in a Quantum Cascade Laser Using a Short Free-Space Delay Line, oral SW4N.5, CLEO US 2019, San Jose, USA, May 13-18, 2019

5. S. Schilt, **P. Brochard**, A. Shehzad, R. Matthey, A. Hugi, P. Jouy, F. Kapsalidis, M. Shahmohammadi, M Gianella, J. Faist, L. Emmenegger, T. Südmeyer, Strategies for frequency stabilization and noise reduction in dual-QCL-comb spectroscopy, invited, PIERS-2019, Roma, Italy; June 17-20, 2019

6. **P. Brochard**, E. Lucas, R. Bouchand, S. Schilt, T. Kippenberg, T. Südmeyer, Ultra-low Phase Noise Microwave Synthesis with a Kerr Frequency Comb used as Transfer Oscillator, oral ED-5.2, CLEO-Europe 2019, Munich, Germany; June 23-27, 2019

7. A. Shehzad, **P. Brochard**, R. Matthey, T. Südmeyer, S. Schilt, Sub-10-kHz Linewidth Quantum Cascade Laser achieved by Stabilization to a Short Free-Space Delay Line, oral CB-7.2, CLEO-Europe 2019, Munich, Germany; June 23-27, 2019

8. **P. Brochard**, B. Rudin, F. Emaury, V.J. Wittwer, S. Schilt, T. Südmeyer, Extraction and amplification of a single frequency comb tooth using an auxiliary laser in a feedforward scheme, poster,

Advanced Solid State Lasers Conference (ASSL), Vienna, Austria; Sept. 29 – October 3 2019

9. **P. Brochard**, B. Rudin, F. Emaury, V.J. Wittwer, S. Schilt, T. Südmeyer, Extraction and amplification of an optical comb line using an auxiliary continuous-wave laser in a feedforward scheme, poster, Ultrafast Optics XII, Bol, Croatia; October 6-11, 2019

10. A. Shehzad, **P. Brochard**, R. Matthey, F. Kapsalidis, M. hahmohammadi, M. Beck, A. Hugi, P. Jouy, Faist, T. Südmeyer, S. Schilt, Investigation of the Noise Properties of the Offset Frequency in a Quantum Cascade Laser Frequency Comb, poster, Ultrafast Optics XII, Bol, Croatia; October 6-11, 2019

11. N. Jornod, K. Gürel, V.J. Wittwer, **P. Brochard**, S. Hakobyan, S. Schilt, D. Waldburger, U. Keller, T. Südmeyer, Carrier-envelope offset frequency stabilization of an ultrafast semiconductor laser, oral 10515-18, SPIE LASE Photonics West Conference, San Francisco, USA, January 27 - February 1, 2018

12. **P. Brochard**, S. Schilt, T. Südmeyer, Optical-to-RF Frequency Division for Ultra-low Noise Microwave Generation Using a Transfer Oscillator Method, oral B1L-C-2, EFTF-2018, Torino, Italy, April 10-12, 2018

13. N. Modsching, C. Paradis, **P. Brochard**, N. Jornod, K. Gürel, C. Kräankel, S. Schilt, V.J. Wittwer, T. Südmeyer, Frequency Comb Stabilization of a 4 W, 50-fs Thin-Disk Laser Oscillator, oral B2L-A-6, EFTF-2018, Torino, Italy, April 10-12, 2018

14. N. Jornod, K. Gürel, V.J. Wittwer**, P. Brochard**, S. Hakobyan, S. Schilt, D. Waldburger, U. Keller, T. Südmeyer, Optical frequency comb stabilization of a gigahertz semiconductor disk laser, invited presentation, SPIE DCS18 Ultrafast Bandgap Photonics Conference, Orlando, USA, April 16-19, 2018

15. N. Modsching, C. Paradis, **P. Brochard**, N. Jornod, K. Gürel, C. Kränkel, S. Schilt, V.J. Wittwer, T. Südmeyer, Frequency Comb Stabilization of a 50-fs Thin-Disk Laser Oscillator Operating in a Strongly SPM-broadened Regime, oral PM SM4L.6, CLEO US 2018, San Jose, USA, May 13-18, 2018

16. A. Shehzad, **P. Brochard**, R. Matthey, A. Bismuto, S. Blaser, T. Gresch, R. Maulini, A. Muller, T. Südmeyer, S. Schilt, Pure Amplitude or Frequency Modulation of a Quantum Cascade Laser by Use of an Integrated Heater, oral SF2G.7, CLEO US 2018, San Jose, USA, May 13-18, 2018

17. S. Hakobyan, **P. Brochard**, V.J. Wittwer, K. Gürel, S. Schilt, T. Südmeyer, Compact GHz Frequency Comb from an Ultrafast Solid-State Laser with Cost-Efficient 3D-Printed Plastic Cavity Base, poster JW2A.161, CLEO US 2018, San Jose, USA, May 13-18, 2018

18. A. Shehzad, **P. Brochard**, R. Matthey, S. Blaser, T. Gresch, R. Maulini, A. Muller, T. Südmeyer, S. Schilt, Generation of pure amplitude and frequency modulation in a quantum cascade laser using an integrated heater, oral #413, Annual Meeting of the Swiss Physical Society, Lausanne, Switzerland, August 28-31, 2018

19. M. Gaponenko, F. Labaye, **P. Brochard**, N. Modsching, K. Gürel, V.J. Wittwer, C. Paradis, C. Kränkel, S. Schilt, T. Südmeyer, CEO frequency stabilization of a thin disk laser with intra-cavity high harmonic generation, oral #FrM2.6, 8th EPS-QEOD Europhoton conference, Barcelona, Spain, September 2-7, 2018

20. **P. Brochard**, S. Schilt, T. Südmeyer, Ultra-low Noise Microwave Generation based on a Free-Running Optical Frequency Comb, oral, best student paper award, International Topical Meeting on Microwave Photonics, Toulouse, France, October 22-25, 2018

21. S. Hakobyan, V.J. Wittwer, **P. Brochard**, K. Gürel, S. Schilt, A.S. Mayer, U. Keller, T. Südmeyer, Fully-Stabilized Optical Frequency Comb from a Diode-Pumped Solid-State Laser with GHz Repetition Rate, oral #SF1C.1, CLEO US 2017, San Jose, USA, May 14-19, 2017

22. **P. Brochard**, S. Bilicki, A. Shehzad, S. Schilt, T. Südmeyer, Laser Linewidth Optimization in a Feedback Loop, oral #CH-4.3, CLEO Europe 2017, Munich, Germany, June 25-29, 2017

23. S. Hakobyan, V.J. Wittwer, K. Gürel, **P. Brochard**, S. Schilt, A.S. Mayer, U. Keller, T. Südmeyer, Opto-Optical Modulator for CEO Control and Stabilization in an Yb:CALGO GHz Diode-Pumped Solid-State Laser, oral #CF-1.1, CLEO Europe 2017, Munich, Germany, June 25-29, 2017

24. N. Jornod, K. Gürel, V.J. Wittwer, **P. Brochard**, S. Hakobyan, S. Schilt, D. Waldburger, U. Keller, T. Südmeyer, Towards Self-Referencing of a VECSEL Frequency Comb, oral #CF-1.4, CLEO Europe 2017, Munich, Germany, June 25-29, 2017

25. **P. Brochard**, S. Schilt, T. Südmeyer, Revisiting the Relation between Laser Spectrum and Phase Noise Spectral Density with New Outcomes, poster #B3P-L 1350, EFTF-IFCS, Besançon, France, July 9-13, 2017

26. S. Hakobyan, V.J. Wittwer, **P. Brochard**, K. Gürel, S. Schilt, A.S. Mayer, U. Keller, T. Südmeyer, Fully-Stabilized 1-GHz Optical Frequency Comb from a Diode-Pumped Solid-State Laser, oral #D1L-A.3, EFTF-IFCS, Besançon, France, July 9-13, 2017

27. S. Hakobyan, V.J. Wittwer, K. Gürel, **P. Brochard**, S. Schilt, A.S. Mayer, U. Keller, T. Südmeyer, Opto-Optical Modulation for Carrier-Envelope-Offset Stabilization in a GHz Diode-Pumped Solid-State Laser, oral #AW1A.4, Advanced Solid State Lasers Conference and Exhibition (ASSL), Nagoya, Japan; October 1-5, 2017

28. N. Jornod, K. Gürel, V.J. Wittwer, **P. Brochard**, S. Hakobyan, S. Schilt, D. Waldburger, U. Keller, T. Südmeyer, Carrier-envelope offset frequency stabilization of a mode-locked semiconductor laser, oral #AW1A.6, Advanced Solid State Lasers Conference and Exhibition (ASSL), Nagoya, Japan; October 1-5, 2017

29. **P. Brochard**, N. Jornod, V.J. Wittwer, S. Schilt, D. Waldburger, S.M. Link, C.G.E. Alfieri, M. Golling, L. Devenoges, J. Morel, U. Keller, T. Südmeyer, Carrier-envelope offset characterization in a semiconductor mode-locked laser without f-to-2f interferometry, Oral #1070, EFTF 2016, 30th European Frequency and Time Forum, York, UK, April 4-7, 2016

30. W. Moreno, R. Matthey, F. Gruet, **P. Brochard**, S. Schilt, G. Mileti, Rb-stabilized optical frequency reference at 1572 nm, Poster #1073, EFTF 2016, 30th European Frequency and Time Forum, York, UK, April 4-7, 2016

31. **P. Brochard**, S. Schilt, T. Südmeyer, New insights on the determination of the linewidth of low-noise signals with the emergence of a coherent peak, Poster #1220, EFTF 2016, 30th European Frequency and Time Forum, York, UK, April 4-7, 2016

32. W. Moreno, R. Matthey, F. Gruet, **P. Brochard**, S. Schilt, G. Mileti, Rb-based optical frequency reference at 1572 nm, Poster #3133, IEEE International Frequency Control Symposium (IFCS), New-Orleans, USA; May 9-12, 2016

33. K. Balskus, S. Schilt, V.J. Wittwer, **P. Brochard**, T. Ploetzing, N. Jornod, R.A. McCracken, Z. Zhang, A. Bartels, D.T. Reid, T. Südmeyer, Frequency comb metrology with a near-infrared optical parametric oscillator, Oral #SM1H.6, CLEO 2016, San Jose, USA, June 5-10, 2016

34. W. Moreno, R. Matthey, F. Gruet, **P. Brochard**, S. Schilt, G. Mileti, Rb-stabilized compact optical frequency comb acting as a versatile wavelength reference, Oral #SM2H.5, CLEO 2016, San Jose, USA, June 5-10, 2016

35. N. Jornod, **P. Brochard**, V.J. Wittwer, S. Schilt, S. Hakobyan, D. Waldburger, S.M. Link, C.G.E. Alfieri, M. Golling, L. Devenoges, J. Morel, U. Keller, T. Südmeyer, First Investigation of the Noise and Modulation Properties of the Carrier Envelope Offset Frequency in a Mode-locked Semiconductor Laser, Oral #SM2H.5, CLEO 2016, San Jose, USA, June 5-10, 2016

36. **P. Brochard**, S. Schilt, T. Südmeyer, CEO noise assessment in an optical frequency comb without direct CEO beat detection, Poster, Optical Clock School, Turin, Italy, June 29 – July 3, 2015

37. **P. Brochard**, S. Schilt, V.J. Wittwer, T. Südmeyer, Characterizing the Carrier-Envelop Offset in an Optical Frequency Comb without Direct Detection, Oral ATh1A.7, Advanced Solid State Lasers Conference and Exhibition, Berlin, Germany, October 4-9, 2015

38. S. Schilt, K. Balskus, V.J. Wittwer, **P. Brochard**, T. Ploetzing, N. Jornod, R.A. McCracken, Z. Zhang, A. Bartels, D.T. Reid, T. Südmeyer, Noise characterization and optical frequency measurement with an optical parametric oscillator frequency comb, Poster, 8th Frequency Standard and Metrology Symposium, Potsdam, Germany, October 12-16, 2015

39. **P. Brochard**, S. Schilt, T. Südmeyer, Characterization of the carrier-envelop offset in an optical frequency comb without direct detection, Poster, 8th Frequency Standard and Metrology Symposium, Potsdam, Germany, October 12-16, 2015

Awards and Honors

1. **P. Brochard**, E. Lucas, R. Bouchand, S. Schilt, T. Südmeyer, and T. J. Kippenberg, Optical-to-Microwave Frequency Division with a Kerr-Frequency-Comb Transfer Oscillator, EFTF-IFCS, Orlando, USA, April 14-18, 2019, **"best student paper award" finalist**

2. **P. Brochard**, S. Schilt, T. Südmeyer, Ultra-low Noise Microwave Generation based on a Free-Running Optical Frequency Comb, International Topical Meeting on Microwave Photonics, Toulouse, France, October 22-25, 2018, **"best student paper award" Winner**

3. **P. Brochard**, S. Schilt, T. Südmeyer, Optical-to-RF Frequency Division for Ultra-low Noise Microwave Generation Using a Transfer Oscillator Method, EFTF-2018, Torino, Italy, April 10-12, 2018, **"best student paper award" finalist**

4. **P. Brochard**, N. Jornod, V.J. Wittwer, S. Schilt, D. Waldburger, S.M. Link, C.G.E. Alfieri, M. Golling, L. Devenoges, J. Morel, U. Keller, T. Südmeyer, Carrier-envelope offset characterization in a semiconductor mode-locked laser without f-to-2f interferometry, EFTF 2016, 30th European Frequency and Time Forum, York, UK; April 4-7, 2016, **"best student paper award" finalist**

Content

Chapter 1

Introduction

For centuries, humans have been looking for periodical effects in nature or produced in more complex systems, with the willingness to have a clock, i.e., a time measurement instrument. It started by systems based on the Earth rotation, the Moon and stars. Inventive flow rate systems using water or sand were developed and the lifetime of objects like a candle was also used. Time measurement has become more precise and accurate with the emergence of mechanical clocks such as pendula. Nowadays, the most accurate and precise periodical systems are based on electronic or optical oscillators. They are involved in a wide type of everyday life tools on one side, but are also the basis for extreme fundamental physics experiments, for example for gravitational wave detection[1].

Frequency is the physical quantity that is measured with the highest level of accuracy. Therefore, frequency measurements are used in many high precision experiments to quantify other physical quantities. The recent optical atomic clocks based on strontium (Sr) features a record relative precision of $2.5 \cdot 10^{-19}$ equivalent to an imprecision of 100 ms over the estimated lifetime of the Universe[2]. This impressive precision is enabled by the use of optical frequencies in the range of 10^{14} Hz and is expected to further improve with the use of higher and higher frequencies going to the ultra-violet or extreme ultra-violet spectral range. However, no electronic system is fast enough to "count" optical oscillations (~2.3 fs at 698 nm for a Sr clock) in order to realize a complete clock. Furthermore, an ultra-stable optical oscillator is generally not directly usable, but needs to be frequency-divided by a large number in order to deliver a usable radio-frequency or microwave signal that is compatible with nowadays electronic. This division as well as the absolute measurement of optical frequencies can be realized with the use of an optical frequency comb (stabilized mode-locked laser), which was the major contribution to the 2005 Nobel Prize in Physics awarded to T.W. Hänsch[3] and J.L Hall[4].

Hence, state-of-the-art clocks deliver an **electrical oscillation** with unprecedented frequency precision and accuracy, generated from an **optical oscillator** using a **pulsed optical oscillator** to link the optical and electronic domains. In this respect, a deep understanding and characterization capabilities of these oscillators are needed.

Continuous-wave electrical or optical oscillators are described in the same way, only their carrier frequency strongly differs (in the MHz-GHz range for electrical oscillators vs THz range for optical oscillators). Pulsed optical oscillators (mode-locked lasers) appear in the frequency domain as an optical comb, meaning a composition of a multitude (hundreds/thousands to millions) of equally spaced optical lines as displayed in Figure 1.1. Each comb line is determined by three parameters which are the comb mode index N (integer number), the repetition rate

frequency f_{rep} that corresponds to the frequency spacing between the lines, and the carrier-envelop offset (CEO) frequency f_{CEO}, which represents the offset frequency of the optical spectrum. Therefore, the absolute optical frequency of each comb line is straightforwardly determined by only two measurable electrical signals (f_{CEO}, f_{rep}), making the comb a key tool for various applications[3–5]. f_{CEO} and f_{rep} are electrical signals/oscillations that can be directly measured by electronic counters.

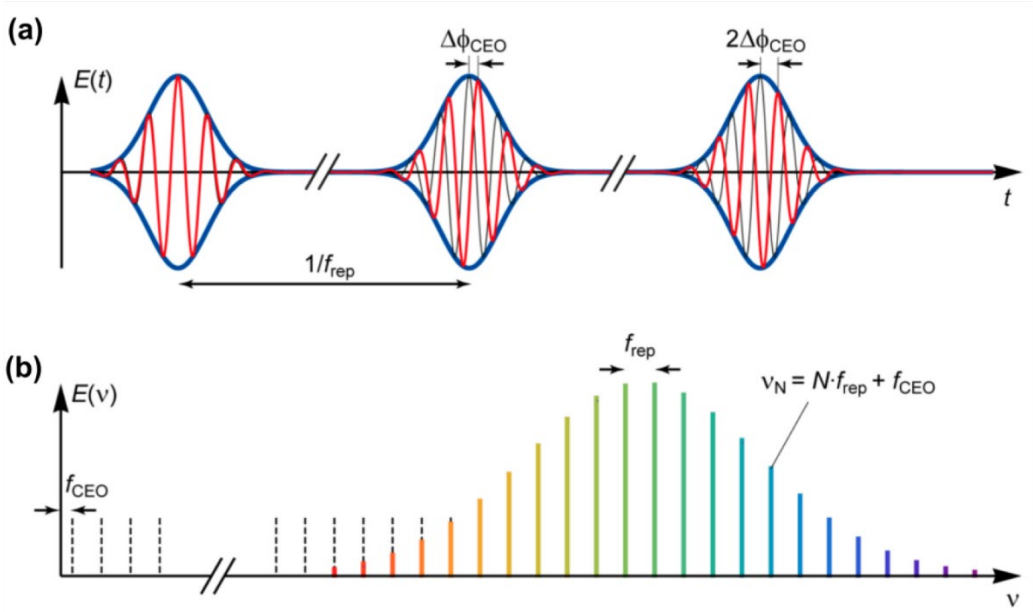

Figure 1.1: Time (a) and frequency (b) domain representation of the frequency comb from a mode-locked laser. Figure taken from Schilt and Südmeyer[6].

The comb repetition rate frequency is generally directly detectable and easy to characterize by sending the laser light onto a fast enough photodetector. However, the detection of the second comb parameter f_{CEO} is much more challenging as this frequency is not present in the optical spectrum emitted by the laser. The standard method to detect it is based on non-linear interferometry, which requires a wide coherent optical spectrum covering one frequency octave (*f*-to-2*f* interferometry[7]).

This has to be realized by external spectral broadening in a non-linear medium such as a highly non-linear fiber, which is demanding to achieve, especially for combs with repetition rates in the GHz range[8]. Nevertheless, it is interesting to get insights into the noise level of this offset frequency even before being able to detect it directly by the aforementioned self-referencing method.

In this thesis, an alternative versatile method has been developed, based on the transfer oscillator concept[9], to indirectly detect and characterize the offset frequency of a comb spectrum without non-linear interferometry, therefore without special requirements on the comb source. This method constitutes the core of the work presented in this thesis manuscript. It enabled the full characterization of four totally different types of comb sources. Basically, the developed method provides a radio-frequency (RF) signal that contains the difference between the comb offset frequency and an auxiliary continuous-wave (cw) laser, electrically-divided by a large integer number. Hence, this scheme makes an electrical division of optical frequencies.

Based on the same basic idea, this scheme was modified to perform optical-to-microwave frequency division with a self-referenced comb to generate an ultra-low noise microwave signal from an ultra-stable laser without the need to optically lock the comb to the optical reference, as done in the traditional approach[10]. Instead, the division is performed electrically, relying on the same transfer oscillator principle. This method paves the way for the realization of compact systems, e.g., based on micro-combs as shown in the last part of the thesis by a proof-of-principle demonstration of optical frequency division realized with such a micro-comb for the first time.

On another side, current-state-of-the-art ultralow phase noise and frequency-stable lasers are based on frequency stabilization onto a high-finesse ultralow expansion (ULE) Fabry-Pérot cavity placed under vacuum, thermally regulated, and mounted onto on a vibration insulation platform, which leads to fairly cumbersome systems. An alternative technology based

on a time delay approach[11,12], which is simpler and more affordable, has demonstrated impressive performance with a sub-Hz-level linewidth and relative frequency stability of 10^{-14} at a few seconds of averaging time[13,14]. The basic principle consists of comparing the laser frequency to a delayed version of itself in an interferometer in order to detect and reduce its frequency fluctuations. This method has been previously implemented with long fiber delay lines at telecom wavelengths, but its use with a much shorter delay in the meter scale has been investigated in this thesis in the mid-infrared spectral range to reduce the linewidth of a quantum cascade laser to the sub-10-kHz range, which led to a very simple, compact and cost-effective narrow-linewidth mid-infrared laser.

Organization of the thesis

This thesis addresses novel approaches for ultra-low phase noise optical and microwave oscillators. The content of the manuscript is organized as follows:

Chapter 2 introduces the mathematical tools used to describe and characterize electrical or optical oscillators, and presents a simple guideline to compute the power spectrum of an oscillator from its phase noise, enabling to qualitatively understand the shape of the spectrum corresponding to different regimes of phase noise.

In Chapter 3, a new method is introduced to characterize the offset frequency of a comb spectrum without the traditional use of *f*-to-2*f* interferometry. The method is first introduced and validated using a self-referenced fiber comb, then it is applied to characterize three totally different frequency combs with a high mode spacing in the multi-GHz range and at a variety of different wavelengths: a vertical external-cavity surface-emitting semiconductor laser with 1.8-GHz repetition rate at 1-μm wavelength, a diode-pumped solid-state laser with 25-GHz repetition rate

at 1.5 μm, and finally a quantum cascade laser frequency comb at 8-μm wavelength with a mode spacing of 7.5 GHz.

Chapter 4 reports proof-of-principle demonstrations towards compact ultra-low noise optical and microwave signal generation. A mid-infrared continuous-wave quantum cascade laser is frequency-stabilized using a very simple scheme made of a free-space delay line to reduce its linewidth by a factor of 60. Then, a method based on a transfer oscillator is presented to perform optical-to-microwave frequency division for ultra-low noise microwave generation in a different approach than traditionally realized. This method is finally applied to generate a low phase noise microwave signal at 14 GHz using a Kerr-comb for optical division.

Finally, Chapter 5 concludes the thesis with an overview of this 4-year work and provides a short outlook of possible future of the developed methods.

Chapter 2

Noise characterization of oscillators

2.1 Basics of oscillators

In simple words, an oscillator is a "system with a variable quantity that oscillates"*.

Relevant examples include the Moon revolving around the Earth, the day-night cycle, a mechanical pendulum, the voltage produced by an electrical oscillator, or the periodical variation of the electromagnetic field emitted by a laser. As an oscillation constitutes a periodical variation of a physical quantity, it is described by two parameters that are the frequency (i.e., the number of cycles per second made by the system, in Hz) and the amplitude (i.e., the maximum deviation of the quantity around its average value) of the varying quantity. Since nothing is perfect, both the amplitude and the frequency of the oscillation fluctuate over time, which is referred to as noise. A real oscillator is always affected by noise to some extent. Some mathematical tools are used to characterize the quality of an oscillator, based on the temporal fluctuations of the amplitude and/or frequency. The most relevant tools used in this manuscript are the power spectrum, the amplitude, phase and frequency noise power spectral densities, the relative frequency stability and some single values obtained by integrating the power spectral densities over a given spectral interval. These tools will be used all along the manuscript and are described in the following sub-sections as they are important for the characterization of all types of oscillators.

* translated from the LAROUSSE dictionnary

2.1.1 Power spectrum

The power spectrum of a temporal signal describes the spectral distribution of the signal, i.e., how the signal power is distributed among its different frequency components. The power spectrum $S_E(\nu - \nu_0)$ of an electrical signal $E(t)$ oscillating at frequency ν_0 corresponds to the Fourier transform (written as $\mathcal{F}$) of the autocorrelation function $R_E(\tau) = \langle E(t) \cdot E(t+\tau) \rangle$ of the signal (where $\langle . \rangle$ denotes an ensemble average)[15]:

$$S_E(\nu - \nu_0) = \mathcal{F}[R_E(\tau)] \, . \tag{1}$$

This power spectrum is simply a frequency representation of the temporal signal. In the case of a noiseless oscillator (pure sine function), the resulting power spectrum is a delta-Dirac function at the oscillating frequency ν_0. For a real signal, both the amplitude and the phase vary temporally around their average value, which leads to a different spectrum that is no longer composed of a single delta-Dirac function.

The unit of the power spectrum depends on the measured signal; for an electrical signal it is generally displayed in dBm, V^2, or W. The power spectrum is sometimes normalized to the resolution bandwidth (the frequency band in which the signal is integrated), leading to the power spectral density (PSD), in a unit of dBm/Hz, V^2/Hz or W/Hz. The power spectrum can also be normalized to the mean power of the signal, leading to a relative spectrum that is unitless or expressed in dBc (dB relative to the carrier) or to a relative PSD in 1/Hz in linear scale or in dBc/Hz in decibel scale.

Figure 2.1 shows the measured power spectrum of a laser as a representative example. The evolution of the power spectrum from the ideal Dirac peak to a real spectrum resulting from the frequency fluctuations of the signal is described in more detail in Section 2.2.

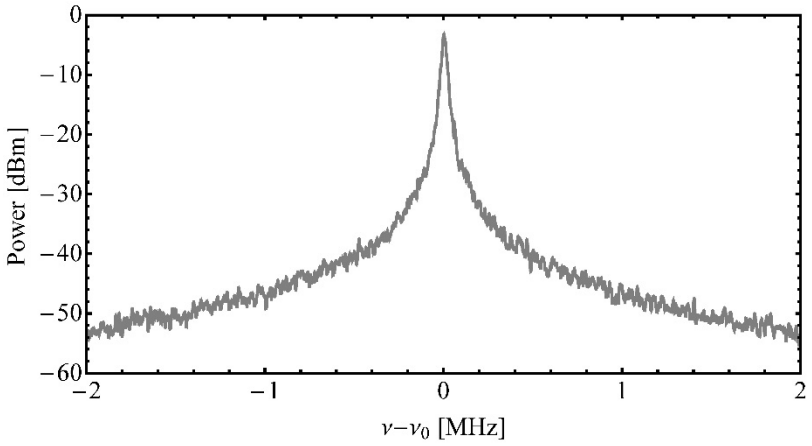

Figure 2.1: Power spectrum in logarithmic scale (dBm unit) of a laser emitting at a telecom wavelength (1.5 µm) measured by heterodyning with an ultra-narrow linewidth reference laser.

2.1.2 Amplitude noise spectrum

An oscillator with a fluctuating amplitude is characterized by its amplitude noise spectrum (or amplitude noise power spectral density, AN−PSD), which is the power spectrum (or PSD) of the time series of the amplitude fluctuations. For an optical oscillator (a laser), the fluctuations of the optical intensity are generally considered and the corresponding noise spectrum is referred to as the intensity noise spectrum (or relative intensity noise - RIN).

The unit of the amplitude noise PSD depends on the measured signal. In this thesis that mainly considers optical or electrical oscillators, the units are dBm/Hz, V^2/Hz, W/Hz. When the amplitude noise PSD is normalized by the mean signal power, the relative amplitude noise is obtained in units of 1/Hz or dB/Hz.

Figure 2.2 shows an example of the relative intensity noise PSD measured for a laser.

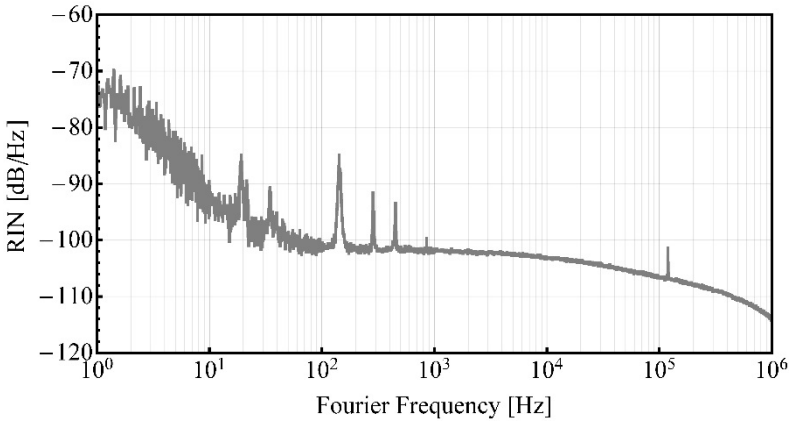

Figure 2.2: Example of relative intensity noise (RIN) power spectral density of a laser emitting at 1.5 µm.

2.1.3 Phase and frequency noise spectra

Frequency and phase noise spectra (or frequency/phase noise power spectral densities, FN-PSD/PN-PSD) result from temporal fluctuations of the frequency or phase, respectively, of the oscillator. They describe the spectral distribution of the frequency/phase fluctuations of the oscillator around its carrier frequency.

The unit of the frequency noise or phase noise PSD does not depend on the nature of the measured signal as it is only linked to the frequency/phase fluctuations of the oscillator. The frequency noise spectrum has a unit of Hz^2/Hz in terms of PSD, and sometimes the square root of this quantity is used (in $Hz/\sqrt{Hz}$). The phase noise is measured in rad^2/Hz, $rad/\sqrt{Hz}$ or dBc/Hz. The frequency and phase noise PSDs $S_\nu(f)$ (Hz^2/Hz) and $S_\phi(f)$ (rad^2/Hz) are directly linked to each other by the following expression:

$$S_\nu(f) = f^2 \cdot S_\phi(f) \tag{2}$$

Additional theoretical aspects that help understanding frequency and phase noise will be discussed in Section 2.2. Figure 2.3 shows an example of the frequency noise PSD of a laser.

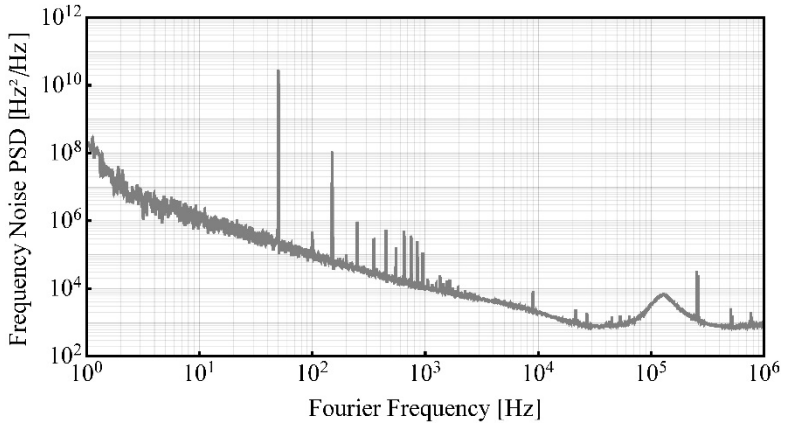

Figure 2.3: Example of frequency noise PSD of a laser emitting at 1.5 µm measured by heterodyning with an ultra-narrow linewidth reference laser and by measuring the frequency noise of the heterodyne signal.

2.1.4 Frequency stability: Allan variance

The frequency noise PSD introduced in the previous Section 2.1.3 is a powerful tool to characterize the frequency fluctuations of an oscillator over short timescales (typically shorter than 1 s, corresponding to Fourier frequencies above 1 Hz). The frequency fluctuations over longer timescales (Fourier frequencies typically below 1 Hz) are generally characterized differently, from the time series of the oscillator frequency ν recorded with a frequency counter. This time series is generally normalized by the averaged oscillator frequency ν_0: $y = \nu/\nu_0$. The frequency stability of the oscillator is characterized by the so-called Allan variance (AVAR), which describes how well the oscillator reproduces the same frequency over a given time τ and is given by [16]:

$$\sigma_y^2(\tau) = \frac{1}{2(N-1)} \sum_{i=1}^{N-1} (\bar{y}_{i+1} - \bar{y}_i)^2 \tag{3}$$

where N is the number of frequency samples averaged during the integration time τ. The Allan variance $\sigma_y^2(\tau)$, or the Allan deviation $\sigma_y(\tau)$, are unitless and represent the relative frequency stability of the oscillator.

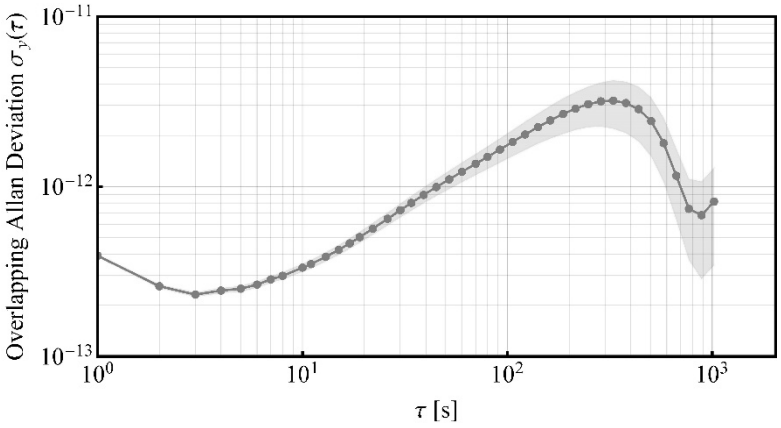

Figure 2.4: Example of Allan deviation of a free-running laser emitting at 1.5 µm measured by heterodyning with an ultra-narrow linewidth reference laser.

2.1.5 Oscillator integrated parameters

The amplitude and frequency/phase noise spectra previously introduced in Sections 2.1.2 and 2.1.3 contain most of the information about the fluctuations and instabilities of an oscillator. However, it is sometimes more convenient to compare the performance of different oscillators by a single number. Several such parameters are widely used in the community. They are generally obtained by integrating the noise PSD over a certain frequency interval. Therefore, these values depend on the observation (integration) time of the signal and this integration time (alternatively the frequency range of the integration) should always be specified when reporting such integrated parameters. Table 2.1 summarizes some of the main used integrated values that are listed below.

- **FWHM** or **HWHM**: full width at half maximum or half width at half maximum, respectively. It represents the actual linewidth of an oscillator, usually in Hz, which is directly derived from the power spectrum. It is also called the linewidth at -3 dB. This quantity can go down to zero for low noise oscillators.
- **Lorentzian linewidth**: hypothetical FWHM of an oscillator with a pure white frequency noise, which corresponds to a Lorentzian power spectrum. It generally gives information on the frequency noise at high Fourier frequencies and on the pedestal of the power spectrum. This linewidth is also referred to as the Schawlow-Townes linewidth[17], the instantaneous linewidth, the intrinsic linewidth or the fundamental linewidth.
- **FWHM$_\beta$**: approximated FWHM calculated from the frequency noise PSD using the concept of the β-separation line introduced in 2010 by Di Domenico *et al*[18].
- **Integrated phase noise** ϕ_{rms}: square root of the integrated value of the phase noise spectrum (in rad^2/Hz) in a given frequency interval. This value, in radians (rad), also corresponds to the root mean square (rms) value of the temporal phase fluctuations.
- **Integrated frequency noise** ν_{rms}: square root of the integrated value of the frequency noise spectrum (in Hz^2/Hz) in a given frequency interval. This value, in Hz, also corresponds to the root mean square (rms) value of the temporal frequency fluctuations.
- **Integrated amplitude noise**, in Volt (V), represents the square root of the integrated value of the amplitude noise spectrum in a given frequency interval. It also corresponds to the root mean square (rms) value of the temporal amplitude fluctuations.

The linewidth (FWHM or HWHM) is one of the most common parameters used to characterize and compare optical oscillators (i.e., lasers), but also sometimes noisy radio-frequency (RF) oscillators. However, this parameter has to be used with caution. The definition of the linewidth (i.e., at half the maximum value of the lineshape) is somehow arbitrary. Moreover, this value depends on the observation time and could significantly differ when looking at the power spectrum of an oscillator over 1 µs or 1 s, for example. In spite of this, the linewidth is a widely used parameter to compare lasers, as it is convenient to use a single value. However, one should notice that this is very restrictive, as the performance of an oscillator cannot be reduced to a single value.

A direct mathematical link exists between the frequency noise PSD and the lineshape of the spectrum[19,20]. Therefore, the linewidth can in principle be assessed from the frequency noise spectrum and can thus be determined for different integration times. However, the exact calculation is fairly complex and Di Domenico *et al.*[18] introduced in 2010 a simple tool to obtain an approximate value of the FWHM linewidth from the frequency noise spectrum. We call this value FWHM_β here. This approximation provides a good accuracy for signals with a relatively high integrated phase noise (typically higher than a few radians). More explanations are given in Section 2.2. The FWHM_β value is obtained in a simple way by integrating the frequency noise PSD that exceeds the so-called β-separation line displayed in Figure 2.5. The β-separation line and the approximated linewidth are given by the following formulas:

$$\beta(f) = \frac{8 \cdot \ln(2)}{\pi^2} \cdot f \ , \tag{4}$$

$$\mathrm{FWHM}_\beta = \sqrt{8 \cdot \ln(2) \cdot A} \ , \tag{5}$$

where A is the surface below the frequency noise PSD for all frequency components for which the frequency noise is higher than the β-separation line, represented by the blue area in Figure 2.5.

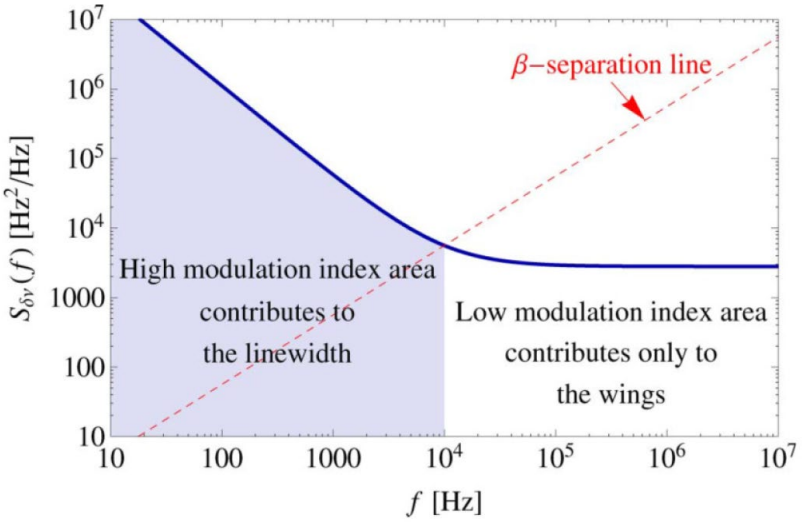

Figure 2.5: Figure from Di Domenico et al.[18]. A typical laser frequency noise PSD made of 1/f noise at low Fourier frequencies and white frequency noise at high Fourier frequencies. The red dashed line is the β-separation line which separates the spectrum into the two regions: the violet area contributes to the linewidth, the white one contributes only to the wings of the line shape function.

The β-separation line is a very simple and powerful tool that has been widely used in the laser community since its introduction. However, it remains an approximation that does not provide insights onto the spectral line shape of the oscillator with respect to the amplitude and spectral distribution of the frequency/phase fluctuations. Building on some old statistical tools as developed by D. Middleton[20,21] more than 70 years ago to link the power spectrum and the frequency noise spectrum, it is explained in details in the next section how the power spectrum evolves from a coherent Dirac peak (FWHM = 0) to a Gaussian-like spectrum when the frequency noise of the oscillator increases. This section is a reprint of an article published in IEEE Transactions on Ultrasonics, Ferroelectrics, and Frequency Control[22].

Oscillator Integrated Parameters			
name	*formula*	*derived from*	*unit*
FWHM, HWHM	----------	Power spectrum	Hz, nm
Lorentzian linewidth	$\pi \cdot S_\nu^0$, where S_ν^0 is the white frequency noise PSD[17]	Power spectrum/frequency noise PSD	Hz
FWHM_β	$\sqrt{8 \cdot \ln(2) \cdot A}$	Frequency / Phase noise PSD	Hz
Integrated phase noise	$\sqrt{\int_{f1}^{f2} S_\phi(f)\, df}$	Phase noise PSD	rad
Integrated frequency noise	$\sqrt{\int_{f1}^{f2} S_\nu(f)\, df}$	Frequency noise PSD	Hz
Integrated amplitude noise	$\sqrt{\int_{f1}^{f2} S_{AN}(f)\, df}$	Amplitude noise PSD	V

Table 2.1 Oscillator integrated parameters.

2.2 Power spectrum computation for an arbitrary phase noise using Middleton's convolution series: implementation guideline and experimental illustration

Pierre Brochard[1]*, Thomas Südmeyer*[1]*, and Stéphane Schilt*[1]

[1]Laboratoire Temps-Fréquence, Institut de Physique, Université de Neuchâtel, CH-2000 Neuchâtel, Switzerland.

In this work, we revisit the convolution series initially introduced by Middleton several decades ago to determine the power spectrum (or spectral lineshape) of a periodic signal from its phase noise power spectral density. This topic is of wide interest as it has an important impact in many scientific areas that involve lasers and oscillators. We introduce a simple guideline that enables a fairly straightforward computation of the power spectrum corresponding to an arbitrary phase noise. We show the benefit of this approach on a computational point of view, and apply it to various types of experimental signals with different phase noise levels, showing a very good agreement with the experimental spectra. This approach also provides a qualitative and intuitive understanding of the power spectrum corresponding to different regimes of phase noise.

2.2.1 Introduction

Many scientific areas rely today on stable and low-noise optical or microwave oscillators. For instance, ultra-narrow-linewidth cavity-stabilized lasers are a key element in optical atomic clocks that have surpassed the best microwave frequency standards in terms of fractional frequency stability in the last decade [1,2]. Such lasers have also produced microwave signals with the lowest phase noise to-date by optical-to-microwave frequency division using an optical frequency comb [3,4].

Other types of frequency-stabilized lasers with less stringent frequency stability requirements are used in microwave atomic clocks [5] or in optical sensing applications, e.g., in differential absorption lidars for the monitoring of pollutants or greenhouse gases in the atmosphere [6]. Low-noise microwave signals are needed, for example, in radar systems, large baseline interferometry, or in telecommunications and time synchronization. When dealing with low-noise oscillators, it is primordial to characterize their noise properties. This is also the case for other types of lasers with a higher noise (broader linewidth), even for free-running laser sources in some cases.

The most complete quantity to characterize the noise of an oscillator is the phase noise power spectral density (PN-PSD) $S_\phi(f)$ or the frequency noise power spectral density (FN-PSD) $S_\nu(f)$, which are directly related to each other by the well-known relation $S_\nu(f) = f^2 S_\phi(f)$, where f is the offset frequency (or Fourier frequency). However, other simpler values are often preferred by the scientific community to characterize and compare oscillators, such as the integrated phase noise ϕ_{rms} or the full width at half maximum (FWHM) of the oscillator power spectrum. Therefore, it is important to understand how these values can be obtained from an experimental noise spectrum.

A simple method to retrieve the linewidth of an oscillator (e.g., a laser) directly from its FN-PSD without first calculating the corresponding power spectrum was proposed by Di Domenico and co-authors [7]. The method is easy to implement and proved to be accurate to better than 10% in a large range of laser linewidths spanning from kilohertz to megahertz that were experimentally studied [8]. Moreover, this method provides a simple estimation of the feedback bandwidth that is required in a stabilization loop, such as a phase-locked loop (PLL), to suppress the linewidth of the oscillator and achieve a tight lock characterized by the presence of a coherent peak in the spectrum. However, this approach does not provide any information about the shape of the spectrum.

Furthermore, its experimental verification was performed in a regime of high phase noise that leads to a finite spectral linewidth, but the method has not yet been evaluated in a low phase noise regime (with ϕ_{rms} in the range of 1 rad), where larger discrepancies are expected.

The problem of determining the power spectrum of a carrier subjected to an arbitrary phase noise has been a topic of interest for a long time. In the 1950's, Middleton first reported theoretical considerations about the power spectrum corresponding to a signal modulated by stationary random disturbances, especially in the case of a Gaussian noise [9,10]. In this frame, he introduced a series of convolution products of the PN-PSD that is referred to as the Middleton's expansion series. Following this initial work, various theoretical studies have been reported based on Middleton's expansion series applied to other types of noise spectra [11-13]. All these works primarily concerned the case of modulated electrical oscillators, for instance for radio, TV and other kinds of communications signals. They generally dealt either with the limiting case of Middleton's expansion obtained for small integrated phase noise values, or with the different case of large integrated phase noise described by Woodward's theorem [14,15], respectively.

Thirty years after Middleton's initial work, Elliott and co-workers discussed for the first time the general mathematical expression to determine the power spectrum of an optical oscillator, i.e., a laser, from its PN-PSD [16]. As an outcome, the exact linewidth of the laser can be extracted. Elliott's theoretical description is basically similar to Middleton's prior work, but it has been much more spread and used in the laser community, whereas Middleton's work remains poorly known today in this area. The main difference between the two approaches, which will be reviewed in Section 2.2.2 of this article, lies in the fact that Elliott's formula requires the autocorrelation function of the oscillator phase to be calculated, as well as its exponential form, whereas Middleton used an expansion series of this term. Elliott's approach appeared more natural after the

universalization of the fast Fourier transform (FFT) algorithm [17] that was unknown at the time of Middleton's initial work, and which is necessary to compute Elliott's formula. Implementing this formula requires a two-step integration that needs to be performed numerically. A notable exception is the ideal case of an infinite white frequency noise PSD that can be analytically solved, leading to a Lorentzian lineshape described by the Schawlow-Townes-Henry linewidth [18,19]. In the general case, the numerical integration is not easy to implement and some care is required to retrieve the correct lineshape without introducing numerical artifacts [8]. Therefore, the process is not straightforward and can be fairly time-consuming (not in terms of pure computational time, but to determine the proper computation parameters as will be discussed in Section 2.2.3.2). Furthermore, this approach does not provide an intuitive understanding of the shape of the power spectrum retrieved for a given PN-PSD.

At first glance, Middleton's expansion series may appear inappropriate for practical implementation due to its infinite number of terms. So far, it has been applied essentially in the extreme situation of low phase noise ($\phi_{\mathrm{rms}} \ll 1$), whereas the opposite situation of high phase noise ($\phi_{\mathrm{rms}} \gg 1$) has been independently described by the central limit theorem [20] and by Woodward's theorem [14,15]. In both situations, the power spectrum can be determined or approximated. However, the applicability of Middleton's series in the more general case of an intermediate phase noise regime has not been reported so far to the best of our knowledge. A reason is that there was no recognized universal criterion enabling an easy determination of the number of terms of the series that need to be calculated to obtain the proper power spectrum [12].

In this article, we revisit Middleton's expansion and implement it to calculate the power spectra corresponding to different types of PN-PSD. As an important outcome, we theoretically shows that only a limited number of terms of the expansion series have a significant contribution to the power spectrum, and these relevant terms only depend on the integrated phase

noise, but not on the shape of the PN-PSD. As a result, we give a simple guideline to apply Middleton's series to an arbitrary noise, which is valid for any integrated phase noise and type of PN-PSD. We also discuss the benefits of Middleton's series over the usual integration of Elliott's formula to calculate and understand the power spectrum of an oscillator subjected to an arbitrary noise. Middleton's series provides an intuitive comprehension of some characteristic spectral features that appear in the power spectrum for a given PN-PSD. It predicts not only the presence of a coherent peak at the carrier frequency, surrounded by some sideband noise components occurring in the well-known regime of low integrated phase noise, but it also gives insights to understand and qualitatively describe the evolution of the spectrum from a coherent peak to a broader bell-shaped spectrum that occurs when the integrated phase noise increases (this bell-shaped profile tends to a Gaussian spectrum when the variance of the PN-PSD is finite according to the central limit theorem). Such an intuitive understanding cannot be directly obtained from Elliott's general formula.

This article is organized as follows. In Section 2.2.2, we will start by a short review of the basic theoretical concepts that link the PN-PSD to the power spectrum, introducing Elliott's general formula and then deriving the less known Middleton's expansion. In Section 2.2.3, we will explain how to implement Middleton's expansion in practice, based on a simple criterion that we introduce to determine the number of terms of the series that need to be considered in the computation. As an example of application, we will highlight some advantages provided by Middleton's expansion, which circumvents numerical artifacts that can occur with the use of Elliott's formula. Then, we will show how Middleton's expansion series enables understanding the shape of the power spectrum. Finally, we will present in Section 2.2.4 some experimental results obtained from real signals that illustrate the different theoretical aspects considered in the previous sections, and demonstrate the appropriateness of Middleton's approach to compute power spectra from the PN-PSD of different signals.

2.2.2 Theoretical background

We remind in this section the main theoretical aspects leading to the formulas previously derived by Elliott [16] and Middleton [9,10], respectively, which link the power spectrum of a signal to its PN-PSD. The two formulas derive from the exact same formalism, which is known for a long time and commonly used in the community [7,21,22]. We do not introduce here new theoretical aspect, the novelty of our work being presented in the next sections of this article. However, we estimated important to first review the main steps of the derivation of Elliott's and Middleton's formulas. The only difference between these two expressions occurs in their final form, as Middleton's expansion appears as a Taylor series of Elliott's general formula.

An ideal (noise-free) oscillator at frequency ν_0 is characterized in the spectral domain by a Dirac function. However, a real oscillator is affected by some phase noise and is mathematically described by the following expression:

$$E(t) = E_0 \sin[2\pi\nu_0 t + \phi(t)] \tag{6}$$

where E_0 is the amplitude of the signal (the electrical field in the case of a laser), ν_0 is the carrier frequency and ϕ(t) describes the temporal phase fluctuations. The power spectrum $S_E(\nu - \nu_0)$ of this signal corresponds to the Fourier transform (written as $\mathcal{F}$) of the autocorrelation function $R_E(\tau) = \langle E(t) \cdot E(t+\tau) \rangle$ of the signal (where $\langle\ \rangle$ denotes an ensemble average):

$$S_E(\nu - \nu_0) = \mathcal{F}[R_E(\tau)] \tag{7}$$

In the case where the phase variations $[\phi(t+\tau) - \phi(\tau)]$ constitute a stationary random process with Gaussian distribution and zero mean value as generally encountered [22], the autocorrelation function $R_E(\tau)$ of the signal can be obtained from the autocorrelation function of the phase $R_\phi(\tau) = \langle \phi(t) \cdot \phi(t+\tau) \rangle$ through the following expression [16,21,22]:

$$R_E(\tau) = E_0^2 \cdot e^{R_\phi(\tau) - R_\phi(0)} = E_0^2 \cdot e^{R_\phi(\tau)} \cdot e^{-R_\phi(0)} \tag{8}$$

The autocorrelation function of the phase evaluated at a time delay τ corresponds to the Fourier transform of the PN-PSD $S_\phi(f)$:

$$R_\phi(\tau) = \int_0^{+\infty} S_\phi(f) \cdot \cos(2\pi f \tau)\, df \tag{9}$$

whereas its value for $\tau = 0$ corresponds to the squared integrated phase noise ϕ_{rms}:

$$R_\phi(0) = \int_0^{+\infty} S_\phi(f)\, df \;=\; \phi_{\mathrm{rms}}^2 \tag{10}$$

Equations (9) and (10) mathematically involve an integration from zero to infinity, which may diverge on either side, e.g., at zero in the case of $1/f^2$ or $1/f^3$ PN-PSD. However, we are interested in this work in physical experimental signals, which are always observed over a finite time interval, so that these integrals remain finite. By combining equations (6) to (10), and taking into account the properties of Fourier transforms ($\mathcal{F}[\alpha] = \alpha\,\delta(\mathrm{x})$ where α is a constant and $\delta(x)$ is the Dirac function, and $\mathcal{F}[x \cdot y] = \mathcal{F}[x] * \mathcal{F}[y]$, where $*$ denotes the convolution product), the following expression is obtained for the power spectrum:

$$\begin{aligned} S_E(\nu - \nu_0) &= E_0^2\, e^{-\phi_{\mathrm{rms}}^2}\, \delta(\nu) * \mathcal{F}[e^{R_\phi(\tau)}] \\ &= E_0^2\, e^{-\phi_{\mathrm{rms}}^2}\, \delta(\nu) * \mathcal{F}[e^{\int_0^{+\infty} S_\phi(f)\cdot\cos(2\pi f\tau)df}]. \end{aligned} \tag{11}$$

We refer to this expression as Elliott's formula, as it was first introduced by Elliott and co-workers [16] to describe the spectrum of a laser. It links the power spectrum $S_E(\nu - \nu_0)$ to the PN-PSD $S_\phi(f)$ via a two-step integration process, described by equations (1) and (9). This integration can be solved only numerically in most cases, which makes the shape of the power spectrum not intuitive for a given PN-PSD. Some critical points for the implementation of this numerical integration must be considered, as will be discussed in Section 2.2.3.2. Elliott's formula can be transformed into

a more convenient form by exploiting the series expansion of the exponential function.

$$e^{R_\phi(\tau)} = \sum_{n=0}^{\infty} \frac{R_\phi^n(\tau)}{n!} = 1 + R_\phi(\tau) + \sum_{n=2}^{\infty} \frac{R_\phi^n(\tau)}{n!}. \tag{12}$$

This mathematical development is valid for any phase noise. As a physical experimental signal has a finite integrated phase noise ϕ_{rms} as previously mentioned, the infinite series (12) converges in practice. By introducing the series expansion (12) into Elliott's general formula (11), and taking into account the properties of Fourier transforms ($\mathcal{F}[x+y] = \mathcal{F}[x] + \mathcal{F}[y]$) and $\mathcal{F}[x \cdot y] = \mathcal{F}[x] * \mathcal{F}[y]$), the following expression is obtained for the power spectrum, which is valid for any real noise type and magnitude:

$$\begin{aligned} S_E(\nu - \nu_0) = {} & E_0^2 \, \mathrm{e}^{-\phi_{\text{rms}}^2} \, \delta(\nu) + E_0^2 \, \mathrm{e}^{-\phi_{\text{rms}}^2} \, S_\phi(f) \\ & + E_0^2 \, \mathrm{e}^{-\phi_{\text{rms}}^2} \sum_{n=2}^{\infty} \frac{1}{n!} S_\phi(f) *^{n-1} S_\phi(f) \end{aligned} \tag{13}$$

This expression is characterized by an infinite series of self-convolution products of the PN-PSD of different orders n, denoted by the symbol $*^n$. We refer to this expression as Middleton's expansion, as it was first introduced by Middleton [9,10]. In contrast to Elliott's general formula that first requires the phase autocorrelation function (9) to be computed for a large number of values of the time delay τ, Middleton's approach directly deals with multiple self-convolution products of the double side-band PN-PSD $S_\phi(f)$, which are easier to compute and do not depend on the particular choice of some computational parameters. The price to pay is that the expansion series contains an infinite number of terms, which has prevented its implementation in other cases than the extreme condition of small integrated phase noise. We will show in the next section that only a limited number of terms have a significant contribution to the spectrum for finite values of ϕ_{rms} (which is always the case experimentally as previously explained) and we will provide a simple guideline for the numerical implementation of Middleton's expansion for an arbitrary PN-PSD.

The decomposition in different convolution products occurring in Middleton's expansion will also enable us to qualitatively understand the shape of the power spectrum, which is not so easy with Elliott's general formula. By analyzing Middleton's expression (13), one notices that the fundamental term of the series (order n = 0) is a delta (Dirac) function centered at the carrier frequency ν_0. The amplitude of this term ($E_0^2\ e^{-\phi_{\mathrm{rms}}^2}$) depends on the squared integrated phase noise. This delta function corresponds to the commonly called coherent peak. This term is always present in the series, but its amplitude is significant only when the signal has a low integrated phase noise, typically in the range of 1 rad or smaller, otherwise its exponential decay with respect to ϕ_{rms}^2 makes it negligible [22]. The important parameter to assess the presence of a coherent peak is its relative power, i.e., the ratio between the carrier power and the integrated signal power, which corresponds to $e^{-\phi_{\mathrm{rms}}^2}$. For instance, for an integrated phase noise $\phi_{\mathrm{rms}} = 2$ rad, approximatively 2% of the signal power is contained in the coherent peak. It is experimentally possible to observe it using a spectrum analyzer with a sufficiently high resolution.

The first-order term (n = 1) of Middleton's expansion (13) is directly proportional to the PN-PSD and is located on each side of the coherent peak centered at ν_0. This term is the dominant contribution, besides the 0-th order term responsible for the coherent peak, in the low phase noise regime ($\phi_{\mathrm{rms}} \ll 1$), as well-known from textbooks on the subject [15]. The higher order terms (n >1) correspond to higher order convolution products. Their expression for the terms of lowest orders (n = 0, 1, 2, 3) is listed in Table II.

Order n = 0	$E_0^2\ e^{-\phi_{\mathrm{rms}}^2}\ \delta(\nu)$
Order n = 1	$E_0^2\ e^{-\phi_{\mathrm{rms}}^2}\ S_\phi(f)$
Order n = 2	$\frac{1}{2}E_0^2\ e^{-\phi_{\mathrm{rms}}^2}\ S_\phi(f) * S_\phi(f)$
Order n = 3	$\frac{1}{6}E_0^2\ e^{-\phi_{\mathrm{rms}}^2}\ S_\phi(f) * S_\phi(f) * S_\phi(f)$

Table II. First Terms of Middleton's Expansion in a Series of PN-PSD Self-Convolution Products

2.2.3 Computation of Middleton's expansion

2.2.3.1 Practical implementation of Middleton's expansion

Middleton's expansion (13) is made of an infinite series of convolution products of the PN-PSD. The number of terms to be considered to accurately compute the power spectrum depends on their respective weight, which is characterized by the relative power contained in each term, i.e., its integrated value or area A_n (moment of order 0):

$$\begin{aligned} A_0 &= e^{-\phi_{rms}^2} \\ A_n &= e^{-\phi_{rms}^2}\frac{1}{n!}\int S_\phi(f) *^{n-1} S_\phi(f)df, \qquad \text{for } n > 0 \end{aligned} \tag{14}$$

To calculate the relative power in each term of the series, one makes use of the following general property of the convolution products: the integral $A[y(x)]$ of any function $y(x)$ corresponding to the convolution product of two functions $g(x)$ and $f(x)$, $y(x) = g(x) * f(x)$, is equal to the product of the areas of the two functions: $A[y(x)] = A[g(x)] \cdot A[f(x)]$. Applying this property to the self-convolution product of order $n > 0$ of a function $h(x)$, $y(x) = h(x) *^{n-1} h(x)$, leads to $A[y(x)] = (A[h(x)])^n$. In our case, the considered function is the phase noise spectrum $S_\phi(f)$ and its area corresponds to the squared integrated phase noise $A[S_\phi(f)] = \phi_{\mathrm{rms}}^2$.

Therefore, $A\left[S_\phi(f) *^{n-1} S_\phi(f)\right] = A[S_\phi(f)]^n = (\phi_{\text{rms}}^2)^n$ and the relative power contained in the term of order n of Middleton's series (13) is given:

$$A_n = e^{-\phi_{\text{rms}}^2} \frac{(\phi_{\text{rms}}^2)^n}{n!} \tag{15}$$

This expression indicates that the relative power of each term of order n of Middleton's series follows a Poisson distribution that is independent of the amplitude and shape of the phase noise spectrum $S_\phi(f)$, but depends only on the squared integrated phase noise ϕ_{rms}^2. Summing the relative power A_n of all terms with $n > 0$ leads to a value of $\left(1 - e^{-\phi_{\text{rms}}^2}\right)$ that corresponds to the total power of the signal out of the coherent peak.

The Poisson distribution has a median value that is very close to ϕ_{rms}^2 and a variance rigorously equal to ϕ_{rms}^2, so that its width (standard deviation) corresponds to ϕ_{rms}. This distribution tends to a normal (Gaussian) distribution centered at ϕ_{rms}^2 with a variance ϕ_{rms}^2 at high integrated phase noise. In this case, one can determine the term of maximum order n_{max} that needs to be taken into account in Middleton's series to accurately determine the power spectrum, by requiring that the cumulated contribution (in terms of relative power) of all higher order terms that are neglected is smaller than a given tolerance factor ε. Using the cumulative distribution function of the Gaussian distribution, the following expression is obtained:

$$n_{\text{max}} = \lfloor \phi_{\text{rms}}^2 + \phi_{\text{rms}} \sqrt{-2 \cdot \ln(\varepsilon)} \rceil \tag{16}$$

where the symbol $\lfloor . \rceil$ represents the nearest integer, but $n_{\text{max}} \geq 1$ in all cases (the first order term $n = 1$ is always considered in addition to the coherent peak given by $n = 0$ when the argument in the nearest integer function in (16) is smaller than 0.5). The simple parameter n_{max} can be straightforwardly and unambiguously determined prior to the spectrum computation for any PN-PSD. Equation (16) is strictly valid for a Gaussian distribution, i.e., in the case of high integrated phase noise values. However, it remains a very

good approximation also for a Poisson distribution, i.e., in the general case of any integrated phase noise values as shown below.

With this criterion, Middleton's series of convolution products is fairly easy to implement for any noise spectrum. Such a simple condition has not been proposed before to the best of our knowledge. From our numerous experimental observations (see some examples in Section 2.2.4) and considering the cumulative distribution function of the Poisson distribution, a tolerance factor $\varepsilon = 1\%$ is sufficient to accurately compute the power spectrum from the PN-PSD, as more than 98.4% of the total signal power is contained in the considered terms for any value of ϕ_{rms}. This fraction increases even up to ~99.86% for a Gaussian distribution of the relative power of the different terms of Middleton's series that is obtained at high ϕ_{rms}. With $\varepsilon = 1\%$, the previous expression (16) can be simplified into the simpler following formula that involves only the integrated phase noise:

$$n_{\max} = \lfloor \phi_{\mathrm{rms}}^2 + 3\phi_{\mathrm{rms}} \rceil \tag{17}$$

A double-sideband PN-PSD must be used in the computation of Middleton's expansion to retrieve a correct power spectrum. The PN-PSD must be known with the same spectral resolution as targeted for the power spectrum. Furthermore, we used the following recurrence relation to calculate the successive convolution orders:

$$S_\phi(f) *^n S_\phi(f) = S_\phi(f) * \left[S_\phi(f) *^{n-1} S_\phi(f) \right] \tag{18}$$

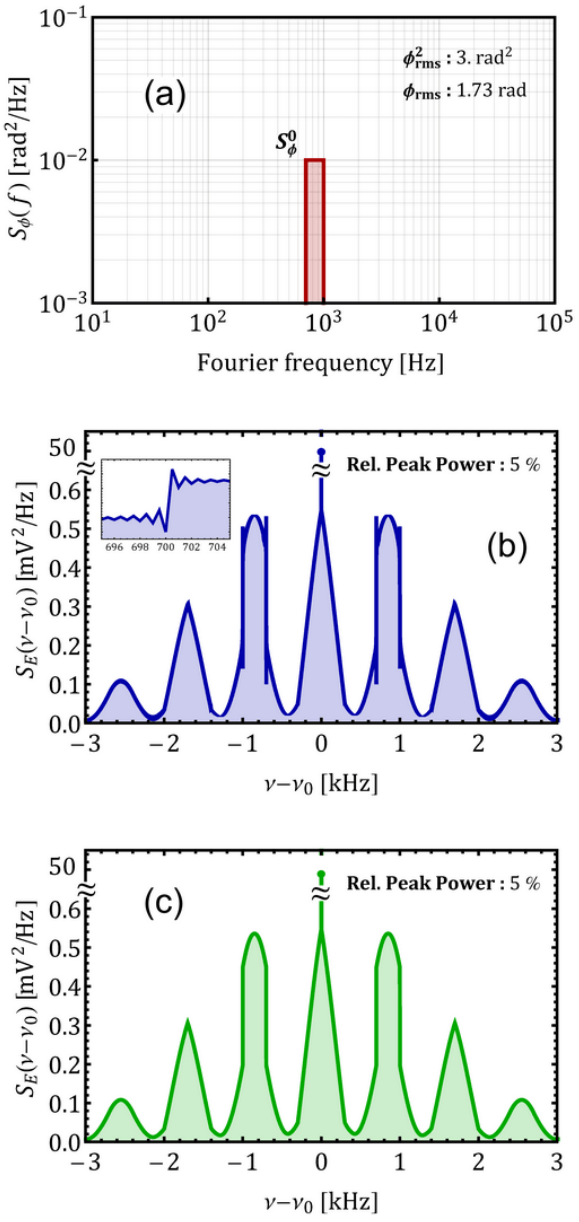

Fig. 2.6. Comparison of the power spectra computed using Elliott's general formula (by Fourier transform of the autocorrelation function) and Middleton's expansion method (using a series of convolution products). (a) PN-PSD used in the simulations, made of a rectangular narrow-band noise centered at 850 Hz with a bandwidth of 300 Hz and an amplitude of 0.01 rad²/Hz (integrated phase noise of 1.73 rad). (b) Power spectrum retrieved with Elliott's standard method. (Inset) Zoom on Gibbs' artifact [23-26] occurring at the transition of the rectangular first sideband resulting from the Fourier transform involved in Elliott's standard method. (c) Power spectrum retrieved using Middleton's convolution products expansion.

2.2.3.2 Benefit of Middleton's approach over Elliott's formula

To compare the use of Middleton's expansion with Elliott's general formula for the computation of power spectra, we first considered a rectangular PN-PSD bounded between 700 Hz and 1 kHz and of amplitude S_ϕ^0 = 0.01 rad²/Hz as displayed in Fig. 2.6-a (corresponding to $\phi_{\text{rms}}^2 = 3$ rad²). Very similar results are numerically obtained for the same resolution bandwidth of 1 Hz using Elliott's formula (see Fig. 2.6-b) and Middleton's expansion series (see Fig. 2.6-c) computed up to the term of order $n_{\max}$ = 8 according to our reported criterion (17). In both cases, the coherent peak reaches ≈50 mV²/Hz (here $E_0 = 1$ V) and similar sidebands (same shape, same amplitude) are observed at the various harmonics of the noise center frequency f_0. However, the spectrum obtained using Elliott's formula, which involves a Fourier transform, presents some oscillations at the transition of the rectangular part of the first order sidebands (see inset of Fig. 2.6-b). These oscillations constitute a computational artifact, which is a typical effect of Fourier transforms known as Gibbs' phenomenon [23-26]. The spectrum obtained using Middleton's expansion is not affected by such artifact and is more accurate.

The numerical implementation of Elliott's formula to simulate the power spectrum corresponding to an arbitrary PN-PSD is not a straightforward procedure. Great care is required in this implementation to retrieve a correct spectral lineshape. The method requires the autocorrelation function of the signal to be calculated from the PN-PSD for an ensemble of correlation times τ. Therefore, the integral (9) needs to be computed a large number of times for different values of τ. The overall range of values of the correlation time τ and the sampling rate of the autocorrelation function must be properly set to obtain the correct spectrum lineshape by Fourier transform (6), but they cannot be chosen fully independently. An improper choice of these parameters may lead to numerical artifacts, resulting in an incorrect spectrum. We illustrate this effect with a real example shown in Fig. 2.7. For this purpose, we generated

an experimental test signal using a waveform generator frequency-modulated by a band-pass-filtered white noise (more details about the experimental conditions will be given in Section 2.2.4). We measured both the PN-PSD of this signal (Fig. 2.6-a) and its power spectrum using a phase noise analyzer (FSWP from Rohde & Schwarz). We also separately computed the corresponding power spectrum using both Elliott's formula and Middleton's expansion series (see Fig. 2.6-c). The computation of Elliott's formula requires the autocorrelation function of the phase of the signal to be calculated in a first step according to (9). The result is shown in Fig. 2.6-b. When only the central part of this signal in the range of ±0.1 s was considered in the Fourier transform (6), a correct power spectrum was retrieved, similar to the measured spectrum (not show in the figure). However, the resulting spectral resolution was only 10 Hz in this case. To achieve a 1-Hz resolution that is straightforwardly obtained using Middleton's expansion, the autocorrelation function needs to be considered in a larger range of ±1 s. In this case, an erroneous power spectrum was obtained as illustrated in Fig. 2.6-c, which results from artifacts occurring in the autocorrelation function at $|\tau| > 0.2$ s. In contrast, Middleton's series computed up to the term of order $n_{\max} = 10$ (for an integrated phase noise $\phi_{\mathrm{rms}} = 2$ rad) is in excellent agreement with the experimental spectrum measured with 1-Hz resolution. For the computation of Elliott's formula, the choice of the τ values is not trivial as the spectrum to be retrieved is not known *a priori*, and may require an iterative process. Therefore, this process may be fairly time-consuming. On the opposite, the number of terms of Middleton's expansion series to be used in the computation is unambiguously determined prior to the calculation according to our simple expression (17). Then, the computation only requires multiple self-convolution products of the PN-PSD, which may be simpler and faster to implement, and circumvents some artifacts that can occur in the computation of Elliott's formula.

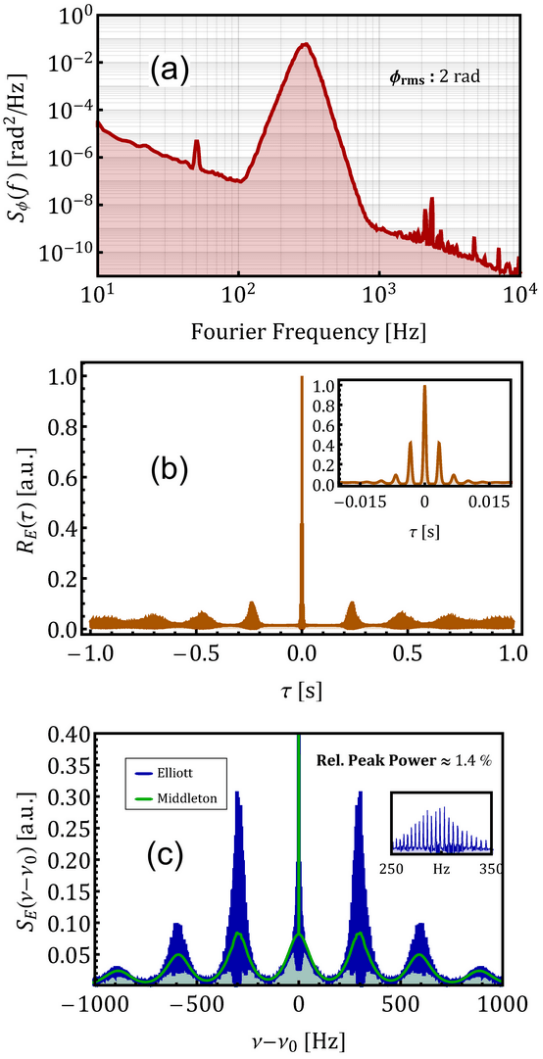

Fig. 2.7. Example of artifact that can occur in the computation of the power spectrum using Elliott's formula, in comparison with the use of Middleton's expansion series. (a) Experimental PN-PSD used in the computations, which was delivered by a waveform generator frequency-modulated by a band-pass-filtered white noise (with an integrated phase noise of 2 rad). (b) Autocorrelation function calculated from Eq. (9) that is used in Elliott's formula. (Inset) Zoom on the central part (-0.02 s to 0.02 s). (c) Power spectrum retrieved using Middleton's expansion (green line) and Elliott's formula (blue line). The measured experimental spectrum, not displayed here for the clarity of the plot, coincides with the spectrum obtained with Middleton's series. (Inset) Zoom on the graph between 250 Hz and 350 Hz showing the discrepancies obtained with the computation of Elliott's formula.

2.2.3.3 Qualitative power spectrum description

Computing the power spectrum with Middleton's expansion has the major advantage that the shape of the spectrum can be qualitatively explained. It also elucidates the transformation of the power spectrum from a zero-linewidth coherent peak to a broader bell-shaped spectrum at increasing integrated phase noise.

By looking at the individual terms of Middleton's series of convolution products (13), the resulting shape of the power spectrum can be clearly understood as illustrated in Fig. 2.8. Here, the same rectangular PN-PSD as shown in Fig. 2.6-a was considered, with a relatively low integrated phase noise of 1.73 rad. The first six terms of lowest orders (n = 0 to 5) of Middleton's series are displayed on the plot, their mathematical form follows the expressions listed in Table II. The coherent peak in the center of the spectrum (dark blue line) corresponds to the 0-th order term. The first order term (n = 1) is directly proportional to the PN-PSD, it has the same rectangular shape centered at $\pm f_0$ (dark red line). The second order term (n = 2) corresponds to the convolution of the PN-PSD with itself, resulting into a triangular shape (blue line). The PN-PSD being double-sideband, three triangular functions are obtained: one is located at the carrier frequency and two sidebands of halved amplitude are located at $\pm 2f_0$. The third order component (n = 3) is made of Gaussian-like (bell-shaped) sidebands centered at $\pm f_0$ and $\pm 3f_0$ (orange line) that results from the convolution between a rectangle and a triangle. Similarly, higher order terms tend more and more towards Gaussian sidebands centered at various harmonics of the noise frequency f_0. The complete power spectrum is the sum of all individual components, leading to a spectrum similar to Fig. 2.6-c, made of sidebands of different shapes (e.g., a triangle at $\nu = \nu_0$ and $\nu = \nu_0 \pm 2f_0$, two deformed rectangles at $\nu_0 \pm f_0$, etc…). An important remark here is that even order terms of the convolution series have a maximum value at the center of the spectrum, but odd order terms do not.

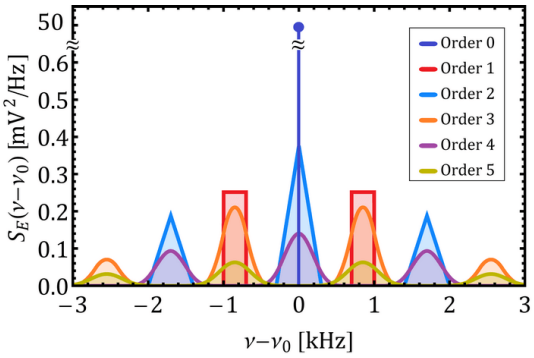

Fig. 2.8. First six individual terms of Middleton's series computed for a rectangular PN-PSD as displayed in Fig. 2.6-a. Dark blue, blue and violet lines are even order terms (n = 0, 2, 4). Red, orange and yellow lines are odd order terms (n = 1, 3, 5).

For an integrated phase noise of 10 rad, the Poisson distribution (15) of the relative power contained in each mode of Middleton's series shows that the low order convolution products become totally negligible and the terms of order $n \approx 100$ are dominant. A high order self-convolution of any real signal (i.e., with a PN-PSD bounded between $f_{\min} > 0$ and $f_{\max} < \infty$, such that its variance - moment of order 2 - is finite) tends towards a Gaussian distribution according to the central limit theorem [20]. Furthermore, the sum of several weighted Gaussian curves remains Gaussian-like. Therefore, it becomes clear that any PN-PSD produces a Gaussian-like (or bell-shaped) spectrum as illustrated in Fig. 2.9 as soon as its integrated phase noise is relatively large, typically higher than some radians in the aforementioned example of a rectangular PN-PSD (however, the transition to a Gaussian-like spectrum may occur at higher ϕ_{rms} values for other types of PN-PSD). This result was already known from Woodward's theorem, which states that the spectrum of a high-index frequency-modulated waveform is approximated by the probability distribution of the modulating wave shifted by the carrier frequency [14,15]. This leads to a Gaussian spectrum in the case of a high integrated phase noise, independently of the use of Middleton's series. However, this approximation is valid only in the case of a high integrated noise. The advantage of the use of Middleton's series that

we revisit in this article is its applicability to any integrated phase noise condition.

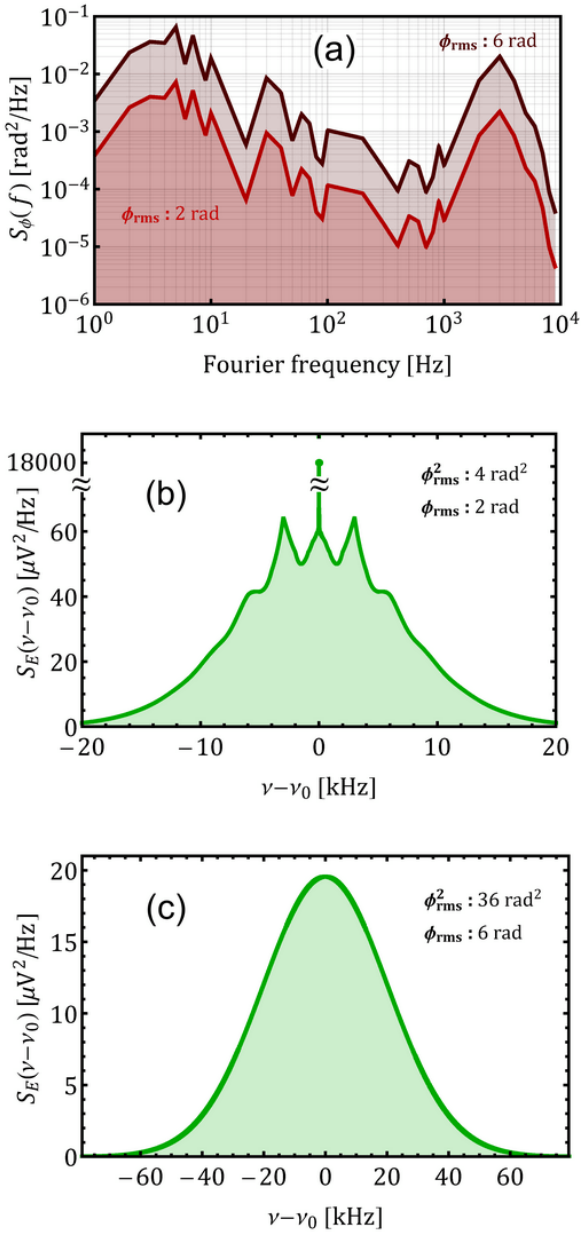

Fig. 2.9. Power spectrum determination using Middleton's expansion series for an arbitrarily distributed PN-PSD with two different amplitudes ($\phi_{\rm rms} = 2$ rad and $\phi_{\rm rms} = 6$ rad, respectively). (a) Arbitrary PN-PSD considered in the simulations. (b, c) Corresponding power spectra computed using Middleton's series (13) up to the order $n_{\rm max}$= 10 and $n_{\rm max}$ = 54, respectively, according to (17).

In complement to our previous theoretical considerations (see Section 2.2.3.1 and earlier in the present section), we numerically confirmed the validity of the transition to a Gaussian-like spectrum at high integrated phase noise for a large number of PN-PSD of various shapes, such as bounded flicker phase noise, white phase noise, or more "exotic" noise PSDs, and of different amplitudes. An example is shown in Fig. 2.9-a for an arbitrarily distributed PN-PSD with two different amplitudes corresponding to an integrated phase noise of 2 and 6 rad, respectively. In the first case (Fig. 2.9-b), a coherent peak is apparent in the power spectrum, surrounded by some bumps at ≈ ±3 kHz which are induced by the noise bump also present in the PN-PSD. This case mimics a real situation encountered in a stabilization loop, for instance a PLL to stabilize an oscillator onto a reference signal, which produces such a servo bump both in the PN-PSD and in the power spectrum. In the second case with a higher integrated noise of 6 rad (Fig. 2.9-c), the computed power spectrum has a Gaussian shape as explained before, as the dominant orders of the convolution products series are fairly large (around 36 here), so that the high order self-convolution terms of the PN-PSD tend toward a Gaussian distribution. This example shows that the regime of high integrated phase noise leading to a Gaussian power spectrum occurs already for ϕ_{rms} values of a few radians in this case (typically $\phi_{\mathrm{rms}} > \pi$).

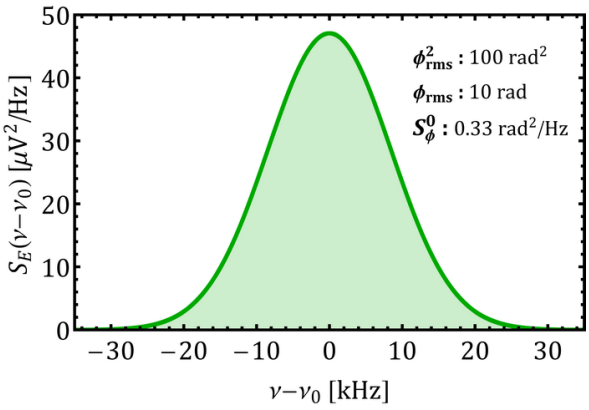

Fig. 2.10. Power spectrum computed using Middleton's series (13) with $n_{\max} = 130$ terms according to (17) for a rectangular PN-PSD with a high integrated phase noise of 10 rad, leading to a Gaussian distribution.

2.2.4 Experimental illustrations and validations

In Sections 2.2.2 and 2.2.3, we have shown how to compute the power spectrum of a signal from its PN-PSD based on Middleton's series of convolution products. Here, we present experimental results that illustrate the different aspects previously addressed on the theoretical point of view for the implementation of Middleton's series. In particular, these results confirm the suitability of the relationship (17) that we have introduced to determine the number of terms of the infinite series to be taken into account in the computation. In a first illustrative example, we will present the dependence of the relative power of the coherent peak as a function of the integrated phase noise that was discussed in Section 2.2.2, in the cases of low and intermediate integrated phase noises. Then, we will apply Middleton's series to different types of experimental PN-PSD covering the regimes of low, intermediate and high integrated phase noise. In all cases, we will show the excellent agreement obtained in comparison with experimentally measured power spectra.

2.2.4.1 Relative power of the coherent peak

A function generator (Agilent 33250A) modulated in frequency by an external voltage was used to generate various types of PN-PSD with a different integrated phase noise. The external voltage was tailored by filtering a white noise source by a narrow-band filter made of two cascaded tunable high-pass and low-pass filters (Stanford Research Systems SIM965) to generate PN-PSDs that approximate the ideal rectangular noise considered in the previous simulations (see Fig. 2.6-a). The cut-off frequencies of the high-pass and low-pass filters were first adjusted at ~600 Hz and ~800 Hz, respectively, to produce a narrow-band noise. Then, the cut-off frequencies were shifted to 3 kHz (high-pass) and 8 kHz (low-pass) to generate a broader PN-PSD. In both cases, the noise level was varied to achieve different values of ϕ_{rms}. In addition, we also used the "real" signal of the carrier envelope offset (CEO) beat of a commercial self-referenced optical frequency comb (FC1500 from Menlo Systems, Germany). More details are given in the next section 2.2.4.2 about the use of this system. In all cases, both the PN-PSD and the power spectrum of the signals under test were measured using a phase noise analyzer (FSWP26 from Rohde & Schwarz). Fig. 2.11 shows the dependence of the relative power of the coherent peak as a function of the integrated phase noise. An excellent agreement is observed between the experimental points obtained for the different aforementioned signals at various noise levels and the theoretical curve $e^{-\phi_{\mathrm{rms}}^2}$ obtained from the first term of Middleton's expansion series (order 0 in Table II).

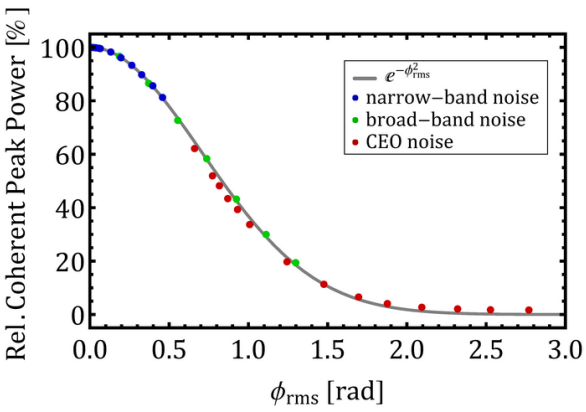

Fig. 2.11. Experimental validation of the dependence of the relative power contained in the coherent peak as a function of the integrated phase noise. Results were obtained for three different types of noise: from signals generated by a frequency-modulated synthesizer with different bandwidths of the induced noise (blue and green dots) and from the CEO beat of an optical frequency comb (red dots). The gray curve represents the theoretical dependence $e^{-\phi_{\mathrm{rms}}^2}$.

2.2.4.2 Validation of Middleton's power spectra computation

We have experimentally validated the computation of Middleton's series (13) restricted to the number of terms defined by our formula (17). For this purpose, we used the CEO beat signal of our frequency comb as a test signal. As this signal was relatively noisy and did not allow us to directly achieve the phase noise regimes of interest for this study, we frequency-divided it by a factor 16 or 4 using frequency pre-scalers (RF Bay FPS-16-4 or FPS-4-20, respectively). Changing the servo-controller gain in the CEO stabilization loop enabled different shapes of PN-PSD and various values of integrated phase noise to be obtained. To achieve the regime of low phase noise, with directly used the output signal at ~10 MHz of a frequency synthesizer (HP 3314A). These three different cases corresponding to low, intermediate and high phase noise values are displayed in Fig. 2.12. Based on our previous theoretical considerations discussed in Section 2.2.3, we can define a more precise delimitation between these different noise regimes compared to the two extreme cases

that are generally considered (i.e., low noise for $\phi_{\mathrm{rms}} \ll 1$ and high noise for $\phi_{\mathrm{rms}} \gg 1$). In the case of low phase noise characterized by a power spectrum consisting of a coherent peak surrounded on each side by the PN-PSD $S_\phi(f)$ [22], only the terms n = 0 and 1 of Middleton's expansion series (13) contribute to the spectrum. Therefore, we chose to consider $\phi_{\mathrm{rms}}^2 + 3\phi_{\mathrm{rms}} < 1.5$ in (17) as an upper limit, which roughly corresponds to $\phi_{\mathrm{rms}} < \pi/8$. In this low phase noise regime, one has n_{max} = 1, meaning that only the two terms n = 0 and n = 1 are considered in Middleton's series. In this case, at least 85% of the signal power is contained in the coherent peak and more than 98.9% in the two first components n = 0 and n = 1 (calculated from (15)). For integrated phase noise values larger than ~ $\pi/8$ rad, more terms of Middleton's series need to be taken into account ($n_{\mathrm{max}} \geq 2$) to determine the correct power spectrum. We have shown at the end of Section 2.2.3.3 that the regime of high phase noise leading to a bell-shaped envelope spectrum occurs already at a phase noise of a few radians, due to the smoothing behavior of the convolution product. We define the lower limit of this noise regime as $\phi_{\mathrm{rms}} > \pi$. In this case, less than 0.06‰ of the signal power is contained in the coherent peak, and at least 20 terms of Middleton's series need to be considered to accurately compute the power spectrum, which corresponds to a minimum accuracy of 99.5% in terms of the total power of the retrieved spectrum. The range of intermediate phase noise corresponds to $\pi/8 < \phi_{\mathrm{rms}} < \pi$, i.e., to $20 > n_{\mathrm{max}} \geq 2$ in terms of maximum order term in Middleton's series. It leads to a more complex shape of the power spectrum, which is obtained with a relative power accuracy between 98.88% and 99.94%.

For each of our experimental signals, we measured both the PN-PSD and the power spectrum using the same phase noise analyzer as in the previous section. From the measured PN-PSD, we also computed the corresponding power spectrum using Middleton's expansion (13) up to a term of maximum order n_{max} given by (17). In the considered examples, n_{max} = 1, 7 and 31, respectively, for integrated phase noise values

$\phi_{\mathrm{rms}} \approx 0.4$, 1.45 and 4.22 rad. We compared the result of the simulations (green lines in Fig. 2.12) with the directly measured power spectra (blue lines), obtaining an excellent agreement in all cases. The three reported examples represent real signals corresponding to the three characteristic regimes of phase noise where the power spectrum is made of (a) a coherent peak surrounded on both sides by the PN-PSD $S_\phi(f)$ for low phase noise ($\phi_{\mathrm{rms}} < \pi/8$), (b) a sum of successive convolution products of $S_\phi(f)$ around a weaker coherent peak at intermediate phase noise ($\pi/8 < \phi_{\mathrm{rms}} < \pi$) and (c) a bell-shaped (Gaussian) spectrum resulting from the multiple self-convolution products of $S_\phi(f)$ at high phase noise ($\phi_{\mathrm{rms}} > \pi$). Despite the first case is well known from textbooks [22], the two other cases are easily and accurately computed using the proposed approach of Middleton's series restricted to the terms of orders up to $n_{\max}$ given by (17). This is a significant advantage compared to the use of Elliott's general formula that is not so simple to apply in such cases.

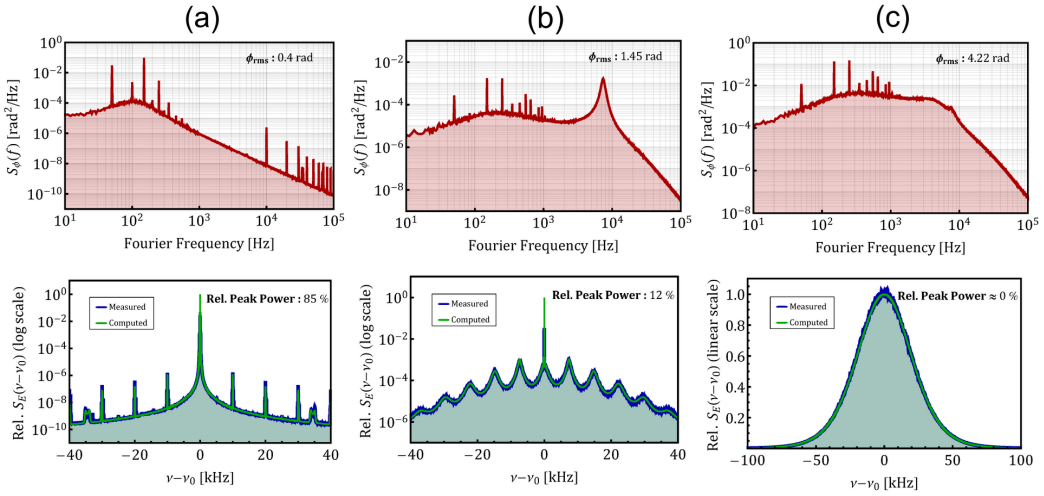

Fig. 2.12. Comparison of the power spectra computed using Middleton's series with experimental spectra. Top: experimental PN-PSD measured for different signals corresponding to the three regimes of low (a), intermediate (b) and high (c) integrated phase noise. Bottom: Corresponding power spectra experimentally measured (blue traces) and computed (green traces) using Middleton's series restricted to the terms of order up to $n_{\max}$ as given by (17). Here $n_{\max}$ = 1 (a), 7 (b) and 31 (c).

2.2.5 Conclusion

In this work, we revisited the relationship that links the PN-PSD of a signal to its power spectrum. The exact formula has been known for a long time, and has been introduced for the first time in the field of lasers by Elliott and co-workers [16]. However, computing this formula with real phase noise data is not straightforward and can be fairly time-consuming. Indeed, it involves a double integration process, which requires a careful adjustment of two parameters, the sampling rate of the autocorrelation function and the overall range of the time delay τ. These parameters cannot be chosen completely independently and their selection depends on the final frequency range and resolution that are targeted for the computed power spectrum, which are generally unknown a priori.

In this work, we presented the high benefits offered by a different approach based on a Taylor expansion of Elliott's formula into a series of self-convolution products of the PN-PSD that was first introduced by Middleton [10]. Despite its anteriority, Middleton's expansion series has been much less known and used than Elliott's formula to our knowledge, especially in the laser community. This is unfortunate, as the use of Middleton's expansion series offers many advantages. On a qualitative point of view, the shape of the power spectrum corresponding to an arbitrary PN-PSD can be easily understood in all different regimes of low, intermediate and high integrated phase noise that are well known for some of them, but much less for others. Our theoretical considerations have also enabled us to better define the boundaries of these three noise regimes. On a quantitative point of view, we have theoretically and experimentally shown that only a limited number of terms of the infinite series have a significant contribution to the power spectrum. We have introduced a simple guideline given by Eq. (17) to determine these terms. This number depends only on the integrated phase noise of the signal, and not on the shape of its PN-PSD. Therefore, this parameter can be easily and unambiguously determined prior to the calculation, which is not the case in

the computation of Elliott's general formula. We have shown that an improper choice of the parameters used to compute Elliott's formula can lead to significant discrepancies in the computed power spectrum. Even with proper parameters, other artifacts (such as Gibbs' artifact) can result from the Fourier transform involved in Elliott's general formula. In contrast, the use of Middleton's series as proposed in this work is very direct and does not rely on some particular choice of computation parameters.

For these reasons, we believe that the computational approach that we have reported in this article based on Middleton's series can benefit many scientists who are interested in precisely determining the spectrum lineshape of an oscillator from its PN-PSD in a simple way, instead of only getting an approximate value of its linewidth [7]. This method deserves to be considered by the laser community as a viable and simpler alternative to the computation of Elliott's general formula. In a next step, we plan to use this computational approach to quantitatively determine the domain of validity and accuracy of the linewidth approximation obtained from the β-separation line concept that is widely used in the laser community [7], especially in the low noise regime where the FN-PSD approaches this limit, and to study in detail the transition from a finite linewidth to a coherent peak spectrum.

Acknowledgments

We thank one of the anonymous reviewers of this article who provided very relevant comments during the review process, which helped improving the quality of the paper and broadening its scope.

References

[1] S. A. Diddams et al., "An Optical Clock Based on a Single Trapped 199Hg+ Ion," Science, vol. 293, no. 5531, pp. 825–828, Aug. 2001.

[2] U. Sterr et al., "The optical calcium frequency standards of PTB and NIST," Comptes Rendus Phys., vol. 5, no. 8, pp. 845–855, Oct. 2004.

[3] T. M. Fortier et al., "Generation of ultrastable microwaves via optical frequency division," Nat. Photonics, vol. 5, no. 7, pp. 425–429, Jun. 2011.

[4] X. Xie et al., "Photonic microwave signals with zeptosecond-level absolute timing noise," Nat. Photonics, vol. 11, no. 1, pp. 44–47, Jan. 2017.

[5] C. Affolderbach and G. Mileti, "A compact laser head with high-frequency stability for Rb atomic clocks and optical instrumentation," Rev. Sci. Instrum., vol. 76, no. 7, p. 073108, Jul. 2005.

[6] R. Matthey, F. Gruet, S. Schilt, and G. Mileti, "Compact rubidium-stabilized multi-frequency reference source in the 1.55-μm region," Opt. Lett., vol. 40, no. 11, pp. 2576–2579, Jun. 2015.

[7] G. Di Domenico, S. Schilt, and P. Thomann, "Simple approach to the relation between laser frequency noise and laser line shape," Appl. Opt., vol. 49, no. 25, pp. 4801–4807, 2010.

[8] N. Bucalovic, V. Dolgovskiy, C. Schori, P. Thomann, G. Di Domenico, and S. Schilt, "Experimental validation of a simple approximation to determine the linewidth of a laser from its frequency noise spectrum," Appl. Opt., vol. 51, no. 20, pp. 4582–4588, 2012.

[9] D. Middleton, "The distribution of energy in randomly modulated waves," Lond. Edinb. Dublin Philos. Mag. J. Sci., vol. 42, no. 330, pp. 689–707, Jul. 1951.

[10] "Wiley: An Introduction to Statistical Communication Theory: An IEEE Press Classic Reissue - David Middleton." [Online]. Available: http://eu.wiley.com/WileyCDA/WileyTitle/productCd-0780311787.html.

[11] N. M. Blachman, "Limiting frequency-modulation spectra," Inf. Control, vol. 1, no. 1, pp. 26–37, Sep. 1957.

[12] N. Abramson, "Bandwidth and Spectra of Phase-and-Frequency-Modulated Waves," IEEE Trans. Commun. Syst., vol. 11, no. 4, pp. 407–414, Dec. 1963.

[13] J. L. Stewart, "The power spectrum of a carrier frequency modulated by Gaussian noise," Proc. IRE, vol. 42, no. 10, pp. 1539–1542, 1954.

[14] N. M. Blachman, "A generalization of woodward's theorem on FM spectra," Inf. Control, vol. 5, no. 1, pp. 55–63, Mar. 1962.

[15] N. Blachman and G. McAlpine, "The spectrum of a high-index FM waveform: Woodward's theorem revisited," IEEE Trans. Commun. Technol., vol. 17, no. 2, pp. 201–208, 1969.

[16] D. S. Elliott, R. Roy, and S. J. Smith, "Extracavity laser band-shape and bandwidth modification," Phys. Rev. A, vol. 26, no. 1, p. 12, Jul. 1982.

[17] J. W. Cooley and J. W. Tukey, "An Algorithm for the Machine Calculation of Complex Fourier Series," Math. Comput., vol. 19, no. 90, p. 297, Apr. 1965.

[18] C. Henry, "Theory of the linewidth of semiconductor lasers," IEEE J. Quantum Electron., vol. 18, no. 2, pp. 259–264, 1982.

[19] A. L. Schawlow and C. H. Townes, "Infrared and Optical Masers," Phys. Rev., vol. 112, no. 6, p. 1940, Dec. 1958.

[20] S. W. Smith, The Scientist and Engineer's Guide to Digital Signal Processing. San Diego, CA: California Technical Publishing, 1999.

[21] A. Godone, S. Micalizio, and F. Levi, "RF spectrum of a carrier with a random phase modulation of arbitrary slope," Metrologia, vol. 45, no. 3, p. 313, May 2008.

[22] F. Riehle, "Wiley: Frequency Standards: Basics and Applications - Fritz Riehle." [Online]. Available: http://eu.wiley.com/WileyCDA/WileyTitle/productCd-3527605959.html.

[23] J. W. Gibbs, "Fourier's Series," Nature, vol. 59, no. 1522, Dec. 1898.

[24] J. W. Gibbs, "Fourier's Series," Nature, vol. 59, no. 1539, Apr. 1899.

[25] H. Wilbraham, "On a certain periodic function," Camb. Dublin Math. J., vol. 3, pp. 198–201.

[26] M. Bôcher, "Introduction to the Theory of Fourier's Series," Ann. Math., vol. 7, no. 3, pp. 81–152, Apr. 1906.

Chapter 3

Characterization of optical frequency combs

The optical spectrum of a frequency comb, for instance generated by a mode-locked laser but also by a micro-resonator[24] or a quantum cascade laser (QCL)[25], is defined by only two radio-frequencies f_{CEO} and f_{rep}. In the frequency domain representation, f_{CEO} corresponds to the offset frequency of the entire optical spectrum (i.e., this parameter affects all modes in the same way) and f_{rep} is the frequency spacing between the modes (i.e., this parameter has a multiplicative effect on the different modes, with a scaling factor *N* that corresponds to the mode number). In this respect, the absolute optical frequency ν_N of each optical line can be derived from only two electrically measurable signals, as described by the comb equation $\nu_N = N \cdot f_{\mathrm{rep}} + f_{\mathrm{CEO}}$ (Figure 1.1). The mode spacing f_{rep} is generally easy to measure and characterize as it can be detected by sending the laser light onto a photodetector with a sufficient bandwidth. The situation is much more difficult for the second comb parameter f_{CEO}. The traditional method

to detect f_{CEO} is based on non-linear interferometry (mainly *f*-to-2*f* interferometry[7]) and requires a wide (one frequency octave) coherent optical spectrum which is challenging to achieve, especially for combs with repetition rates higher than 1 GHz[8]. Indeed, the generation efficiency of the required octave-spanning spectrum that is obtained by spectral broadening in a non-linear medium like an optical fiber directly scales with the optical peak power. The lower the repetition rate and pulse duration, the broader the generated supercontinuum spectrum at constant average optical power. Therefore, detecting the CEO frequency by *f*-to-2*f* interferometry is generally more challenging for high repetition rates. However, getting information about the noise level of the CEO frequency and about its modulation capabilities before being able to detect it directly by *f*-to-2*f* interferometry is attractive to characterize and better understand new comb technologies.

In this chapter, an alternative and versatile method is presented and applied to various laser systems to indirectly characterize the offset frequency of a comb spectrum without the need for non-linear interferometry or an octave-spanning spectrum. This method was developed in the frame of this thesis and is based on the transfer oscillator concept[9]. It was first implemented and validated using a commercial self-referenced fiber-based mode-locked laser operating at a repetition rate frequency of 250 MHz, enabling a direct comparison of the results of this new method with an *f*-to-2*f* interferometer. This is presented in Section 3.1, which is a reprint of an article published in Optics Letters[26].

After its proof-of-principle demonstration and validation, this method was used for the full spectral characterization of three different types of comb spectra. The first one was a prototype of a vertical external-cavity surface-emitting laser (VECSEL) emitting at 1030 nm with a repetition rate frequency of 1.8 GHz. This laser was developed at ETH Zürich and it is based on a semiconductor gain chip that generates sub-300-fs pulses with an average power of 90 mW distributed within a 4-nm broad optical

spectrum. The characterization of the carrier-offset frequency of this laser using the developed method is reported in Section 3.2, which is a reprint of an article published in Optics Letters[27]. A few months later, the CEO frequency of this laser was detected by *f*-to-2*f* interferometry and was stabilized at the LTF[8].

The second laser system that was characterized is an Er:Yb:glass laser oscillator (ERGO) emitting ~4 mW at 1.5 µm with pulses of ~3 ps duration and with a repetition rate of 25 GHz, for which a coherent octave-spanning spectrum cannot be achieved by non-linear spectral broadening which made the proposed method attractive. The results are reported in (Section 3.3), which is a reprint of an article published in IEEE Photonics Journal[28].

Finally, the last comb spectrum characterized with the developed method is based on the completely different technology of QCL frequency combs emitting in the mid-infrared. The used laser emits slightly modulated light (no pulse) at ~8 µm with a mode spacing of 7.4 GHz. In contrast to frequency combs based on passively mode-locked ultrafast lasers, their operation relies on four-wave mixing in the semiconductor gain medium, and so far, no direct self-referencing has been achieved. Therefore, the developed method was very useful to perform the first noise analysis of the offset frequency in a QCL comb, which is reported in Section 3.4.

3.1 Characterizing the carrier-envelope offset in an optical frequency comb without traditional *f*-to-2*f* interferometry

Pierre Brochard[1], *Stéphane Schilt*[1], *Valentin J. Wittwer*[1]

and Thomas Südmeyer[1]

[1]Laboratoire Temps-Fréquence, Institut de Physique, Université de Neuchâtel, CH-2000 Neuchâtel, Switzerland.

We present a new method to measure the frequency noise and modulation response of the carrier-envelope offset (CEO) beat of an optical frequency comb that does not make use of the traditional *f*-to-2*f* interferometry. Instead, we use an appropriate combination of different signals to extract the contribution of the CEO frequency without directly detecting it. We present a proof-of-principle validation realized with a commercial Er:fiber frequency comb and show an excellent agreement with the results obtained using a standard *f*-to-2*f* interferometer. This approach is attractive for the characterization of novel frequency comb technologies for which self-referencing is challenging, such as semiconductor mode-locked lasers, micro-resonator based systems, or GHz repetition rate lasers

Optical frequency combs from mode-locked lasers have revolutionized the field of optical metrology in the last decade. They provide a direct and coherent link between the microwave and optical frequency domains, enabling the measurement of optical frequencies with extreme precision. A frequency comb constitutes a frequency ruler in the optical spectral domain [1], which is characterized by two radio-frequencies (RFs), the repetition rate f_{rep} and the carrier-envelope offset (CEO) frequency f_{CEO}. The repetition rate corresponds to the spacing between the comb modes and f_{CEO} represents the global frequency shift of the comb

spectrum from the origin, such that the frequency ν_N of each comb mode depends on only three parameters (where N is the mode number):

$$\nu_N = N \cdot f_{\mathrm{rep}} + f_{\mathrm{CEO}} \tag{19}$$

Many applications require a fully stabilized comb, where both f_{rep} and f_{CEO} are phase-locked. Whereas the stabilization of f_{rep} is fairly direct by controlling the cavity length using a piezo-electric transducer, the detection and stabilization of f_{CEO} are more challenging. The standard self-referencing method [2] requires an octave-spanning spectrum that is usually obtained by spectral broadening into a nonlinear medium such as a highly nonlinear fiber, a photonic crystal fiber or an integrated waveguides. Other methods that are less demanding in terms of spectral width of the comb spectrum were based on optical frequency dividers in the early days of frequency combs [3] or make use of higher order nonlinear processes, such as 2*f*-to-3*f* [4-5]. The ability to achieve a tight phase-lock of the CEO beat strongly depends on the frequency noise of the free-running CEO beat and in the capability to control f_{CEO} using a suitable actuator and with a sufficient bandwidth. The standard method involves modulating the pump power of the femtosecond laser, which is realized by a direct modulation of the injection current in diode-pumped solid-state lasers (DPSSLs) and fiber lasers.

Today there is a strong demand for novel compact and cost-effective frequency comb systems. One highly promising technology relies on semiconductor lasers such as vertical external cavity surface emitting lasers (VECSELs) or mode-locked integrated external cavity surface emitting lasers (MIXSELs) [6]. Such lasers are promising for future low-cost high-volume production, but no CEO stabilization has ever been demonstrated so far based on this technology, as a consequence of their insufficient peak power. Very recently, the only CEO beat ever detected from a semiconductor mode-locked laser has been reported [7], which required external pulse amplification and compression. So far, no stabilization attempt or noise analysis has been presented, which is most likely due to

the insufficient signal-to-noise ratio achieved for the CEO beat. Before such a mode-locked laser can be fully phase stabilized, it would be valuable to get first insights on its CEO noise level. In addition, knowing the response of f_{CEO} to a modulation of the pump current is a key requirement for the future phase stabilization of f_{CEO}. This is the case for many other novel laser systems.

In this Letter, we suggest and validate a new method to characterize the CEO beat, which does not involve self-referencing, but instead assesses its properties indirectly from an appropriate combination of different signals. Another technique that does not involve nonlinear interferometry to measure f_{CEO} was suggested by Osvay et al. based on spectrally and spatially resolved multiple-path interferometry [8]. This method was able to determine f_{CEO}, but with a precision of a few MHz only, and did not provide any information on the CEO noise spectrum. In contrast, the approach reported here is applicable to the characterization of the CEO beat in terms of frequency noise and modulation response. It is particularly attractive for laser systems for which the self-referencing method is not yet achievable. We should stress out that this approach does not target f_{CEO} stabilization and does thus not intend to replace the powerful self-referencing concept for CEO phase stabilization.

As a proof-of-principle demonstration, we implemented the proposed method with a commercial Er:fiber frequency comb and compared the results with the use of traditional *f*-to-2*f* interferometry to validate this new approach. The work reported in this Letter constitutes a first step for the future implementation of this method for the characterization of novel frequency comb technologies for which the detection of a CEO beat by traditional *f*-to-2*f* interferometry is challenging, such as GHz repetition rate systems, semiconductor lasers, or micro-resonator based systems [9].

The experimental method that we propose here does not require a direct detection of the CEO beat, but indirectly assesses its properties from an appropriate combination of signals that is schematized in Fig. 3.1(a).

These signals are mixed in such a way that the contribution of f_{rep} cancels out, giving access to f_{CEO} only. The method emulates the use of a frequency comb as a transfer oscillator [10] to compare two distant optical frequencies without contribution of the comb noise. Here the concept is modified to combine a high harmonic N_1 of f_{rep} with the signal obtained from the heterodyne beat f_{beat} between a comb line N and a narrow-linewidth continuous-wave (CW) laser. Very limited information about the properties of f_{CEO} could be directly obtained from this beat signal, as it simultaneously contains contributions of f_{CEO} and $N \cdot f_{rep}$. Even if f_{rep} is locked to an RF reference, its contribution to the noise of the beat signal is generally not negligible compared to the noise of f_{CEO}, at least out of its locking bandwidth. The different approach reported here enables suppressing the contribution of f_{rep} and thus assessing the properties of f_{CEO} over a much wider range, both in terms of frequency noise and modulation response. This is a key benefit of the reported approach.

The basic principle of the method is schematized in Fig. 3.1(a) and consists of the combination of two signals. The frequency ν_{laser} of the CW laser and the comb repetition rate are adjusted such that the index N of the comb line that beats with the laser can be factorized as $N = N_1 \cdot N_2$. On one side, the heterodyne beat frequency $f_{beat} = (\nu_N - \nu_{laser})$ is detected using a fast photodiode and is frequency-divided by the large integer number N_2 to produce a signal at a much lower frequency f_B (lower branch in Fig. 3.1). On the other side, a high harmonic signal $f_A = N_1 \cdot f_{rep}$ is detected (upper branch of the scheme). The two signals f_A and f_B are mixed in order to generate the difference frequency $f_{out} = f_B - f_A = (f_{CEO} - \nu_{laser})/ N_2$, in which the contribution of f_{rep} cancels out for a proper choice of the sign of the heterodyne beat signal. Therefore, only the noise of f_{CEO} / N_2 remains, provided that the noise of the CW laser is sufficiently low to have a negligible contribution. Besides the difference frequency component $(f_B - f_A)$, the mixer output also contains the sum frequency component

($f_B + f_A$) and a great care is needed to select the proper signal for the characterization of f_{CEO} (this will be discussed in the last part of this Letter).

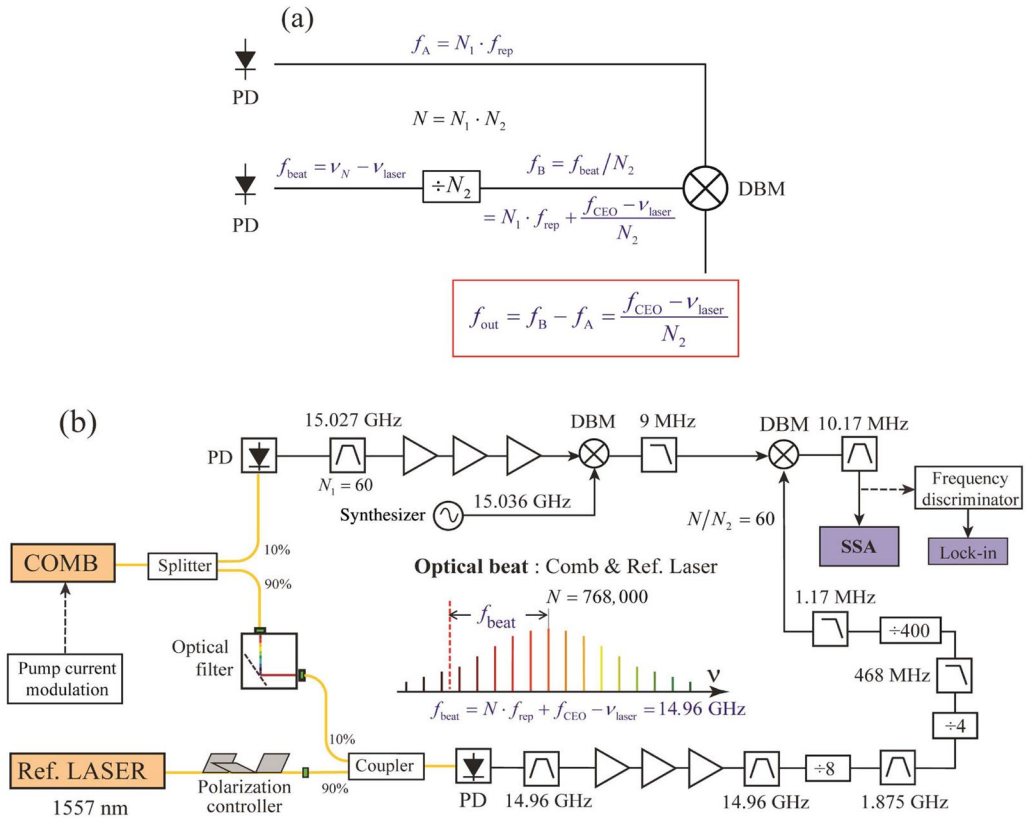

Fig. 3.1: (a) Basic principle of the proposed scheme to characterize the CEO beat without directly detecting it. A high harmonic N_1 of f_{rep} (upper branch, signal f_A) is mixed with the heterodyne beat with a CW laser, frequency-divided by N_2 (lower branch, signal f_B), to produce a signal f_{out} that is exempt of the contribution of f_{rep}. PD: fast photodiode; DBM: double-balanced mixer. (b) Detailed experimental scheme realized for the proof-of-principle implementation of the method with a commercial Er:fiber frequency comb with $f_{rep} \approx 250$ MHz using a narrow-linewidth CW laser at 1557.4 nm. SSA: signal source analyzer. All RF components but the narrow-bandpass filters at ~15 GHz are standard off-the-shelf components.

Figure 3.1(b) displays the detailed experimental setup implemented to validate this method using a commercial Er:fiber frequency comb (FC1500 from MenloSystems, Germany). Its repetition rate was tuned to $f_{rep} \approx 250.45$ MHz in this experiment and the CEO beat was detected using

a standard common-path *f*-to-2*f* interferometer for comparison. In the experimental setup, we used a high harmonic $N_1 = 60$ of f_{rep} at $f_A \approx 15$ GHz, which was detected using a fast photodiode (model 1434 from Newport, with 25 GHz bandwidth), filtered with a narrow-band filter (model TIC 15GB10-01 from Techniwave with ~70 MHz bandwidth) and amplified to a level of ~0 dBm. As a reference CW laser, we used a planar-waveguide external cavity laser at 1557.4 nm (model ORION from Redfern Integrated Optics Inc.) with a free-running linewidth of a few kilohertz only (over a timescale of 1-10 ms). The laser had a negligible contribution to the measured noise as will be shown in Fig. 3.2. Alternatively, the laser can be stabilized to a high-finesse ultra-stable optical cavity to improve its frequency stability and further reduce its optical linewidth, but this was not necessary here.

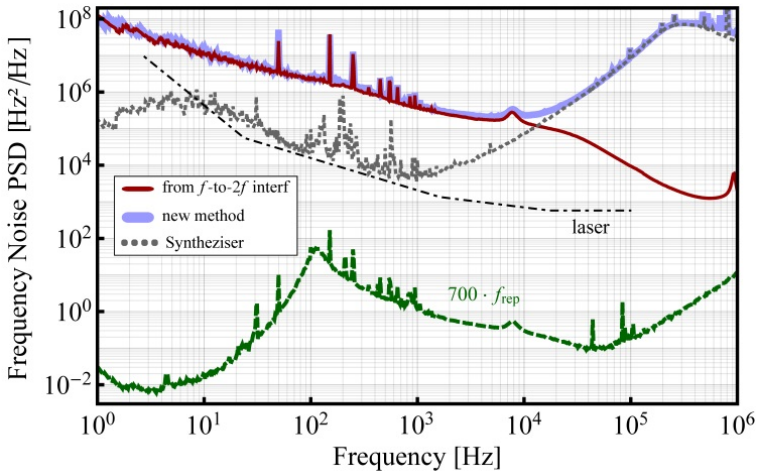

Fig. 3.2: Frequency noise spectrum of the free-running CEO beat of an Er:fiber comb measured with the proposed method (thick light blue line) and comparison with the CEO noise directly measured from an *f*-to-2*f* interferometer (thin dark red line). The dotted grey line represents the noise floor of the measurement introduced by a frequency synthesizer, and the dash-dotted line displays the typical frequency noise PSD previously measured for the free-running CW laser used in this experiment [12]. The residual contribution of f_{rep} in the measured signal resulting from its imperfect cancellation is also displayed (green dashed line).

The beat signal f_{beat} was detected at a high frequency of ~15 GHz using a fast photodiode (model DSC40S from Discovery Semiconductors Inc.,

with 14 GHz bandwidth).After proper filtering with a narrow-band filter (model TWRWC14.95GFC01 from Techniwave with ~70 MHz bandwidth) and subsequent several stages of amplification to a level of around 12 dBm, this signal was frequency-divided by the large number N_2 = 12,800, leading to a signal at $f_B \approx 1.2$ MHz. This division was performed in three subsequent steps using off-the-shelf frequency pre-scalers (÷8, 4 and 400, respectively), with proper filtering in between. As the signals in the two branches of the setup had a very different frequency ($f_A \approx 15$ GHz vs $f_B \approx 1.2$ MHz), their direct combination in a frequency mixer was not possible due to the impracticality to isolate and analyze the adequate signal among the two close components at the mixer output (15 GHz ± 1.2 MHz). In the present implementation of the method, we proceeded differently by first frequency downconverting the high harmonic $N_1 \cdot f_{rep}$ with the signal of a low-noise synthesizer (Rohde & Schwarz SMF100A) tuned to the frequency $f_{synth} = N_1 \cdot f_{rep} + 9$ MHz. The resulting downconverted signal at 9 MHz was then combined with the frequency-divided signal $f_B = f_{beat} / N_2$ in a double balanced mixer to produce two signals at (f_{synth} $f_A \pm f_B$). The contribution of f_{rep} cancelled out in the properly selected signal. After bandpass filtering, the resulting RF signal at ~10 MHz contained only the contributions of f_{CEO} and of the CW laser, both divided by the large integer number N_2. This signal was analyzed using a signal source analyzer (SSA, Keysight E5052B) for phase noise measurements, or processed by a phase-locked loop (PLL) frequency discriminator [11] and a lock-in amplifier to measure the transfer function of f_{CEO} when the current of the pump diode of the mode-locked laser was modulated by a small amplitude sine waveform.

The frequency noise power spectral density (PSD) of the CEO beat assessed using our experimental setup is displayed in Fig. 3.2, where it is compared to the CEO noise spectrum directly obtained from the output of the *f*-to-2*f* interferometer. An excellent agreement is observed between the two measurements up to an offset frequency of ~10 kHz, which demonstrates the suitability of the proposed method. At higher frequency,

the measurement is limited by the noise of the 15 GHz synthesizer used for frequency downconverting the high harmonic $N_1 \cdot f_{rep}$, which is also displayed in Fig. 3.2 (measured with Keysight E5052B and E5053A). In this proof-of-principle demonstration, the available CW laser at 1557.4 nm did not lead to an exact cancellation of f_{rep} in the output signal f_{out}. The targeted comb mode number $N = N_1 \cdot N_2 = 768{,}000$ would have required a repetition rate of 250.65 MHz, which was not achievable with our frequency comb. Alternatively, the nominal comb repetition rate of 250 MHz would have requested a CW laser wavelength of 1561.4 nm to achieve a perfect cancellation of the repetition rate. With our experimental conditions of f_{rep} = 250.45 MHz and ν_{laser} = 192.5 THz, the output signal f_{out} still contained a contribution of $\sim 0.055 \cdot f_{rep}$, corresponding to a residual contribution of $\sim 700 \cdot f_{rep}$ when scaled up by the factor N_2 = 12,800. However, this residual contribution is completely negligible as shown by the independently measured noise of f_{rep} also displayed in Fig. 3.2. The comb repetition rate was locked in these noise measurements to minimize the residual contribution resulting from its imperfect cancellation. However, it turns out that this residual contribution would be negligible even for a free-running f_{rep}. This demonstrates that the proposed method is not too challenging to be implemented, as it is not necessary to exactly fulfill the condition $N = N_1 \cdot N_2$.

In addition to the characterization of the CEO noise, our experimental setup was also applied to measure the frequency modulation response of f_{CEO} to a small modulation of the frequency comb pump current. The knowledge of this transfer function is an important step to assess the possibility to achieve a tight CEO lock in a stabilization loop using the common method of pump current modulation. In this experiment, we applied a sine modulation to the input voltage of the pump driver and the output signal f_{out} was demodulated using a PLL frequency discriminator [11]. A lock-in amplifier was used to measure the amplitude and phase of the change of f_{CEO} induced by the modulation. The pump current

modulation was kept small, typically <1 mA for an average current in the order of 800 mA. The result of this measurement is shown in Fig. 3.3, where it is compared to the result directly obtained from the CEO beat detected in the *f*-to-2*f* interferometer using the same measurement principle. Here, also, an excellent agreement is obtained, both in terms of amplitude and phase.

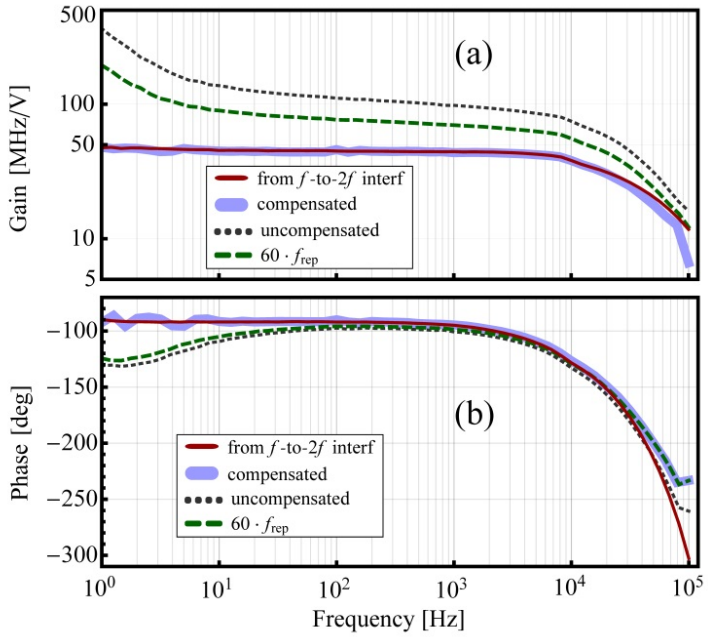

Fig. 3.3: Transfer function (amplitude (a) and phase (b)) of f_{CEO} measured with the proposed method (thick light blue line) for a modulation applied to the input voltage of the pump driver and comparison with the curve directly measured from the CEO beat (thin dark red line). The signal corresponding to the other frequency component at the output of the mixing process is also shown (uncompensated signal, dotted black line). This signal contains 120 δf_{rep} and is compared to the transfer function measured directly for 60 $\cdot f_{rep}$ from the high harmonic of the repetition rate at ~15 GHz (green dashed line).

To cross-check the operation of our novel method, we also measured the transfer function for the other frequency component in the output signal. In practice, this was realized by simply shifting the synthesizer frequency f_{synth} without changing any filter in the setup in order to exchange the sign of the output signal ($f_A + f_B$ instead of $f_A - f_B$), but it could also be achieved by tuning the CW laser. As modulating the pump current does not only affect f_{CEO}, but also f_{rep} [13], the contribution of the repetition rate

modulation δf_{rep} in this uncompensated signal is doubled (i.e., it contains $120 \cdot \delta f_{rep}$) instead of being cancelled. The result is also displayed in Fig. 3.3, where the transfer function of $60 \cdot f_{rep}$ (measured from the 60th harmonic of f_{rep} at ~15 GHz in the upper branch of the setup of Fig. 3.1) is shown as well for comparison.

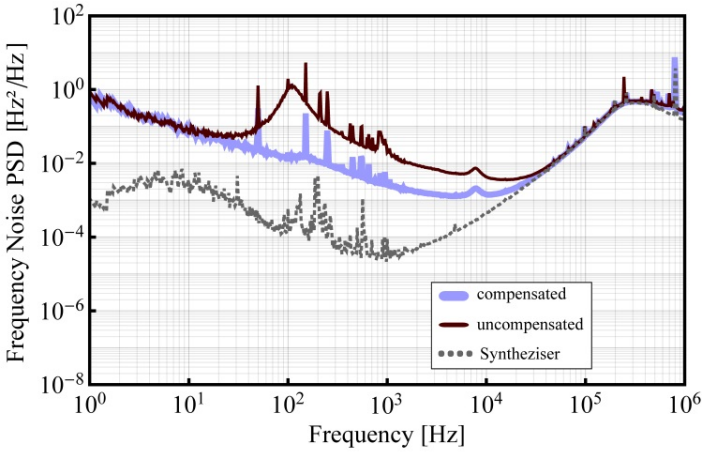

Fig. 3.4: Comparison of the signals measured for the two signs of the heterodyne beat between the CW laser and the comb line, corresponding to the cases where the contribution of f_{rep} is either suppressed (compensated) or doubled (uncompensated). The noise of the raw signals is displayed here (i.e., not re-scaled by the factor N_2).

We performed a similar cross-check for the CEO noise measurement using the other frequency component in the output signal (Fig. 3.4). The noise measured at low frequency was unchanged as the repetition rate stabilization led to a much weaker contribution to the beat signal than the free-running CEO. At frequencies higher than ~30 Hz, a significant difference was observed between the two curves, which confirmed that the contribution of f_{rep} in the measured signal was efficiently suppressed. If the measurements of the uncompensated signal shown in Fig. 3.3 for the transfer function and in Fig. 3.4 for the noise spectrum do not bring any additional information about the properties of f_{CEO}, they constitute important inputs to ensure the correctness of the results. It is not relevant for the measurements reported here that aimed at comparing the results of the novel method with the standard self-referencing technique. However, a

practical verification performed by measuring both signals at the mixer output becomes important when no CEO beat is available. This will be the case in future implementations of the method with novel comb technologies.

In conclusion, we demonstrated a new method to characterize both the frequency noise and the transfer function of the CEO beat in a frequency comb without directly detecting f_{CEO}, e.g., using a standard *f*-to-2*f* interferometer. The method was validated with an Er:fiber comb at 1560 nm and an excellent agreement was obtained with the CEO properties directly measured from the CEO beat at the output of an *f*-to-2*f* interferometer. The results of this Letter pave the way to using this approach for the characterization of mode-locked lasers for which the generation of a CEO beat by *f*-to-2*f* interferometry is challenging, such a GHz mode-locked DPSSLs, micro-resonator-based systems [9], or for novel semiconductor mode-locked lasers which is our next target.

In the current implementation of the repetition rate compensation scheme reported here, a limitation to the measurable CEO noise arose from a frequency synthesizer used for frequency downconversion of the high harmonic of f_{rep} before its subtraction from the frequency-divided beat signal. We expect this limitation to be removed and the setup to be improved with the use of a single sideband (SSB) mixer that would enable us to directly mix the signals from the two branches of our setup ($f_A \approx 15$ GHz and $f_B \approx 1.2$ MHz, respectively) and analyze the resulting signal without using the 15 GHz synthesizer. With this update, we expect to lower the noise floor of the system, resulting in the possibility to measure the frequency noise PSD of the CEO beat in a wider frequency range.

Funding

EU-FP7 (ITN FACT (PITN-GA-2013-607493)), Nano-Tera.ch (MIXSEL II (20NA21_145932))

Acknowledgments

We thank Computer Controls AG (Switzeland) and Keysight Technologies Deutschland GmbH for the loan of a signal source analyzer (E5052B and E5053A).

References

[1] T.W. Hänsch, Rev. Mod. Phys. 78, 1297 (2006).

[2] H. R. Telle, G. Steinmeyer, A. E. Dunlop, J. Stenger, D. H. Sutter, and U. Keller, Appl. Phys. B 69, 327 (1999).

[3] J. Reichert, R. Holzwarth, T. Udem, and T.W. Hänsch, Opt. Comm 172, 59 (1999).

[4] C.R. Locke, E.N. Ivanov, P.S. Light, F. Benabid, and A.N. Luiten, Opt. Express 17, 5897 (2009).

[5] K. Hitachi, A. Ishizawa, O. Tadanaga, T. Nishikawa, H. Mashiko, T. Sogawa, and H. Gotoh, Appl. Phys. Lett. 106, 231106 (2015).

[6] M. Hoffmann, O.D. Sieber, V.J. Wittwer, I.L. Krestnikov, D.A. Livshits, T. Südmeyer, and U. Keller, Opt. Express 19, 8108 (2011).

[7] C.A. Zaugg, A. Klenner, M. Mangold, A.S. Mayer, S.M. Link, F. Emaury, M. Golling, E. Gini, C.J. Saraceno, B.W. Tilma, and U. Keller, Opt. Express 22, 16445 (2014).

[8] K. Osvay, M. Görbe, C. Grebing, and G. Steinmeyer, Opt. Lett. 32, 3095 (2007).

[9] T.J. Kippenberg, R. Holzwarth, and S.A. Diddams, Science 332, 555 (2011).

[10] H.R. Telle, B. Lipphardt, and J. Stenger, Appl. Phys. B 74, 1 (2002).

[11] S. Schilt, N. Bucalovic, L. Tombez, V. Dolgovskiy, C. Schori, G. Di Domenico, M. Zaffalon, and P. Thomann, Rev. Scient. Instr. 82, 123116 (2011).

[12] V. Dolgovskiy, "All-optical microwave generation using frequency combs," PhD dissertation, University of Neuchâtel (2012).

[13] V. Dolgovskiy, N. Bucalovic, P. Thomann, C. Schori, G. Di Domenico, and S. Schilt, J. Opt. Soc. America B 29, 2944 (2012).

3.2 First investigation of the noise and modulation properties of the carrier-envelope offset in a mode-locked semiconductor laser

P. Brochard,[1] N. Jornod,[1] S. Schilt,[1] V. J. Wittwer,[1] S. Hakobyan,[1] D. Waldburger,[2] S. M. Link,[2] C. G. E. Alfieri,[2] M. Golling,[2] L. Devenoges,[3] J. Morel,[3] U. Keller,[2] and T. Südmeyer[1]

[1]Laboratoire Temps-Fréquence, Institut de Physique, Université de Neuchâtel, CH-2000 Neuchâtel, Switzerland.

[2]Department of Physics, Institute of Quantum Electronics, ETH Zurich, CH-8093 Zürich, Switzerland.

[3]Federal Institute of Metrology METAS, CH-3003 Bern-Wabern, Switzerland.

We present the first characterization of the noise properties and modulation response of the carrier-envelope offset (CEO) frequency in a semiconductor mode-locked laser. The CEO beat of an optically-pumped vertical external-cavity surface-emitting laser (VECSEL) at 1030 nm was characterized without standard *f*-to-2*f* interferometry. Instead, we used an appropriate combination of signals obtained from the mode-locked oscillator and an auxiliary continuous-wave laser to extract information about the CEO signal. The estimated linewidth of the free-running CEO beat is approximately 1.5 MHz at 1-s observation time, and the feedback bandwidth to enable a tight CEO phase lock to be achieved in a future stabilization loop is in the order of 300 kHz. We also characterized the amplitude and phase of the pump current to CEO-frequency transfer function, which showed a 3-dB bandwidth of ~300 kHz for the CEO frequency modulation. This fulfills the estimated required bandwidth and indicates that the first self-referenced phase-stabilization of a mode-locked semiconductor laser should be feasible in the near future.

Optical frequency combs from mode-locked solid-state lasers have been a revolution in the field of high precision metrology by directly and coherently linking the optical and microwave parts of the electromagnetic spectrum [1–3]. Such stabilized frequency combs enable the measurement of optical frequencies with an extreme precision [4,5] and constitute a key element of novel optical atomic clocks that have surpassed the best microwave frequency standards in terms of fractional frequency stability [6,7].

Most comb applications today require self-referencing, i.e., the detection and stabilization of the carrier envelope offset (CEO) frequency f_{CEO} [1,8]. This has been achieved in various fiber laser systems [9] and solid-state lasers (Ti:Sapphire [2] or diode-pumped solid-state lasers – DPSSLs [10,11]). Electronic feedback modulating the pump power of the femtosecond laser is the most common approach to phase-stabilize f_{CEO} to an external reference frequency [3]. Alternative methods have been demonstrated, which make use of an intra-cavity loss modulator enabling the modulation bandwidth to be extended beyond the gain lifetime limitation, such as a graphene electro-optic modulator [12] or an opto-optical modulation of a semiconductor saturable absorber mirror (SESAM) [13]. Other solutions are based on feedforward corrections applied to the CEO frequency [14] or passive CEO cancellation using a difference frequency generation (DFG) process [15].

Self-referencing mode-locked lasers with a higher repetition rate in the GHz range is much more challenging, as the CEO noise typically scales with the repetition rate [16], therefore requiring larger feedback bandwidths. In addition, the standard self-referencing method most often involves *f*-to-2*f* interferometry to detect the CEO frequency [1]. This requires a coherent supercontinuum (SC) spectrum that covers at least one frequency octave, which is fairly challenging to achieve for some novel comb technologies that are presently being developed. The use of higher order nonlinear processes,

such as 2*f*-to-3*f* [1], slightly reduces the requirements in terms of spectral width of the SC spectrum, but at the expense of a higher complexity.

Among the emerging comb technologies, mode-locked semiconductor lasers are promising for future low-cost high-volume production owing to the benefits of semiconductor manufacturing. Vertical external-cavity surface-emitting lasers (VECSELs) or mode-locked integrated external-cavity surface-emitting lasers (MIXSELs) [17] can lead to compact and cost-effective frequency comb systems in the future. However, no such mode-locked laser has ever been CEO-frequency-stabilized yet. The main reason is the insufficient peak power and too long pulse duration that have prevented so far the generation of a suitable SC spectrum for CEO detection.

A CEO beat signal from a semiconductor mode-locked laser has been detected for the first time by Zaugg et al. after external pulse amplification and compression [18], but no further investigation has been reported since then. The 1038-nm VECSEL was first amplified to 5.5 W average power using a fiber amplifier, then the pulses were compressed to 85 fs to generate the necessary octave-spanning SC spectrum in a photonic crystal fiber (PCF). However, the detected CEO signal was not suitable for noise analysis or stabilization as the signal-to-noise ratio (SNR) of ~15 dB (in a 100-kHz resolution bandwidth) was insufficient. Extra noise may have been induced in the amplification.

In this Letter, we present the first detailed characterization of the CEO frequency in a mode-locked VECSEL, showing promising results for future self-referencing stabilization. For this purpose, we implemented a characterization method of the CEO beat that does not require *f*-to-2*f* interferometry and therefore circumvents the need for a coherent octave-spanning comb spectrum that has not yet been achieved directly from the output of this laser. The information about the CEO noise and modulation response was obtained directly from the output of the oscillator, without any further spectral broadening, pulse compression or amplification. We recently showed a proof-of-principle demonstration of this method

implemented with an Er:fiber frequency comb for which the CEO beat was separately detected using an *f*-to-2*f* interferometer for cross validation [19]. The method proved to be suitable to infer both the frequency noise spectrum of the free-running CEO beat and the transfer function of f_{CEO} for a modulation of the laser pump current. Here we report on the implementation of this method for the characterization of the CEO frequency of a mode-locked VECSEL.

The investigated ultrafast laser oscillator was a prototype developed at ETH Zurich. The laser cavity had a semiconductor gain chip as folding mirror, and a SESAM and an output coupler (1% transmission) as end mirrors. It generated sub-300-fs pulses at around 1030 nm [20]. The VECSEL was pumped with up to 17 W of optical power from a commercially-available fiber-coupled 808-nm multimode pump diode. The average output power was 90 mW with a spectral width of ~4 nm. The pump diode was driven in-parallel by a low-cost constant current source and a home-built voltage-current transducer providing a fast modulation channel for the pump power. A dedicated low-pass filter was implemented between the two current sources to avoid undesirable cross-talks. A 3-dB modulation bandwidth of the pump power of around 1 MHz was therewith achievable with this home-made transducer. Fast modulation capabilities of the pump power are important for future comb self-referencing with direct control of the CEO frequency via pump current modulation. The VECSEL repetition rate $f_{rep} \approx 1.77$ GHz was phase-stabilized to a radio-frequency (RF) signal referenced to an H-maser for stable long-term operation at the required level of accuracy. This stabilization was implemented by a phase-locked loop operating at $5 \cdot f_{rep}$ (~8.85 GHz), with a feedback signal applied to a piezoelectric transducer (PZT) controlling the position of the output coupler within the VECSEL cavity.

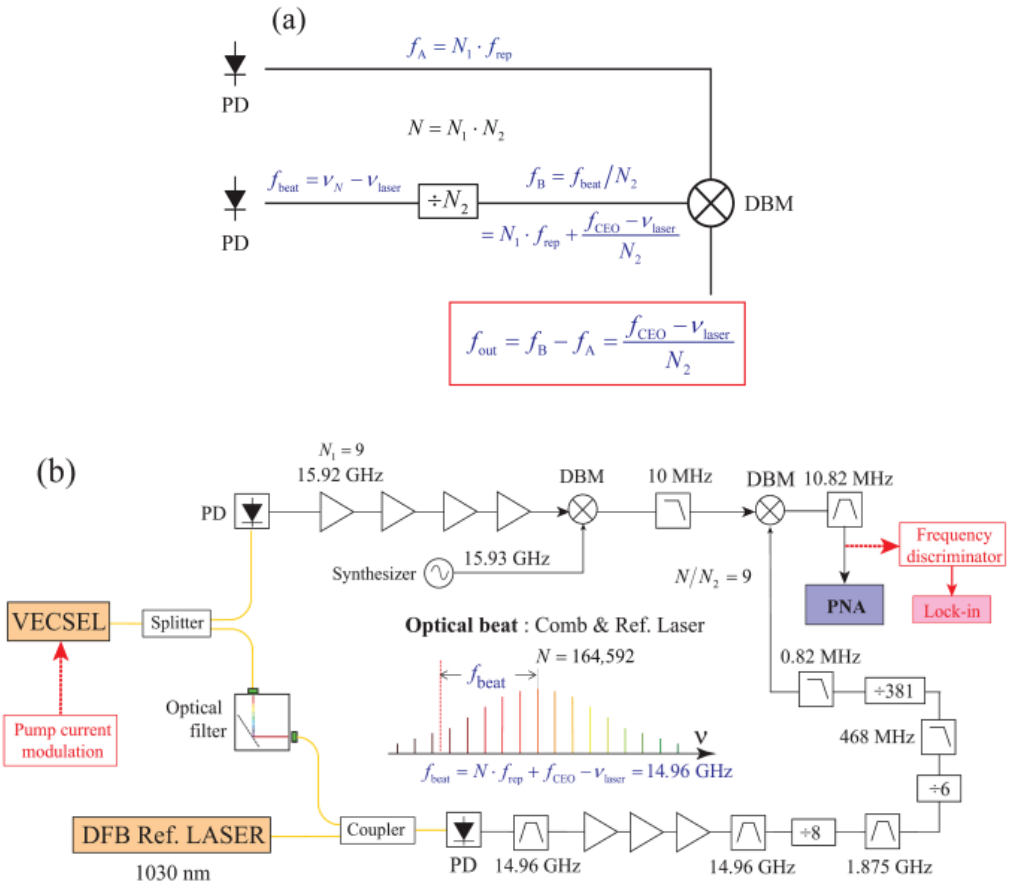

Figure 3.5: (a) Basic principle of the proposed scheme to characterize the CEO beat without directly detecting it [19]. A high harmonic N_1 of the repetition rate (upper branch, signal f_A) is mixed with the heterodyne beat with a cw laser, frequency-divided by N_2 (lower branch, signal f_B), to produce a signal f_{out} that is exempt from the contribution of f_{rep}. PD: fast photodiode; DBM: double-balanced mixer. (b) Detailed experimental scheme realized for the implementation of the method with a mode-locked VECSEL with $f_{rep} \approx 1.77$ GHz using an auxiliary DFB laser at 1030 nm. PNA: phase noise analyzer. All radio-frequency components except the narrow band-pass filters at ~15 GHz are standard off-the-shelf components. The frequency discriminator and lock-in amplifier are used for the transfer function.

The principle of the method applied to characterize the CEO beat without directly detecting it was recently presented in Ref. [19]. It requires an auxiliary continuous wave (cw) laser. Whereas a planar waveguide external-cavity laser with a very low frequency noise was used in our proof-

of-principle experiment at 1.55 µm, this type of laser is not available at the 1030-nm emission wavelength of our VECSEL. Therefore, a distributed feedback (DFB) laser (Eagleyard) with a specified linewidth <2 MHz was used in the work reported here. Its frequency noise power spectral density (PSD) has first been measured to assess its suitability for this application. This was realized by heterodyning the laser with the SC spectrum generated in a highly nonlinear fiber from a fully-stabilized Er:fiber frequency comb (Menlo FC 1500-250). The SC spectrum was spectrally filtered using a fibered tunable bandpass filter with a bandwidth of ~1 nm and amplified in a semiconductor optical amplifier (Innolume) before being combined with the auxiliary cw laser in a 90/10 fiber coupler. The resulting beat signal was bandpass filtered and its frequency noise was measured using a frequency discriminator [21] and a fast Fourier transform spectrum analyzer. The noise of the auxiliary DFB laser was the dominating contribution in this measurement, leading to the frequency noise spectrum displayed in Figure 3.6.

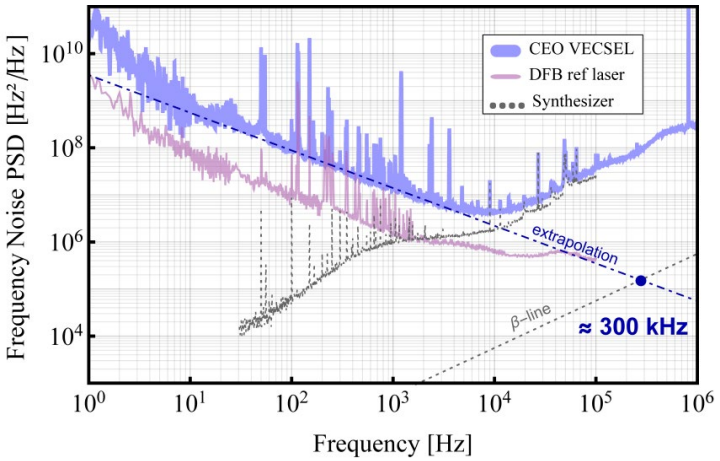

Figure 3.6: Frequency noise PSD of the free-running CEO beat of the VECSEL assessed with the proposed method (thick light blue line). The thin light purple line represents the frequency noise PSD of the free-running cw laser used in this experiment. The CEO noise at frequencies higher than ~10 kHz is limited by the noise of a synthesizer used in the experiment (dashed grey line). Therefore an estimation of the feedback bandwidth required for a future phase stabilization of f_{CEO} was assessed by extrapolating the $1/f$ noise (dashed blue line) up to its crossing point with the β-separation line [22].

The experimental setup for the characterization of f_{CEO} was implemented in a similar way as in our previous proof-of-principle demonstration. However, different RF components (filters, frequency dividers, amplifiers) were used to account for the different repetition rate and mode number N involved here. Basically, two RF signals were detected, corresponding to a harmonic $N_1 = 9$ of the repetition rate (at 15.92 GHz) and to the beat signal f_{beat} between one mode of the VECSEL (with a nominal mode number $N = N_1 \cdot N_2$) and the auxiliary laser, which was detected at a frequency of 14.96 GHz. In order to remove the contribution of the VECSEL repetition rate, these signals were processed and combined according to the general principle reported in Ref. [19] and to the detailed scheme displayed in Figure 3.5. Finally, only a frequency-divided contribution of the CEO frequency fluctuations δf_{CEO} (division by a factor $N_2 = 18{,}288$ here) occurred in the noise of the output signal $\delta f_{out} = \delta f_{CEO}/N_2$. This signal also contained the frequency noise of the cw laser (divided by the same factor N_2), but it had a negligible impact as it was significantly lower than the noise of the free-running CEO beat (as shown in Figure 3.6). Therefore, the CEO noise was retrieved by up-scaling by a factor N_2^2 the phase noise of the output signal measured with a phase noise analyzer (FSWP from Rohde & Schwarz). The assessed CEO frequency noise displayed in Figure 3.6 is not affected by the noise of the auxiliary laser (apart from some isolated peaks) and was thus correctly retrieved. In order to verify the correctness of the CEO noise measurement and to check if the considered combination of signals resulted in the expected compensation of the repetition rate noise, we also measured the sum-frequency component signal at the mixer output as discussed in Ref. [19]. This signal contains two times the noise of the repetition rate and thus shows the same noise features as the repetition rate as displayed in Figure 3.7, which enabled identifying the correct difference-frequency signal.

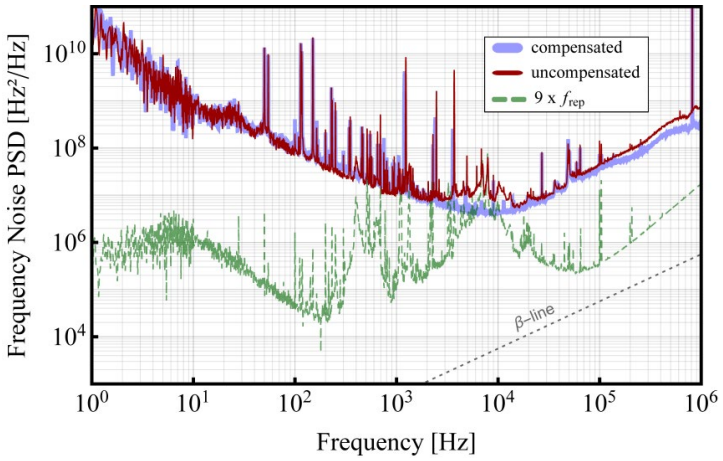

Figure 3.7: Frequency noise PSD corresponding to the up-scaled noise obtained for the two signals at the mixer output (thick light blue line: compensated signal corresponding to the frequency-difference component; thin red line: uncompensated signal corresponding to the sum-frequency component) and comparison with the 9th harmonic signal of the repetition rate (thin dashed green line).

At frequencies higher than ~10 kHz, the measured CEO noise was limited by the noise floor of the experimental setup, which resulted from an RF synthesizer used to frequency down-convert the signal of the harmonics of f_{rep}, as previously discussed [19]. Therefore, we extrapolated the $1/f$ noise of the CEO signal to higher frequencies (blue dashed line in Figure 3.6) to estimate the feedback bandwidth that would be required to achieve a tight CEO lock in a future self-referencing setup. From the crossing point of the extrapolated noise spectrum with the β-separation line [22], we assessed a full width at half maximum of the CEO beat of ~1.5 MHz (1-s observation time) and a corresponding required feedback bandwidth of ~300 kHz.

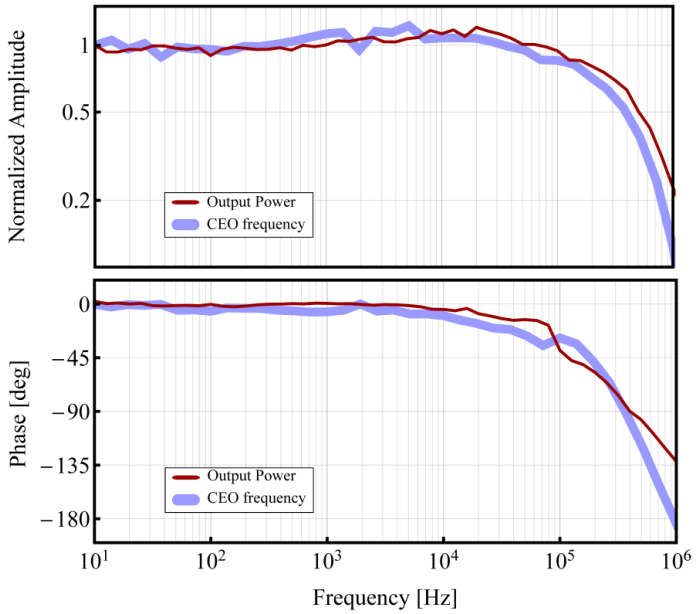

Figure 3.8: Normalized amplitude (top) and phase (bottom) of the measured transfer functions of the VECSEL CEO frequency (thick blue line) and output power (thin red line) obtained for a direct modulation of the pump current. The phase of f_{CEO} has been offset by 180° to facilitate the comparison with the phase of the output power transfer function.

To assess if such bandwidth would be achievable using a direct modulation of the pump power via the pump current, we measured the modulation response of f_{CEO}. We used the same general setup as before, but demodulated the output signal using a frequency discriminator [21] and a lock-in amplifier referenced to the pump diode modulation applied using our fast modulation electronics. Figure 3.8 shows the measured amplitude and phase of the pump current to f_{CEO} transfer function. For comparison, we also measured the transfer function of the VECSEL output power for the same pump current modulation, as it generally has a similar behavior [23], which is indeed the case here. The amplitude of the transfer functions is constant up to at least 100 kHz, resulting in a 3-dB bandwidth of ~300 kHz for f_{CEO} modulation. At this frequency, the corresponding phase shift is approximately -90°. The CEO modulation capability of this VECSEL is significantly faster than usually encountered in DPSSLs or fiber lasers, resulting from the much shorter upper state lifetime in the semiconductor

gain. The VECSEL CEO transfer function reported here is not limited by the carrier lifetime, which is much shorter, but by the cavity dynamics [23]. The fast modulation capability of the VECSEL is promising for a future self-referencing stabilization loop.

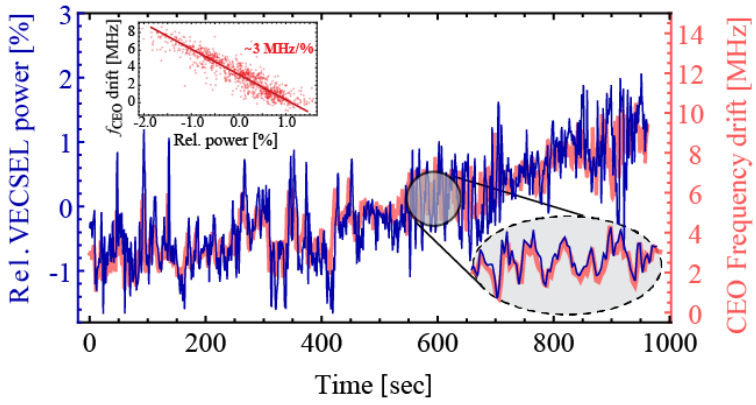

Figure 3.9: CEO frequency drift (thick light red trace) measured by heterodyning the VECSEL emission with the DFB auxiliary laser frequency-locked to an Er:fiber comb fully-stabilized to an H-maser and comparison with the VECSEL output power (thin dark blue line). The inset in the right-bottom corner displays a zoom of the traces over 70 seconds and the top-left inset shows the high correlation between the drift of f_{CEO} and the relative variations of the VECSEL output power with a slope of ~3 MHz/%.

Finally, we also measured the frequency drift of f_{CEO} by recording the beat signal between an optical frequency reference ν_{laser} and one optical mode of the VECSEL (with f_{rep} stabilized to an RF synthesizer that was referenced to an H-maser). The optical reference was made of the cw DFB laser stabilized to a line of the SC spectrum of a commercial fully-stabilized Er:fiber frequency comb referenced to the H-maser. In this scheme, the slow frequency fluctuations of the beat signal only reflect the variations of the VECSEL CEO frequency, as all other frequencies (f_{rep}, ν_{laser}) were stabilized. A slow drift of ~8 MHz was observed in 15 min. Furthermore, we measured at the same time the relative variations of the VECSEL output power. A strong correlation was observed between the variations of f_{CEO} and the VECSEL output power as shown in Figure 3.9. The intensity noise of the pump diode was likely responsible for this effect. Therefore, a feedback

loop acting on the pump diode current is expected to be highly efficient for f_{CEO} noise reduction with a large bandwidth, enabling a tight CEO lock to be reached in future self-referencing experiments.

In conclusion, we reported the first thorough analysis of the noise and modulation properties of the CEO beat in a mode-locked VECSEL. This was realized using a novel approach that we recently proposed to characterize the CEO beat without directly detecting it using standard *f*-to-2*f* interferometry. Our results show that a modulation of f_{CEO} can be achieved by direct pump current modulation with a 3-dB bandwidth of around 300 kHz, which is comparable to the feedback bandwidth needed to achieve a tight CEO lock in a future self-referencing scheme estimated from our noise measurements. These results pave the way for the first self-referencing of a mode-locked semiconductor laser that is our next target.

Funding

Nano-Tera.ch MIXSEL II (20NA21_145932); EU-FP7 ITN FACT (PITN-GA-2013-607493).

References

[1] H. R. Telle, G. Steinmeyer, A. E. Dunlop, J. Stenger, D. H. Sutter, and U. Keller, "Carrier-envelope offset phase control: A novel concept for absolute optical frequency measurement and ultrashort pulse generation," Appl. Phys. B **69**(4), 327–332 (1999).

[2] D. J. Jones, S. A. Diddams, J. K. Ranka, A. Stentz, R. S. Windeler, J. L. Hall, and S. T. Cundiff, "Carrier-Envelope Phase Control of Femtosecond Mode-Locked Lasers and Direct Optical Frequency Synthesis," Science **288**(5466), 635–639 (2000).

[3] A. Apolonski, A. Poppe, G. Tempea, C. Spielmann, T. Udem, R. Holzwarth, T. W. Hänsch, and F. Krausz, "Controlling the Phase

Evolution of Few-Cycle Light Pulses," Phys. Rev. Lett. **85**(4), 740–743 (2000).

[4] T. W. Hänsch, "Nobel Lecture: Passion for precision," Rev. Mod. Phys. **78**(4), 1297–1309 (2006).

[5] J. Ye, H. Schnatz, and L. W. Hollberg, "Optical frequency combs: from frequency metrology to optical phase control," IEEE J. Sel. Top. Quantum Electron. **9**(4), 1041–1058 (2003).

[6] S. A. Diddams, L. Hollberg, and V. Mbele, "Molecular fingerprinting with the resolved modes of a femtosecond laser frequency comb," Nature **445**(7128), 627–630 (2007).

[7] S. Schiller, "Spectrometry with frequency combs," Opt. Lett. **27**(9), 766–768 (2002).

[8] U. Keller, "Ultrafast solid-state laser oscillators: a success story for the last 20 years with no end in sight," Appl. Phys. B **100**(1), 15–28 (2010).

[9] B. R. Washburn, S. A. Diddams, N. R. Newbury, J. W. Nicholson, M. F. Yan, and C. G. Jrgensen, "Phase-locked, erbium-fiber-laser-based frequency comb in the near infrared," Opt. Lett. **29**(3), 250–252 (2004).

[10] S. Schilt, N. Bucalovic, V. Dolgovskiy, C. Schori, M. C. Stumpf, G. Di Domenico, S. Pekarek, A. E. H. Oehler, T. Südmeyer, U. Keller, and P. Thomann, "Fully stabilized optical frequency comb with sub-radian CEO phase noise from a SESAM-mode-locked 1.5-μm solid-state laser," Opt. Express **19**(24), 24171–24181 (2011).

[11] A. Klenner, S. Schilt, T. Südmeyer, and U. Keller, "Gigahertz frequency comb from a diode-pumped solid-state laser," Opt. Express **22**(25), 31008 (2014).

[12] C.-C. Lee, C. Mohr, J. Bethge, S. Suzuki, M. E. Fermann, I. Hartl, and T. R. Schibli, "Frequency comb stabilization with bandwidth beyond the limit of gain lifetime by an intracavity graphene electro-optic modulator," Opt. Lett. **37**(15), 3084–3086 (2012).

[13] M. Hoffmann, S. Schilt, and T. Südmeyer, "CEO stabilization of a femtosecond laser using a SESAM as fast opto-optical modulator," Opt. Express **21**(24), 30054 (2013).

[14] S. Koke, C. Grebing, H. Frei, A. Anderson, A. Assion, and G. Steinmeyer, "Direct frequency comb synthesis with arbitrary offset and shot-noise-limited phase noise," Nat. Photonics **4**(7), 462–465 (2010).

[15] G. Krauss, D. Fehrenbacher, D. Brida, C. Riek, A. Sell, R. Huber, and A. Leitenstorfer, "All-passive phase locking of a compact Er: fiber laser system," Opt. Lett. **36**(4), 540–542 (2011).

[16] B. R. Washburn, W. C. Swann, and N. R. Newbury, "Response dynamics of the frequency comb output from a femtosecond fiber laser," Opt. Express **13**(26), 10622–10633 (2005).

[17] B. W. Tilma, M. Mangold, C. A. Zaugg, S. M. Link, D. Waldburger, A. Klenner, A. S. Mayer, E. Gini, M. Golling, and U. Keller, "Recent advances in ultrafast semiconductor disk lasers," Light Sci. Appl. **4**(7), e310 (2015).

[18] C. A. Zaugg, A. Klenner, M. Mangold, A. S. Mayer, S. M. Link, F. Emaury, M. Golling, E. Gini, C. J. Saraceno, B. W. Tilma, and U. Keller, "Gigahertz self-referenceable frequency comb from a semiconductor disk laser," Opt. Express **22**(13), 16445–16455 (2014).

[19] P. Brochard, S. Schilt, V. J. Wittwer, and T. Südmeyer, "Characterizing the carrier-envelope offset in an optical frequency comb without traditional *f*-to-2*f* interferometry," Opt. Lett. **40**(23), 5522–5525 (2015).

[20] D. Waldburger, S. M. Link, M. Mangold, C. G. E. Alfieri, E. Gini, M. Golling, B. W. Tilma, and U. Keller, "High-power 100 fs semiconductor disk lasers," Optica **3**(8), 844–852 (2016).

[21] S. Schilt, N. Bucalovic, L. Tombez, V. Dolgovskiy, C. Schori, G. Di Domenico, M. Zaffalon, and P. Thomann, "Frequency discriminators for the characterization of narrow-spectrum heterodyne beat signals: Application to the measurement of a sub-hertz carrier-envelope-offset beat in an optical frequency comb," Rev. Sci. Instrum. **82**(12), 123116 (2011).

[22] G. Di Domenico, S. Schilt, and P. Thomann, "Simple approach to the relation between laser frequency noise and laser line shape," Appl. Opt. **49**(25), 4801–4807 (2010).

[23] F. Emaury, A. Diebold, A. Klenner, C. J. Saraceno, S. Schilt, T. Südmeyer, and U. Keller, "Frequency comb offset dynamics of SESAM mode-locked thin disk lasers," Opt. Express **23**(17), 21836 (2015).

3.3 Frequency noise characterization of a 25-GHz diode-pumped mode-locked laser with indirect carrier-envelope offset noise assessment

P. Brochard,[1] V. J. Wittwer,[1] S. Bilicki,[2] B. Resan,[3,4] K. J. Weingarten,[3] S. Schilt,[1] and T. Südmeyer[1]

[1] Laboratoire Temps-Fréquence, Université de Neuchâtel, Avenue de Bellevaux 51, CH-2000 Neuchâtel, Switzerland

[2] SYRTE, Observatoire de Paris, PSL Research University, CNRS, Sorbonne Université, LNE, Paris F-75014, France

[3] Lumentum Switzerland, Ruetistrasse 12, CH-8952 Schlieren, Switzerland

[4] School of Engineering, University of Applied Sciences and Arts Northwestern Switzerland, CH-5210 Windisch, Switzerland

We present a detailed frequency noise characterization of an ultrafast diode-pumped solid-state laser operating at 25-GHz repetition rate. The laser is based on the gain material Er:Yb:glass and operates at a wavelength of 1.55 μm. Using a beating measurement with an ultra-low-noise continuous-wave laser in combination with a dedicated electrical scheme, we measured the frequency noise properties of an optical mode of the 25-GHz laser, of its repetition rate and indirectly of its carrier-envelope offset (CEO) signal without detecting the CEO frequency by the standard approach of nonlinear interferometry. We observed a strong anti-correlation between the frequency noise of the indirect CEO signal and of the repetition rate in our laser, leading to optical modes with a linewidth below 300 kHz in the free-running laser (at 100-ms integration time), much narrower than the individual contributions of the carrier envelope offset and repetition rate. We explain this behavior by the presence of a fixed point located close to the optical carrier in the laser spectrum for the dominant noise source.

3.3.1 Introduction

Mode-locked lasers with a high repetition rate are attractive for applications in optical telecommunications, such as ultra-high speed transmission systems up to 30 Tbits/s [1], optical clocking or multi-wavelength sources [2]. With a mode spacing of 12.5 GHz, 25 GHz, 50 GHz or 100 GHz in the C or L spectral band, a mode-locked laser can act as a single light source simultaneously covering a large number of channels in dense wavelength division multiplexing (DWDM) optical telecommunications. This can advantageously replace a large number of continuous-wave singlemode distributed feedback (DFB) lasers with their associated own drive electronics and temperature control, which each acts as an optical source for a single wavelength channel only. In addition, the high frequency spacing between the modes of an optical frequency comb with a high repetition rate can be beneficial to other applications such as ultra-low-noise microwave generation [3], [4] or astronomical spectrographs calibration [5], [6]. However, a frequency comb requires the second degree of freedom of the mode-locked laser spectrum, i.e., the carrier-envelope offset (CEO) frequency f_{CEO}, to be stabilized or at least detected, which constitutes the fundamental difference between any mode-locked laser and a frequency comb [7].

Diode-pumped solid-state lasers (DPSSLs) constitute a proven technology for high repetition rate mode-locked lasers, with repetition rates up to 100 GHz achieved in fundamentally mode-locked operation [8]. They are also particularly suitable for optical frequency combs with a large mode spacing. The standard approach to detect the CEO beat based on supercontinuum spectrum generation in a non-linear fiber and *f*-to-2*f* interferometry [9] is particularly challenging with high repetition rate lasers due to their low peak power and usually long pulse duration. For this reason, the highest repetition rates for a frequency comb produced from a mode-locked laser are 10 GHz demonstrated for a self-referenced Ti:Sapphire mode-locked laser [10] and 15 GHz reported more recently for

an Yb:Y2O3 ceramic DPSSL locked to an ultra-stable laser [11]. However, this comb was not self-referenced and suffered from the frequency drift of the reference laser.

Even if not CEO-stabilized, a high repetition rate mode-locked laser can act as a regular grid of equispaced optical frequencies when its repetition rate is phase-locked to a stable radio-frequency reference source, which can be straightforwardly realized by controlling the cavity length using a piezo-electric transducer (PZT). Such stabilized laser could serve as a multi-wavelength light source for dense wavelength division multiplexing (DWDM) optical networks using multi-level quadrature-amplitude modulation (mQAM) with digital coherent receivers to address the needs for increased network capacity [12]. A critical constraint for such coherent detection systems is the phase noise of the laser source and the corresponding linewidth of the laser modes, which typically needs to be significantly smaller than 100 kHz in coherent transmission systems [13]. A naïve expectation from the stabilization of the repetition rate is that the frequency stability of the individual laser modes would be improved at the same time (i.e., their low-frequency noise would be reduced). Here, we present a study of the noise properties of a mode-locked DPSSL with 25 GHz repetition rate, notably obtained by beating the laser with a narrow-linewidth continuous-wave reference laser. We locked the repetition rate of the mode-locked laser to a stable radio-frequency reference source and show that it leads to a degradation of the phase noise of the analyzed optical line and to a corresponding increase of its linewidth. To understand this behavior, we separately characterized the phase noise of the optical line and of the repetition rate frequency of the laser, which is the controlled parameter in the considered stabilization scheme of our laser. As the optical spectrum of a mode-locked laser is fully determined by only two parameters, the mode spacing f_{rep} and the global frequency offset f_{CEO}, we furthermore implemented a dedicated scheme to characterize the noise properties of the second degree of freedom f_{CEO}, to have a complete picture.

Hence, the two characteristic frequencies defining the optical modes of the DPSSL spectrum have been separately analyzed. The measurement of the phase noise of the CEO frequency involves an electrical scheme that circumvents the standard *f*-to-2*f* interferometry method that cannot be implemented here due to the too low output power and too long pulses emitted by the laser for coherent octave-spanning supercontinuum spectrum generation. Nevertheless, we have been able to indirectly measure the frequency noise spectrum of the CEO signal without detecting f_{CEO}. This result constitutes to the best of our knowledge the highest repetition rate CEO noise measurement realized for a mode-locked laser. We observed a very similar and anti-correlated phase noise between f_{rep} and f_{CEO}, leading to a much lower phase noise of the optical mode. We explain this behavior using the elastic tape model of a frequency comb [14], [15] and the presence of a fixed point located close to the carrier frequency in the laser spectrum.

3.3.2 Experimental setup

We have used a picosecond Er:Yb:glass laser oscillator (ERGO), which is schematized Fig. 3.10. It is made of a V-shaped cavity, consisting of an output coupler with 0.5% transmission, a 1-mm thick Er:Yb-doped glass plate (QX/Er from Kigre) as gain medium, a folding high-reflectivity mirror, and a quantum-well-based semiconductor saturable absorber mirror (SESAM). The laser is based on the same design as previously described for a similar 10-GHz ERGO laser [16] and also used in a 12.5-GHz ERGO laser employed for some optical communications proof-of-principle demonstrations [1], [13]. The same components such as gain medium and SESAM are used, only the folding mirror and output coupler have a different radius of curvature that is shorter than 2 mm resulting into a compact standing-wave cavity with an optical length of only 6 mm between its end mirrors. All optics are glued on stainless steel parts. The laser is fundamentally mode-locked, meaning that a single pulse circulates within

the cavity with 25-GHz pulse repetition rate of the output beam. The SESAM is mounted on a PZT for fine cavity length adjustment and stabilization. The laser is pumped by a single-mode fiber-pigtailed diode, emitting up to 600 mW at 976 nm (model 300076 from EM4), but only a fraction of up to ~300 mW of pump power was used here. This is the same type of pump diode used at a similar power as in the 10-GHz ERGO laser reported in [16].The pump beam is coupled into the laser cavity through a dichroic mirror placed in the output beam, after the output coupler (Fig. 3.10). The laser generates pulses with a duration of ~3 ps at a center wavelength of 1547 nm. Passive fundamental SESAM mode-locking enables ultralow pulse timing jitter and optical pulse-to-pulse phase coherence, which is essential for high data rate communication systems with coherent modulation formats [1]. As the 25-GHz ERGO laser is very similar to the previously reported versions with 10-GHz and 12.5-GHz repetition rates [1], [13], [16], which are built on the same mechanical platform and pumped by the same type of laser diode, similar noise properties are expected, just scaled up by the higher repetition rate. However, these noise properties have not been studied in detail before. In a basic heterodyne beat measurement made with a narrow-linewidth continuous-wave (CW) laser, a linewidth of an optical mode of the 12.5 GHz ERGO laser was claimed to be at the kHz level for an observation time of a few ms only [13]. However, this result was obtained by fitting the measured beat signal by a Lorentzian lineshape in a logarithmic scale, so that the 3-dB linewidth was not properly assessed and strongly underestimated in our opinion. Here, we present a detailed analysis of the noise properties of the 25-GHz mode-locked laser obtained by measuring the complete frequency noise power spectral density (FN-PSD) of an optical line, as well as of the individual contributions of the repetition rate and CEO frequency down to a Fourier frequency of 1 Hz. The FN-PSD is the most complete quantity to characterize the noise properties of a signal, and contains much more information than the power spectrum [17].

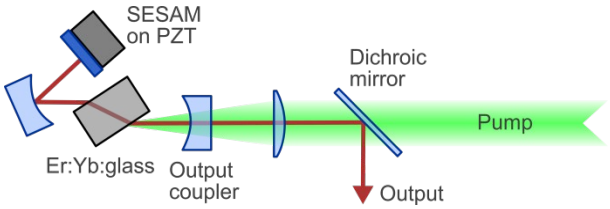

Fig. 3.10: Layout of the 25-GHz ERGO laser. The gain medium is an Er:Yb-doped glass plate and a quantum well SESAM is placed at the end of the cavity, mounted on a PZT for cavity length control.

The experimental setup shown in Fig. 3.11 was implemented to beat one mode of the laser with an ultra-low-noise continuous-wave reference laser to measure the frequency noise of one of its individual modes. Additionally, this setup enabled us to indirectly assess the frequency noise of the CEO signal of the ERGO laser without directly detecting the CEO beat by the traditional method of *f*-to-2*f* interferometry. This was not possible with this laser as the required octave-spanning supercontinuum spectrum cannot be achieved with the present laser power and pulse duration. The general principle of the implemented approach was previously presented and validated using a self-referenced Er:fiber frequency comb [18]. We recently applied it to perform the first detailed investigation of the noise properties of the CEO frequency in a mode-locked semiconductor laser [19]. Here we have applied it in a similar way to the 25-GHz ERGO laser. In brief, the method consists of suppressing the contribution of the repetition rate in the frequency noise of an optical line $\nu_N = (N \cdot f_{rep} + f_{CEO})$ of the mode-locked laser, measured from the heterodyne beat with a narrow-linewidth laser. The repetition rate suppression was achieved using an electrical scheme (see Fig. 3.11) and not optically as with *f*-to-2*f* interferometry. As a result, the frequency noise originating from f_{CEO} is the dominant noise contribution in the analyzed signal, which could be measured even if the CEO frequency itself remained unknown.

More specifically, we first detected the heterodyne beat signal $f_{beat} = \nu_{laser} - N \cdot f_{rep} - f_{CEO}$ between a CW reference laser of frequency ν_{laser} and one mode ν_N of the 25-GHz ERGO laser at ~1547 nm, corresponding to a mode number $N \approx 7{,}760$. The reference laser was an external cavity diode laser (ECDL) stabilized to an ultra-low thermal expansion (ULE) optical cavity using the Pound-Drever-Hall locking technique [20]. It has a negligible frequency noise (with a corresponding linewidth in a range of a few Hz) compared to the CEO signal to be analyzed. The 10 GHz heterodyne beat signal f_{beat} was detected using a fast photodiode (Discovery Semiconductors DSC40S, PD-1 in Fig. 3.11). It was subsequently band-pass filtered, amplified and frequency-divided by a large integer number $N_{div} = 7{,}620$ using three successive off-the-shelf frequency dividers with a division factor of 2, 10 and 381, respectively. The resulting frequency-divided signal $f_A = f_{beat} / N_{div} \approx 1.3$ MHz contained the frequency fluctuations Δf_{CEO} of the unknown CEO signal divided by the large number N_{div}, plus the frequency fluctuations Δf_{rep} of the repetition rate scaled by the factor $(N/ N_{div}) \approx 1$, i.e., $\Delta f_A = (N/ N_{div}) \cdot \Delta f_{rep} + \Delta f_{CEO} / N_{div}$. In this expression, the frequency fluctuations $\Delta\nu_{laser}$ of the reference laser have been omitted as they are negligible compared to the noise of the CEO signal. The noise of the repetition rate was removed by mixing the frequency-divided beat signal f_A with the repetition rate f_{rep} separately detected using another fast photodiode (New-Focus 1014-IR, PD-2 in Fig. 3.11). A perfect cancellation of the noise of f_{rep} was not achieved as the required condition $N_{div} = N$ was not exactly fulfilled in the setup. However, the residual noise contribution of f_{rep} was negligible as $N/ N_{div} \approx 1$. Due to the large frequency difference occurring between the two signals $f_A \approx 1.3$ MHz and $f_{rep} = 24.899$ GHz, the repetition rate was first frequency down-converted using a frequency synthesizer (Agilent E8257D, Synth-1 in Fig. 3.11) tuned at $f_{synth} \approx 24.889$ GHz, prior to be mixed with the frequency-divided beat signal f_A in order to make possible the filtering of the proper signal at the mixer output. Alternately, a single-sideband mixer could be used to circumvent the use of Synth-1. The resulting signal

fout = $f_A + (f_{rep} - f_{synth}) \approx (\nu_{laser} - f_{CEO})/ N_{div} - f_{synth} \approx 11.3$ MHz comprised the frequency noise of the free-running CEO signal, scaled down by the large number N_{div}, i.e., $\Delta fout \approx \Delta f_{CEO} / N_{div}$. This signal was analyzed using a phase noise analyzer (Rohde & Schwarz FSWP26).

To stabilize the repetition rate at ~25 GHz, the down-converted repetition rate signal ($f_{rep} - f_{synth}$) was phase-locked to a 10 MHz signal (Agilent 33250A, Synth-2 in Fig. 3.11) by applying feedback to the PZT holding the SESAM in the laser cavity. For this stabilization, both synthesizers Synth-1 and Synth-2 (at 24.899 GHz and 10 MHz, respectively) were referenced to an H-maser to ensure their long-term frequency stability.

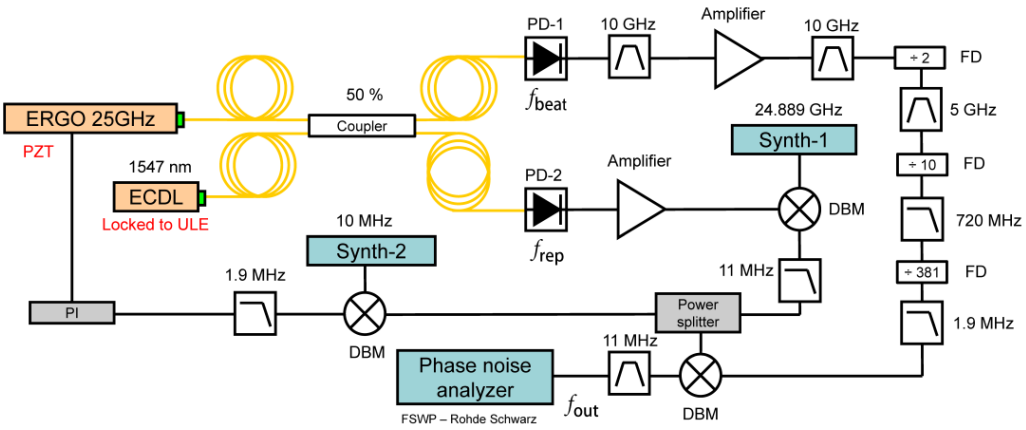

Fig. 3.11: Overall scheme of the experimental setup implemented to measure the frequency noise of the unknown free-running CEO signal of the 25-GHz ERGO laser and to lock its repetition rate to an external frequency reference. The CEO frequency noise is indirectly measured by separately detecting the heterodyne beat between one optical line of the ERGO laser and a narrow-linewidth external cavity diode laser (ECDL) at 1547 nm, filtered and frequency-divided (FD) by a large number N_{div} = 7,620 (upper branch of the scheme) and the repetition rate f_{rep}, down-converted to a low frequency of 10 MHz (lower branch of the scheme). The two signals are then combined (mixed) to remove the noise contribution of f_{rep}, such that the resulting signal f_{out} is representative of the noise of f_{CEO}. The down-converted repetition rate signal is also used for phase stabilization using a proportional-integral (PI) servo-controller and a feedback signal applied to a PZT in the laser cavity (bottom part of the scheme).

3.3.3 Experimental results

The FN-PSD measured for an optical mode ν_N of the free-running ERGO laser (from the beat signal with the narrow linewidth CW laser) is displayed in Fig. 3.12. For comparison, the frequency noise spectra separately measured for the repetition rate f_{rep} and indirectly assessed for the unknown CEO signal using our experimental scheme are also plotted on the same graph. A very similar noise spectrum is observed for the indirect CEO signal and for the repetition rate up-scaled to the optical frequency (i.e., $N \cdot f_{rep}$), whereas the noise of the optical line is significantly lower. This indicates that the fluctuations of f_{rep} and f_{CEO} are anti-correlated and partially compensate each other in the optical line. This behavior indicates the existence of a fixed point [21], [22] in the vicinity of the optical carrier in the spectrum of our laser according to the elastic tape model of the frequency comb [14], [15]. This fixed point results from the dominant noise source in our laser, which is believed to be the amplitude noise of the pump laser. It has been previously shown that pump noise leads to a fixed point located at the carrier frequency in diode-pumped frequency combs [21] and we recently observed that the pump noise was also the main contribution in the frequency noise of the CEO beat in a 1-GHz DPSSL frequency comb [29].

However, the noise of an optical line of the comb was dominated in this case by mechanical noise in the laser cavity, which strongly affected the repetition rate. At Fourier frequencies higher than ~30 kHz, the measured CEO FN-PSD is limited by the experimental noise floor arising from the synthesizer used to frequency down-convert the repetition rate signal (Synth 1 in the setup of Fig. 3.11). However, from the very similar noise observed at lower frequencies for $N \cdot f_{rep}$ and f_{CEO} and its interpretation in terms of the laser fixed point, one can also expect a comparable correspondence at high frequency. Therefore, one can assume the presence of the same white frequency noise plateau in the FN-PSD of f_{CEO} as for $N \cdot f_{rep}$, at a level of $\sim 2 \cdot 10^6$ Hz²/Hz. This assumption is justified by the

flattening of the indirect CEO signal FN-PSD observed in the range of 10 to 30 kHz compared to its regular $1/f$ behavior occurring at lower frequencies. Furthermore, the FN-PSD of the optical beat is much lower than the measured noise of $N \cdot f_{rep}$ in this frequency range, which shows that here also f_{CEO} and $N \cdot f_{rep}$ have a similar noise level and are anti correlated.

By considering the same white frequency noise as for $N \cdot f_{rep}$, a CEO linewidth of ~5 MHz is obtained at an integration time of 100 ms using the approximation of the β-separation line [23]. This value results to a large extent from the high white FN PSD of f_{CEO} at Fourier frequencies above ~30 kHz. This high white frequency noise is believed to result from the low optical power of the laser (~4 mW output power), leading to high quantum noise. Using typical parameters for our laser (0.5% output coupler, ~0.5% parasitic losses leading to ~1% gain per round trip, ~3-ps pulse duration), the quantum noise level estimated from the theoretical formula introduced by Schlatter and co-workers [24] is on the same order of magnitude as the observed white noise level. However, this estimation is fairly imprecise due to the poor knowledge of some of the relevant laser parameters for this calculation. In contrast, the resulting linewidth estimated for the optical mode $\nu_N = (N \cdot f_{rep} + f_{CEO})$ is only ~270 kHz at 100-ms integration time, which is indeed significantly narrower than the estimated CEO linewidth of ~5 MHz. This is also much smaller than the value of ~10 MHz that would result from a completely uncorrelated noise of f_{CEO} and f_{rep}. The noise observed at Fourier frequencies higher than 20 kHz in the FN-PSD of the optical beat note has not been considered in the linewidth calculation, as it mainly arises from the CW laser locked to the cavity (especially its servo bump at ~250 kHz) and from other RF components used in the measurement scheme, therefore it is not representative of the actual laser noise. The noise peak occurring at ~14 kHz in the FN-PSD of f_{rep}, but not of f_{CEO}, does not originate directly from the mode-locked laser. We discovered afterwards that it arose from a parasitic noise peak occurring in the servo-controller used in the repetition rate stabilization loop. This technical noise

peak was present even when f_{rep} was not stabilized, but with the PZT connected to the servo-controller. This technical noise peak was amplified in the optical beat as there is no compensation by the CEO signal. However, its contribution to the calculated linewidth of the optical line is small (it contributes only for 10 kHz in the linewidth calculate at 100 ms integration time). The degree of correlation between the frequency noise of $N \cdot f_{rep}$ and f_{CEO} was assessed from our measurements to further confirm our previous statement about the laser fixed point. It was obtained by calculating the sum of the complex coherence Γ_Δ between the frequency variations of the indirect CEO signal and repetition rate in the free-running ERGO laser from the measured FN PSD of ν_N, f_{rep} and f_{CEO} following the approach presented by Dolgovskiy and co-workers [25]. The calculated value of Γ_Δ shown in Fig. 3.12 (b) is close to -2 in the entire spectral range of 10 Hz to >10 kHz, which demonstrates a strong anti-correlation of the frequency noise of $N \cdot f_{rep}$ and f_{CEO}. This outcome, combined with the similar amplitude of the FN-PSD separately measured for f_{rep} and indirectly for f_{CEO}, confirms the existence of a fixed point in the spectrum of our laser. This explains the lower observed frequency noise of the optical mode of the ERGO laser compared to the individual noise contributions of $N \cdot f_{rep}$ and f_{CEO}. The Γ_Δ value matches -2 in the frequency range of 1 kHz to 10 kHz, whereas it is somehow smaller (in absolute value) at lower Fourier frequencies. This indicates that there is in fact not a true fixed point in the spectrum of our laser as generally considered by the simplified comb elastic tape model [14], [15]. Instead, the fixed point varies with the considered noise frequency as previously observed in an Er:fiber comb and described in details in [25]. This is the reason why the FN-PSD of the optical mode is much lower than the individual noise of f_{rep} or f_{CEO} in the frequency range of 1 kHz to 10 kHz (by two orders of magnitude), whereas the difference is reduced at lower frequency (only one order of magnitude at f = 100 Hz) despite the similar amplitude of the frequency noise of f_{rep} and f_{CEO}. This may indicate that another noise source affects the laser at low Fourier frequencies, and has a

different impact on f_{CEO} and f_{rep} (in other words it corresponds to a different fixed point).

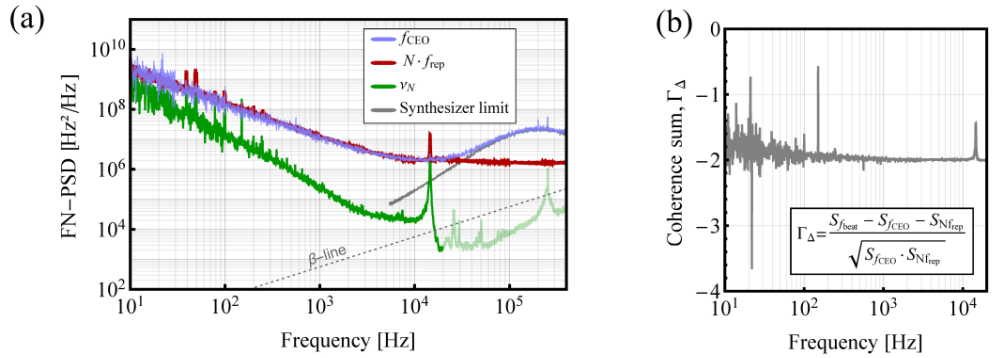

Fig. 3.12: (a) Frequency noise power spectral density (FN-PSD) measured for an optical mode ν_N (green), in comparison to the laser repetition rate scaled to the optical frequency ($N f_{rep}$, red) and indirectly assessed for the CEO signal (light blue). At high Fourier frequency, the noise spectrum of f_{CEO} is limited by the 25-GHz synthesizer used for frequency down-conversion (grey curve), whereas the noise spectrum of the comb line is limited by the reference CW laser and some RF components used in the setup (displayed by the light green part of the curve). The noise peak at ~14 kHz visible in the spectra of $N f_{rep}$ and ν_N arises from a spurious noise peak present in the output signal of the PID controller that was connected to the laser cavity PZT. (b) Frequency dependence of the sum of the complex coherences Γ_Δ between the frequency variations of f_{CEO} and f_{rep} in the free-running ERGO laser.

We stabilized the repetition rate of our laser to a reference signal from a synthesizer as schematized in Fig. 3.11 and we measured the resulting frequency noise spectra of f_{rep}, f_{CEO} and of the optical line ν_N in a similar way as for the free-running laser. Results obtained with the locked repetition rate are displayed in Fig. 3.13(a) and a comparison between the free-running and stabilized cases is separately shown in Fig. 3.13(b-d) for f_{rep}, the indirect CEO signal and the optical line ν_N. One observes that the repetition rate is properly stabilized with a feedback bandwidth of around 1.5 kHz, assessed

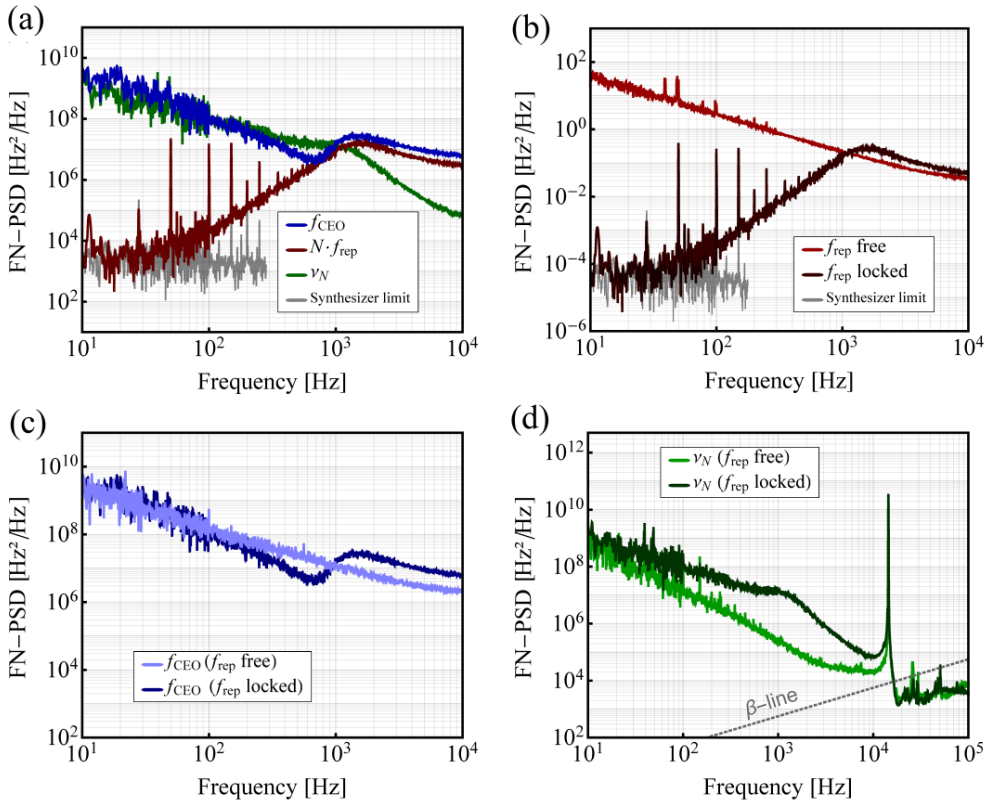

Fig. 3.13: (a) Comparison of the FN-PSD of the repetition rate up-scaled to the optical frequency ($N f_{rep}$, red), of the indirect CEO signal (blue) and of the optical line ν_N (green) of the ERGO laser measured when the repetition rate is locked. The low-frequency noise floor resulting from the ~25-GHz synthesizer used as a reference in the stabilization of f_{rep} is also displayed (gray), showing that it limits the FN-PSD of the repetition rate at frequencies below ~30 Hz. (b-d) FN-PSD of the repetition rate (b), of the indirect CEO signal (c) and of the optical line (d) of the ERGO laser in locked (darker colors) and free-running (lighter colors) conditions. The strong noise peak at ~14 kHz visible in the spectra of the optical line arises from a spurious noise peak present in the output signal of the PID controller and is not inherent to the laser itself.

from the servo bump in its FN-PSD [see Fig. 3.13(b)]. The achieved FN-PSD coincides with the noise of the reference synthesizer at Fourier frequencies below ~50 Hz. However, the frequency noise of the optical line ν_N is significantly degraded by the repetition rate stabilization, while the frequency noise of f_{CEO} is not reduced by the feedback loop, despite its strong negative correlation with the noise of f_{rep}. The reason is that the effect

of the PZT on the laser operation corresponds to a different fixed point than the principal noise source that affects the free-running laser, which is believed to be the amplitude noise of the pump diode.

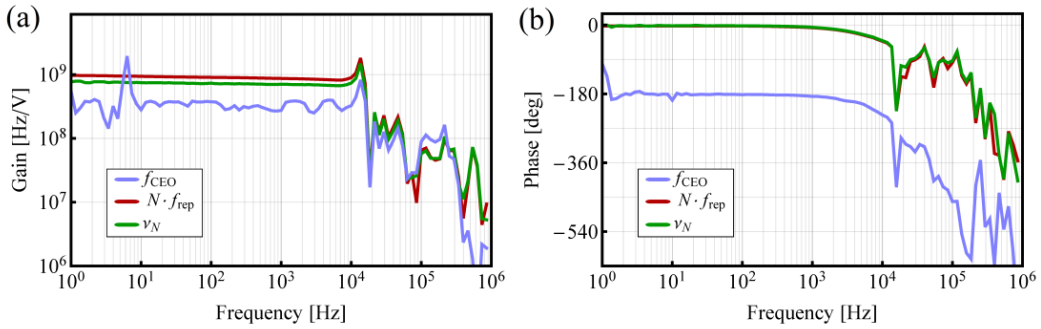

Fig. 3.14: Transfer functions in amplitude (a) and phase (b) of $N f_{rep}$ (red), f_{CEO} (light blue) and ν_N (optical line, green) for a modulation of the PZT voltage.

To further investigate the noise behavior observed in Fig. 3.13 for the stabilized repetition rate, we measured the transfer function of ν_N, f_{rep} and f_{CEO} for a modulation of the cavity length. This was realized by modulating the PZT voltage with a sine waveform and by demodulating the corresponding signals (optical beat, repetition rate or indirect CEO signal) using a frequency discriminator [26] and a lock-in amplifier. The indirect CEO signal was obtained using the scheme of Fig. 3.11. The different transfer functions, displayed in Fig. 3.14 present the same behavior, both in amplitude and in phase, with a constant amplitude response up to ~10 kHz. A phase shift of 180° is observed between the transfer functions of f_{rep} and f_{CEO}, which indicates that a change of the cavity length produces an opposite effect on f_{rep} and f_{CEO}. The PZT produces a significant change of f_{CEO}, which is a factor ~3,000 larger than the corresponding tuning coefficient of f_{rep}. This corresponds to a fixed point $N_{fix} \approx 3{,}000$ or to a fixed frequency $N_{fix} \cdot f_{rep} \approx 75$ THz for the cavity length change, which is substantially lower than the fixed frequency resulting from the noise in the free-running laser, located close to the optical carrier of ~194 THz. The fixed frequency for a change of the cavity length is two orders of magnitude higher than values

reported in a 250-MHz Er:fiber frequency comb [25] and in another Er:Yb:glass DPSSL comb with 75-MHz repetition rate [27], both in the same wavelength range of 1.56 μm. This factor is of the same order of magnitude as the ratio of the considered repetition rates.

The repetition rate has a slightly more important contribution (by a factor ~2.7) than f_{CEO} to the modulation of the optical line ν_N resulting from a change of the cavity length, as a result of its scaling by the mode number $N \approx 7{,}760$. From the theoretical model of coupled stabilization loops in a frequency comb presented by Dolgovskiy and co-workers [25], the impact of the repetition rate stabilization loop on the CEO signal is given by the following expression if a fully anti-correlated noise of similar amplitude is considered between f_{CEO} and $N \cdot f_{rep}$ (i.e., $\Delta f_{CEO} \approx -N \cdot \Delta f_{rep}$):

$$\delta f_{CEO} = \Delta f_{CEO} \frac{1+\left[1-(C_{f_{CEO}}/C_{f_{rep}})/N\right]H}{1+H} \tag{20}$$

where Δf_{CEO} and δf_{CEO} represent the frequency fluctuations of f_{CEO} with the repetition rate stabilization loop open and closed, respectively, $H(f)$ is the total open loop transfer function of the repetition rate stabilization, while $C_{f_{CEO}}$ and $C_{f_{rep}}$ are the transfer functions of f_{CEO} and f_{rep} for a modulation of the PZT shown in Fig. 3.14. All transfer functions in Eq. (20) are complex numbers that incorporate both the amplitude and phase information.

The stabilization loop of f_{rep} might have a significant effect on f_{CEO} in our laser only in the case where $C_{f_{CEO}}/C_{f_{rep}} \approx N$, i.e., if the ratio of the transfer functions of f_{CEO} and f_{rep} $(C_{f_{CEO}}/C_{f_{rep}})$ was approximately equal to the ratio of the free-running frequency fluctuations of f_{CEO} and f_{rep} (i.e., if $\Delta f_{CEO}/\Delta f_{rep} \approx -N$). In other words, the fixed points corresponding to the effect of the PZT and to the dominant noise source in the free-running laser should coincide. In the present case, $(C_{f_{CEO}}/C_{f_{rep}})/N \approx 0.3$, so that the FN-PSD of f_{CEO} is reduced in the best case by a factor of $(1\text{-}0.3)^{-2} \approx 2$ within the

repetition rate loop bandwidth (i.e., for $|H| >> 1$), which is too small to be visible on the noise spectrum of f_{CEO} displayed in Fig. 3.13(c).

The effect of the repetition rate stabilization on the optical line at ν_N is even more detrimental than for f_{CEO} and its FN-PSD is significantly degraded when the repetition rate is stabilized. Whereas the fluctuations of $N \cdot f_{rep}$ and f_{CEO} did compensate each other to a large extent in the noise of the optical line ν_N in the free-running laser (as ν_N is located close to the fixed point), this situation no longer stands when the repetition rate is locked. The noise of f_{rep} is strongly reduced by the stabilization loop, while f_{CEO} is not affected. Therefore, the FN-PSD of the optical line mainly corresponds to the noise of f_{CEO} when f_{rep} is stabilized (within the loop bandwidth) and is thus higher than in the free-running case. Beyond the loop bandwidth, the frequency noise of the optical mode is still enhanced in the frequency range between ~1 kHz and ~10 kHz in comparison to the unstabilized case. This is believed to result from a slight difference in the noise amplitude of f_{CEO} and $N \cdot f_{rep}$ and from their partially uncorrelated part, which are both introduced by the loop. The parasitic noise peak at ~14-kHz that is coupled onto f_{rep} and ν_N by the servo-controller is strongly enhanced when the repetition rate loop is closed. As this peak arises from a spurious technical noise of the servo-controller and is not inherent to the laser itself, it is not taken into account in the estimation of the optical mode linewidth. Therefore, the linewidth of the optical line obtained by integrating the FN-PSD between 10 Hz and 10 kHz (i.e., without considering the 14-kHz excess noise peak) amounts to ~600 kHz, which is slightly more than a factor 2 broader than the free-running linewidth.

3.3.4 Conclusion

We have presented a detailed analysis of the frequency noise of a 25-GHz ERGO DPSSL, including an indirect assessment of the frequency noise of the CEO signal. This signal was indirectly obtained using an electrical scheme that does not require the detection of the CEO beat using a nonlinear interferometry scheme (such as *f*-to-2*f* or 2*f* to-3*f* [28]). Instead, we assessed the frequency noise of f_{CEO} using an appropriate combination of electrical signals made of the laser repetition rate and of a frequency-divided heterodyne beat with a narrow linewidth laser. A relatively high frequency noise of the CEO signal was estimated from these measurements. The regular $1/f$ noise observed at low frequency is higher by only a factor ~10 compared to a 1-GHz DPSSL at 1 μm that we recently fully stabilized with CEO self-referencing [29], which appears relatively moderate owing to the 25-fold higher repetition rate of the ERGO laser. However, the white frequency noise plateau occurring at Fourier frequencies above 10 kHz has a significant contribution to the large CEO linewidth of ~5 MHz (at 100 ms integration time) assessed from its extrapolated frequency noise.

Despite the frequency noise assessed for the CEO signal, the $1/f$ noise of an optical mode of the laser was lower by at least 1-2 orders of magnitude, leading to a much narrower linewidth < 300 kHz at the same integration time of 100 ms. The reason behind this observation is a partial compensation of the noise of $N \cdot f_{rep}$ and f_{CEO} in the optical mode of the laser that arises from their similar amplitude and strong anti-correlation, leading to a fixed point in the spectrum of the laser that is located in the vicinity of the optical carrier. Amplitude noise of the pump diode is believed to be the dominant noise source responsible for this behavior. The noise compensation no longer holds when the repetition rate is stabilized by active feedback to the cavity length, which strongly reduces the fluctuations of f_{rep} but lets the noise of f_{CEO} almost unchanged within the locking bandwidth. Therefore, the frequency noise and linewidth of an optical mode of the laser are degraded when f_{rep} is stabilized. This degradation is not related to the

quality of the stabilization of f_{rep}, but is a direct consequence of the different fixed points corresponding to the major noise source in the free-running laser and to the PZT actuator used for the stabilization, as shown by our detailed noise analysis. The laser performance, i.e., the optical linewidth, may be improved when the repetition rate is stabilized by additionally phase-locking one mode of the laser to an optical reference. The optical reference can be either a free-running low frequency noise laser, such as a planar-waveguide external cavity laser [30] with a linewidth in the range of a few kilohertz, or a cavity-stabilized laser with a narrower linewidth. In order to faithfully transfer the noise properties of the optical reference to the optical modes of the ERGO laser, i.e., to achieve a tight phase-lock, a feedback bandwidth of less than 50 kHz is estimated to be sufficient from the crossing-point of the FN-PSD of the optical line ν_N with the β separation line [23]. If a modulation of the current of the ERGO laser pump diode was not fast enough to achieve such bandwidth as a result of the laser cavity dynamics, a faster stabilization could be achieved using a feedforward method using an acousto-optic modulator in the laser output beam [11]. In this a way, a multi-wavelength laser source with narrow-linewidth optical modes compatible with the requirements of 16-ary quadrature amplitude modulation (16-QAM) coherent optical telecommunication systems can be obtained [13].

Acknowledgments

We acknowledge funding by the Swiss Commission for Technology and Innovation (CTI) (project 17137.1 PFNM-NM). The ultra-stable laser and experimental scheme used to characterize the comb optical line were developed in the frame of the Marie-Curie International Training Network project FACT (Future Atomic Clock Technologies) of the European Union's Seventh Framework Programme for research, technological development and demonstration, under the grant agreement No PITN-GA-2013-607493.

References

[1] D. Hillerkuss et al., "26 Tbit s-1 line-rate super-channel transmission utilizing all-optical fast Fourier transform processing," Nat. Photonics, vol. 5, no. 6, pp. 364–371, Jun. 2011.

[2] P. Bakopoulos et al., "Multi-Wavelength Laser Source for Dense Wavelength Division Multiplexing Networks," in Optical Fiber Communication Conference and Exposition and The National Fiber Optic Engineers Conference (2007), 2007, p. OWJ2.

[3] T. M. Fortier et al., "Generation of ultrastable microwaves via optical frequency division," Nat. Photonics, vol. 5, no. 7, pp. 425–429, Jun. 2011.

[4] X. Xie et al., "Photonic microwave signals with zeptosecond-level absolute timing noise," Nat. Photonics, vol. 11, no. 1, pp. 44–47, Jan. 2017.

[5] C.-H. Li et al., "A laser frequency comb that enables radial velocity measurements with a precision of 1 cm s-1," Nature, vol. 452, no. 7187, pp. 610–612, Apr. 2008.

[6] T. Steinmetz et al., "Laser Frequency Combs for Astronomical Observations," Science, vol. 321, no. 5894, pp. 1335–1337, Sep. 2008.

[7] S. A. Diddams, "The evolving optical frequency comb [Invited]," J. Opt. Soc. Am. B, vol. 27, no. 11, pp. B51–B62, 2010.

[8] A. E. H. Oehler, T. Südmeyer, K. J. Weingarten, and U. Keller, "100 GHz passively mode-locked Er:Yb:glass laser at 1.5 μm with 1.6-ps pulses," Opt. Express, vol. 16, no. 26, pp. 21930–21935, Dec. 2008.

[9] H. R. Telle, G. Steinmeyer, A. E. Dunlop, J. Stenger, D. H. Sutter, and U. Keller, "Carrier-envelope offset phase control: A novel concept for absolute optical frequency measurement and ultrashort pulse generation," Appl. Phys. B, vol. 69, no. 4, pp. 327–332, 1999.

[10] A. Bartels, D. Heinecke, and S. A. Diddams, "10-GHz Self-Referenced Optical Frequency Comb," Science, vol. 326, no. 5953, p. 681, Oct. 2009.

[11] M. Endo, I. Ito, and Y. Kobayashi, "Direct 15-GHz mode-spacing optical frequency comb with a Kerr-lens mode-locked Yb:Y_2O_3 ceramic laser," Opt. Express, vol. 23, no. 2, pp. 1276–1282, Jan. 2015.

[12] T. N. Huynh, F. Smyth, L. Nguyen, and L. P. Barry, "Effects of phase noise of monolithic tunable laser on coherent communication systems," Opt. Express, vol. 20, no. 26, pp. B244–B249, Dec. 2012.

[13] D. Hillerkuss et al., "High-Quality Optical Frequency Comb by Spectral Slicing of Spectra Broadened by SPM," IEEE Photonics J., vol. 5, no. 5, p. 7201011, Oct. 2013.

[14] H. R. Telle, B. Lipphardt, and J. Stenger, "Kerr-lens, mode-locked lasers as transfer oscillators for optical frequency measurements," Appl. Phys. B Lasers Opt., vol. 74, no. 1, pp. 1–6, Jan. 2002.

[15] R. Paschotta, A. Schlatter, S. C. Zeller, H. R. Telle, and U. Keller, "Optical phase noise and carrier-envelope offset noise of mode-locked lasers," Appl. Phys. B, vol. 82, no. 2, pp. 265–273, Feb. 2006.

[16] B. Resan et al., "10 GHz pulse repetition rate Er:Yb:glass laser mode-locked with quantum dot semiconductor saturable absorber mirror," Appl. Opt., vol. 55, no. 14, pp. 3776–3780, May 2016.

[17] P. Brochard, T. Sudmeyer, and S. Schilt, "Power spectrum computation for an arbitrary phase noise using Middleton's convolution series: implementation guideline and experimental illustration," IEEE Trans. Ultrason. Ferroelectr. Freq. Control, vol. 64, pp. 1766–1775, 2017.

[18] P. Brochard, S. Schilt, V. J. Wittwer, and T. Südmeyer, "Characterizing the carrier-envelope offset in an optical frequency

comb without traditional f-to-2f interferometry," Opt. Lett., vol. 40, no. 23, pp. 5522–5525, Dec. 2015.

[19] P. Brochard et al., "First investigation of the noise and modulation properties of the carrier-envelope offset in a mode-locked semiconductor laser," Opt. Lett., vol. 41, no. 14, pp. 3165–3168, Jul. 2016.

[20] R. W. P. Drever et al., "Laser phase and frequency stabilization using an optical resonator," Appl. Phys. B, vol. 31, no. 2, pp. 97–105, 1983.

[21] N. R. Newbury and W. C. Swann, "Low-noise fiber-laser frequency combs," J. Opt. Soc. Am. B, vol. 24, no. 8, pp. 1756–1770, 2007.

[22] D. R. Walker, T. Udem, C. Gohle, B. Stein, and T. W. Hänsch, "Frequency dependence of the fixed point in a fluctuating frequency comb," Appl. Phys. B, vol. 89, no. 4, pp. 535–538, Dec. 2007.

[23] G. Di Domenico, S. Schilt, and P. Thomann, "Simple approach to the relation between laser frequency noise and laser line shape," Appl. Opt., vol. 49, no. 25, pp. 4801–4807, 2010.

[24] A. Schlatter et al., "Nearly quantum-noise-limited timing jitter from miniature Er:Yb:glass lasers," Opt. Lett., vol. 30, no. 12, pp. 1536–1538, Jun. 2005.

[25] V. Dolgovskiy, N. Bucalovic, P. Thomann, C. Schori, G. Di Domenico, and S. Schilt, "Cross-influence between the two servo loops of a fully stabilized Er: fiber optical frequency comb," J. Opt. Soc. Am. B, vol. 29, no. 10, pp. 2944–2957, 2012.

[26] S. Schilt et al., "Frequency discriminators for the characterization of narrow-spectrum heterodyne beat signals: Application to the measurement of a sub-hertz carrier-envelope-offset beat in an

optical frequency comb," Rev. Sci. Instrum., vol. 82, no. 12, p. 123116, 2011.

[27] S. Schilt et al., "Noise properties of an optical frequency comb from a SESAM-mode-locked 1.5-μm solid-state laser stabilized to the 10−13 level," Appl. Phys. B, vol. 109, no. 3, pp. 391–402, Nov. 2012.

[28] C. R. Locke, E. N. Ivanov, P. S. Light, F. Benabid, and A. N. Luiten, "Frequency stabilisation of a fibre-laser comb using a novel microstructured fibre," Opt. Express, vol. 17, no. 7, pp. 5897–5904, 2009.

[29] S. Hakobyan et al., "Full stabilization and characterization of an optical frequency comb from a diode-pumped solid-state laser with GHz repetition rate," Opt. Express, vol. 25, no. 17, pp. 20437–20453, Aug. 2017.

[30] K. Numata, J. Camp, M. A. Krainak, and L. Stolpner, "Performance of planar-waveguide external cavity laser for precision measurements," Opt. Express, vol. 18, no. 22, pp. 22781–22788, Oct. 2010.

3.4 Investigation of the noise properties of the offset frequency in a quantum cascade Laser frequency comb

This section presents a similar noise investigation as shown in Section 3.3, but for a QCL-comb in the mid-infrared. QCLs are unipolar semiconductor lasers emitting in the mid-infrared or THz spectral range, based on intraband transitions in the gain medium[29]. Under certain conditions, Fabry-Perot QCLs can emit a comb spectrum made of equidistant lines due to a nonlinear four-wave mixing process occurring in the semiconductor gain material, which locks the modes together[25]. As a result, a comb spectrum is obtained in the spectral domain, but these lasers do not emit ultrashort pulses in contrast to femtosecond mode-locked lasers, and their output power is nearly constant, only affected by a small amplitude modulation. QCL-combs constitute a relatively novel comb technology with a high potential for dual-comb spectroscopy in the mid-infrared, but their noise properties have not been investigated deeply so far. In particular, the absence of a pulsed emission, combined with the poor availability of optical fibers in this spectral range, prevents the generation of a broad supercontinuum spectrum by spectral broadening for *f*-to-2*f* self-referenced CEO detection. Therefore, no noise investigation of the offset frequency has been reported so far for a mid-infrared QCL-comb.

Using the dedicated scheme introduced in Section 3.1 to characterize the CEO beat in mode-locked frequency combs, a similar noise investigation was performed for the first time for the offset frequency f_0 of a QCL-comb in the mid-infrared. By separately analyzing the noise of the characteristic comb frequencies, f_0, f_{FSR} (mode spacing, equivalent to f_{rep} for pulsed modelocked lasers) and ν_{opt}, it was possible for the first time to quantify the noise contributions of the two degrees of freedom of a QCL-comb.

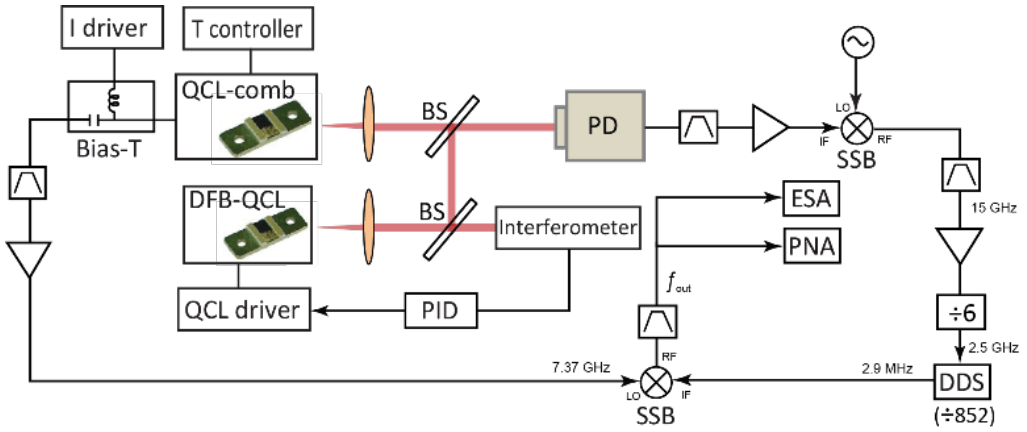

Fig. 3.15: Scheme of the experimental setup implemented to measure the frequency noise of the unknown free-running offset f_0 of the QCL-comb. The frequency noise of f_0 is indirectly measured by separately detecting the heterodyne beat between one optical line of the QCL-comb and a narrow-linewidth DFB-QCL at 1256.7 cm^{-1}, filtered, up-converted and frequency-divided by a large number N = 5,112 using a frequency pre-scaler (÷6) and a direct digital synthesizer (DDS, upper branch of the scheme) and the mode spacing f_{FSR} by RF extraction (lower branch of the scheme) on the chip wires through a bias-T. The two signals are then combined (mixed) to remove the noise contribution of f_{FSR}, such that the resulting signal f_{out} is representative of the noise of f_0 only. SSB: single sideband mixer; BS: beamsplitter; ESA: electrical spectrum analyzer; PNA: phase noise analyzer.

The used QCL-comb has a length of 6 mm, leading to a mode spacing of ~7.4 GHz. Its facets are high-reflection coated and the laser is junction-down-mounted. It was operated at a temperature of 10°C and at a typical current of ~1.7 A. In these conditions, the optical spectrum centered at 1245 cm^{-1} typically extends over 50 cm^{-1} and consists of ~200 lines separated by ~7.4 GHz. This frequency (mode spacing) can be detected electrically from the intermode beating extracted from the modulation of the injected current in the laser[30]. The experimental setup shown in Fig. 3.15 was implemented to beat one mode of the QCL-comb with a low-noise single-mode reference laser in order to measure the frequency noise of one of its individual modes. The reference laser is a distributed feedback (DFB) QCL operating at 1256.7 cm^{-1}. It was temperature-controlled and driven by a home-made low-noise QCL driver, and its linewidth was narrowed by stabilization to a Mach-Zehnder interferometer as described in Section 4.1.2.

Hence, the measured heterodyne beat reflects the noise of the QCL-comb as the resulting linewidth in the 10-kHz range (at 1-s integration time) of the stabilized DFB-QCL is significantly narrower than the linewidth of the QCL-comb presented later.

This setup enabled the frequency noise of the offset frequency f_0 of the QCL-comb to be indirectly assessed without directly detecting it by the traditional method of *f*-to-2*f* interferometry. The frequency noise PSD measured for an optical mode ν_N of the free-running QCL-comb (from the beat signal with the narrow-linewidth QCL) is displayed in Fig. 3.16. It is compared to the mathematically scaled frequency noise spectra separately measured for the up-scaled mode spacing $N \cdot f_{FSR}$ of the QCL-comb and indirectly assessed for f_0 using the experimental scheme. A close frequency noise spectrum (same shape and similar amplitude) is observed for the indirect f_0 signal and for the up-scaled mode spacing, whereas the noise of the optical line is significantly lower. This indicates that the fluctuations of f_{FSR} and f_0 are anti-correlated and partially compensate each other in the optical line. This behavior implies the existence of a fixed point[31,32] in the vicinity of the optical carrier in the spectrum of the QCL-comb according to the elastic tape model of frequency combs introduced for mode-locked lasers[9,33]. This fixed point is calculated in this case as $N_{fix} \approx 4{,}300$, leading to a fixed wave number of ~1056 cm^{-1} located outside of the comb spectrum. It results from the dominant noise source in the used QCL-comb, which is believed to arise from the voltage noise between the QCL terminals as previously observed in single-mode QCLs[34,35], which induces fluctuations of the internal temperature of the gain medium.

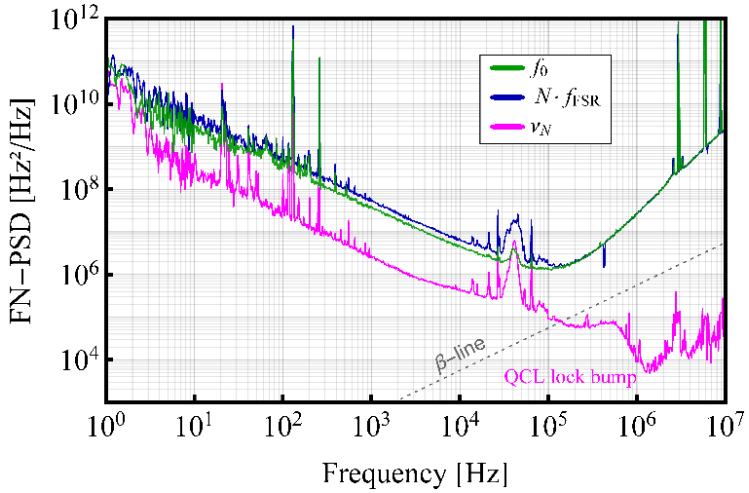

Fig. 3.16: Frequency noise power spectral density (FN-PSD) separately measured for an optical mode ν_N (pink), for the mode spacing scaled to the optical frequency ($N\,f_{FSR}$, blue) and indirectly assessed for the offset signal f_0 (green).

The degree of correlation between the frequency noise of $N\,f_{FSR}$ and f_0 was assessed from the measurements by calculating the sum of the complex coherence Γ_Δ between the frequency variations of the indirect offset signal f_0 and of the mode spacing in the free-running QCL-comb from the measured FN-PSD of ν_N, f_{FSR} and f_0 following the approach presented by Dolgovskiy and co-workers[36]:

$$\Gamma_\Delta = \frac{S_{f_{beat}} - S_{f_{CEO}} - S_{N\cdot f_{FSR}}}{\sqrt{S_{f_{CEO}} - S_{N\cdot f_{FSR}}}} \tag{21}$$

where S_x represents the FN-PSD of the parameter x. The calculated value of Γ_Δ displayed in Fig. 3.17 is close to -2 in the entire considered spectral range, which demonstrates the strong anti-correlation of the frequency noise of $N\,f_{FSR}$ and f_0. This outcome, combined with the similar amplitude of the FN-PSD measured for $N\,f_{FSR}$ and indirectly for f_0, explains the lower frequency noise observed for the optical mode of the QCL-comb compared to the individual noise contributions of $N\,f_{FSR}$ and f_0. This behavior is very similar to the case of comb spectra generated from ultrafast mode-locked lasers as reported in Section 3.3 for a 25-GHz diode-pumped

solid-state laser, even though the comb formation mechanism is completely different.

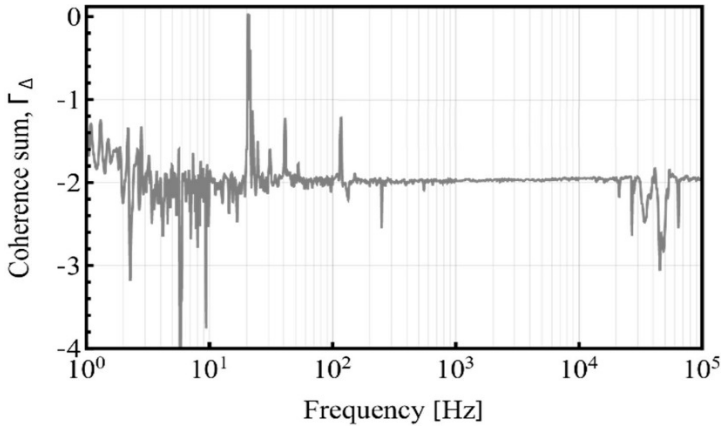

Fig. 3.17: Frequency dependence of the sum of the complex coherences Γ_Δ between the frequency variations of f_0 and f_{FSR} in the free-running QCL-comb

The effect of a modulation of the laser driving current on the two comb parameters f_{FSR} and f_0, as well as on an optical line ν_N, was separately investigated by measuring their transfer functions. For this purpose, the QCL current was modulated with a sine waveform and he corresponding signals (optical beat, mode spacing or indirect offset signal obtained using the scheme of Fig. 3.15) were demodulated using a frequency discriminator[37] and a lock-in amplifier.

The measured transfer functions displayed in Fig. 3.18 present the same behavior, both in amplitude and in phase, with a flat amplitude response up to ~10 kHz. A phase shift of 180° is observed between the transfer functions of f_{FSR} and f_0, which indicates that a change of the QCL current produces an opposite effect on f_{FSR} and f_0.

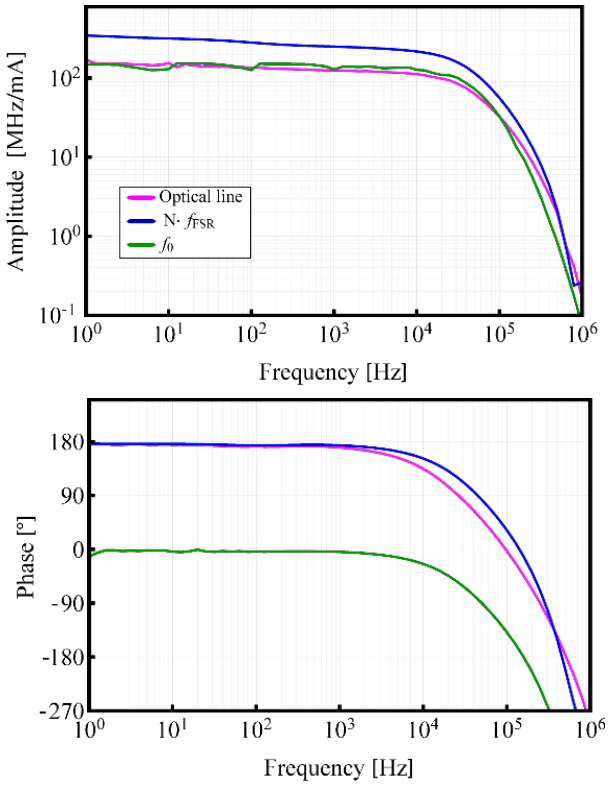

Fig. 3.18: Transfer function in amplitude (top) and phase (bottom) of $N f_{FSR}$ (blue), f_0 (green) and ν_N (optical line, pink) for a modulation of the QCL current.

As a conclusion, the first noise characterization of the offset frequency in a mid-infrared QCL-comb has been realized in this work using an electrical scheme previously presented in Section 3.1 and applied to other types of comb spectra in Sections 3.2 to 3.3. This scheme has been applied for the first time here to a mid-infrared comb. It does not require the direct detection of the offset frequency beat based on a nonlinear interferometry scheme, which is not yet applicable to the unpulsed emission of QCL-combs. With this scheme, the frequency noise of the two parameters of the QCL-comb, the mode spacing and the offset frequency, was separately measured. The strong observed anti-correlation between these two signals explains the lower noise and narrower linewidth obtained for the lines of the QCL-comb, with the presence of a fixed point estimated at 1056 cm^{-1}. This behavior has a high analogy with the high repetition rate DPSSL evaluated with the same approach and reported in Section 3.3.

Chapter 4

Ultralow noise optical and microwave oscillators

Optical oscillators (lasers) with a very low frequency noise, narrow linewidth and high relative frequency stability are generally referred to as ultra-low noise or ultra-stable lasers. Their linewidth is typically in a range of a few Hz to sub-Hz[38] and the fractional frequency instability[39] can be at the level of $4 \cdot 10^{-17}$, which is the highest relative frequency stability achieved so far for any type of oscillator.

Such ultra-stable lasers are also a core element to generate ultralow-noise microwave signals, as the high relative frequency stability of the optical oscillator can be transferred to the microwave domain with the use of an optical frequency comb. At the same time, the phase noise of the optical oscillator is divided by a large factor in the resulting microwave signal. Microwave signals with the lowest phase noise ever produced have been generated in this way[10,40,41], as well as zeptosecond level integrated timing jitter demonstrated for microwave signals[42]. These outstanding oscillators are a key tool for numerous high-level applications in various

domains (GPS, radar, lidar, quantum computing, clocking, spectroscopy, gravimetry, gravitational wave detection…).

In this chapter, ultralow noise optical and microwave oscillators are considered with a focus on unconventional approaches. Section 4.1 deals with ultra-stable lasers, notably an alternative method to the commonly employed ultra-stable optical cavities, which makes use instead of an optical delay line. This approach previously demonstrated with long fibered delays in the near-infrared[12,13] is applied here for the first time to a mid-infrared quantum cascade laser. Using a short, meter-scale free-space delay line, a significant reduction of the frequency noise is demonstrated. Sub-section 4.1.2 is a reprint of an article published in Optics Letters[43].

Then, Section 4.2 deals with ultralow noise microwave oscillators. An alternative approach to generate an ultra-low noise microwave signal by frequency division of an ultra-stable laser using a femtosecond frequency comb is first presented in Section 4.2.1, which is a reprint of an article published in Optics Letters[44]. In contrast to the commonly used method where the comb is optically locked to the ultra-stable lasers, the different approach proposed here makes use of the comb as a transfer oscillator and does not need any fast stabilization, which presents some advantages. Finally, this transfer oscillator method has also been implemented with a crystalline microresonator-based comb, enabling the first proof-of-principle demonstration of optical-to-microwave frequency division realized with a Kerr comb. This is reported in Section 4.2.2 which is a reprint of an article submitted to Nature Communications[45].

4.1 Ultra-low noise continuous-wave lasers

From the Schawlow-Townes laser theory[17], any laser exhibits white frequency noise as a quantum limit. This white frequency noise that is responsible for the Lorentzian linewidth (see Table 2.1) depends on the considered laser technology. It can be very high for laser diodes ($> 10^6$ Hz^2/Hz) and very low for fiber lasers ($< 10^0$ Hz^2/Hz) or mid-infrared quantum cascaded lasers[46,47] ($\sim 10^2$ Hz^2/Hz).

The frequency fluctuations of a laser can be reduced, especially at high Fourier frequency, corresponding to a narrowing of the Lorentzian linewidth, by using an external cavity[48,49]. Moreover, besides the fundamental white frequency noise, some additional noise with different frequency dependence (such as $1/f$, $1/f^2$, or peaks at specific frequencies…) and magnitude, also affects a laser. It notably results from the sensitivity of the laser frequency to external environmental perturbations, such as temperature, pressure, mechanical or acoustic vibrations… In order to further reduce the frequency fluctuations and the linewidth of a laser, active frequency stabilization is needed.

It requires an optical reference to detect the frequency fluctuations and an actuator in the laser to apply a correction signal to reduce the fluctuations. The optical reference can be for example an atomic or molecular transition, an optical filter resulting from multiple-wave interference processes (optical cavity, Bragg grating…), or a time delay interferometer where the laser frequency is compared to a delayed version of itself (see Section 4.1.1). The residual frequency fluctuations of the locked laser directly depend on the quality of the optical reference which, as the laser itself, is generally sensitive to external environmental perturbations.

The state-of-the-art laser stabilization technology that achieved an optical linewidth as narrow as 10 mHz[38] is based on a high-finesse well-isolated single-crystal silicon Fabry-Pérot cavity placed under vacuum and regulated at 124 K where the thermal expansion coefficient of this material

has a zero-crossing point. With a proper isolation of the cavity from environmental noise sources, the thermal noise limit (Brownian noise of the mirror coatings) can be reached, leading to a flicker noise floor of 4.10^{-17}. Different cavity designs, materials and arrangements exist and are being developed by several university research groups or industries[50–52]. These systems have reached tremendous performance, but they are also fairly complex and bulky, which makes them not convenient for field applications.

4.1.1 Optical delay-line

The time delay interferometer, also referred to as optical delay-line, is probably the best candidate to achieve a high ratio of performances over complexity, resulting in a compact system. The laser frequency fluctuations are detected by comparing the emitted frequency at two different times. This is usually made using an imbalanced optical interferometer, such as a Michelson interferometer (MI) or a Mach-Zehnder interferometer (MZI) with a long delay between the two optical paths. From the theory[53,54], the interferometer acts as a laser frequency fluctuations to voltage converter with the following transfer function $T_F(f)$ and $T_\phi(f)$ (for the laser phase):

$$T_\phi(f) = \alpha\left(1 - e^{-i2\pi f\tau}\right) \qquad \text{[V/rad]} \tag{22}$$

$$T_F(f) = \alpha\left(1 - e^{-i2\pi f\tau}\right)/if \qquad \text{[V/Hz]} \tag{23}$$

where α is a multiplicative factor which depends on experimental components (conversion coefficient of the photo-detector, gain of the voltage amplifier…). It implies that the optical delay-line acts as a frequency discriminator with a factor of $2\pi\tau$ at low Fourier frequency ($\ll 1/\tau$), which is directly proportional to the time delay τ.

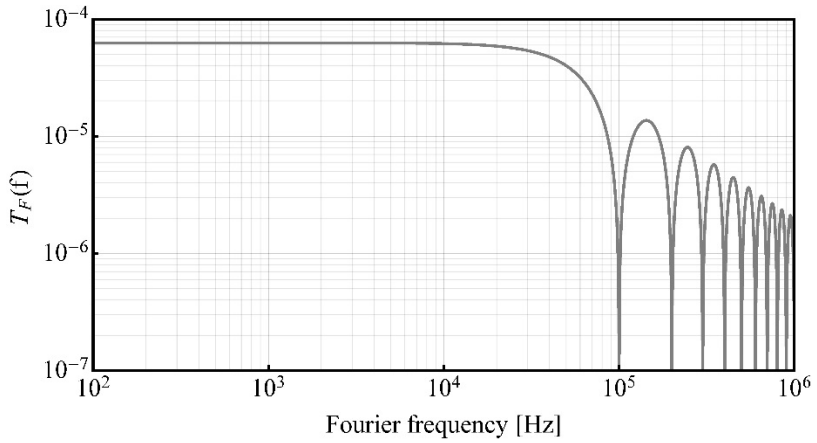

Figure 4.1: Example of a calculated amplitude of transfer function $T_F(f)$ of an optical delay line with $\tau = 10$ µs.

It is important to notice that this transfer function does not depend on the carrier frequency of the signal, but only on the time delay τ. The magnitude of the transfer function is directly proportional to τ. The transfer function has null values at multiples of $1/\tau$ (see Figure 4.1). This is easily understood if one considers that the signal is modulated by a sine function at a frequency f_{mod}. For a time delay equal to a multiple of $1/f_{mod}$, there is no frequency difference measured on the photodetector. The observed low-pass filter response is a direct consequence of the multiple poles occurring in the transfer function.

In this scheme, the photodetector signal depends on the frequency difference between the light that propagates in the two arms of the interferometer. It is sensitive to the laser frequency fluctuations, but also to fluctuations of the interferometer differential length. It implies that in the best case where no other noise is induced in the stabilization loop, the achievable relative frequency fluctuations of the stabilized laser correspond to the relative length fluctuations of the interferometer: $\Delta\upsilon/\upsilon = \Delta L/L$. Interferometer length fluctuations are induced by different environmental perturbations such as temperature, pressure, mechanical and acoustical vibrations, humidity, acceleration…, similarly to other optical references. Moreover, some other sources of extra noise are generally present and

reduce the final system performances, such as photodetection noise. This extra noise originates from the detector itself and its electronics ($1/f$ noise) or from other conversion processes occurring in the photodetection (shot noise, polarisation fluctuations, laser intensity noise). To counter-act these limitations, one possibility is to use a long time delay in order to increase the converted frequency fluctuations compared to the extra noise, which is independent of the time delay. On another side, increasing the time delay decreases the frequency of the first zero of the interferometer transfer function and reduces the possible locking bandwidth. A compromise has to be found to reach the best performance. The photodetection noise limitation can be reduced by using a balanced detection[54], reducing the converted laser intensity noise contribution. It can also be significantly mitigated with the use of a self-heterodyne detection[12] instead of the aforementioned self-homodyne detection[54]. The self-heterodyne detection consists of shifting the light frequency in one arm of the interferometer using a modulator (e.g., an acousto-optic modulator) in order to detect a heterodyne signal at the shifting frequency (typically in the MHz range) on the photodetector and not a signal around DC (0 Hz). The photo-detected signal is demodulated at the shifting frequency in order to generate an error signal that is much less affected by extra $1/f$ noise.

The optical delay-line method has been used to stabilize lasers or characterize their frequency fluctuations since 1980[55]. It has been mainly used at telecom wavelengths (~1.5 μm) based on highly imbalanced fiber interferometers with typical path length difference ranging from 100 m to 100 km (corresponding to a time delay τ of 0.5 μs to 0.5 ms). It is a fairly simple and affordable method, enabling the realization of compact and performant systems, as long as the interferometer is properly isolated from external environmental perturbations. In principle, the method is applicable at any wavelength, but the literature is exempt of results obtained in the mid-infrared spectral region where long fiber delay are difficult and costly to implement. In Section 4.1.2, the application of this approach to a quantum

cascade laser in the mid-infrared region is presented, resulting in a strong reduction of its linewidth from the megahertz range (in the free-running mode) down to <10 kHz (1-s integration time), using a an imbalanced MZI with only 1-m path length difference and a self-homodyne detection.

4.1.2 10-kHz-Linewidth mid-infrared quantum cascade laser by stabilization to an optical delay Line

Atif Shehzad[1]*, Pierre Brochard*[1]*, Renaud Matthey*[1]*, Thomas Südmeyer*[1]*, and Stéphane Schilt*[1]

[1]Laboratoire Temps-Fréquence, Institut de Physique, Université de Neuchâtel, CH-2000 Neuchâtel, Switzerland.

We present a mid-infrared quantum cascade laser (QCL) with a sub-10-kHz full width at half maximum linewidth (at 1-s integration time) achieved by stabilization to a free-space optical delay line. The linear range in the center of a fringe detected at the output of an imbalanced Mach-Zehnder interferometer implemented with a short free-space pathlength difference of only 1 m is used as frequency discriminator to detect the frequency fluctuations of the QCL. Feedback is applied to the QCL current to lock the laser frequency to the delay line. The application of this method in the mid-infrared is reported for the first time. By implementing it in a simple self-homodyne configuration, we have been able to reduce the frequency noise power spectral density of the QCL by almost 40 dB below 10-kHz Fourier frequency, leading to a linewidth reduction by a factor of almost 60 compared to the free-running laser. The present limits of the setup are assessed and discussed.

Distributed-feedback (DFB) quantum cascade lasers (QCLs) offer a unique combination of high output power, single-mode emission, and continuous spectral tunability that make them the most widely used type of continuous-wave laser sources in the mid-infrared (MIR) molecular fingerprint spectral region for gas-phase spectroscopy and trace gas sensing applications. The intrinsic or Schawlow-Townes linewidth [1] of DFB-QCLs that results from the laser white frequency noise can be as low as a few hundred hertz [2]. However, excess electrical flicker noise in the semiconductor structure that induces internal temperature fluctuations of

the laser active region [3,4], as well as technical noise that may arise from the current driver [5] lead to a broadening of the observed QCL emission linewidth (full width at half maximum - FWHM) to the megahertz level, typically, for integration times of milliseconds to hundreds of millisecond [2,3,6–8]. This is most often sufficient for gas sensing and many molecular spectroscopy applications, but more advanced applications that aim at controlling molecular degrees of freedom, for example to test fundamental symmetries, or to measure fundamental constants and their possible time variation [9], require QCLs with a lower frequency noise and, thus, a narrower linewidth.

Different fairly simple approaches have been implemented to reduce the frequency noise of QCLs, e.g., by using the voltage noise detected between the QCL terminals as an error signal in a stabilization loop [10,11], but these methods resulted in a modest reduction of the frequency noise power spectral density (FN-PSD) by typically one order of magnitude. More sophisticated setups involved stabilization to a reference optical cavity. However, high-finesse cavities are much less developed in the MIR than in the near infrared (NIR) range where lasers stabilized down to the sub-hertz level are routinely used [12–15] today in optical clocks or for ultra-low noise microwave generation. Therefore, only few works of direct laser stabilization to a MIR high-finesse cavity have been reported. M.S. Taubman and co-workers measured a heterodyne beat note with a linewidth of a few hertz only between two cavity-stabilized QCLs at 8.5 µm [16], but the measurement did not constitute an absolute assessment of the linewidth of these lasers as the two cavities were locked to each other with a bandwidth of 6 kHz. E. Fasci et al. reported a 1-ms linewidth of less than 4 kHz for a 8.6-µm QCL locked to a high-finesse V-shaped cavity by optical feedback [17]. However, the most stable and low frequency noise lasers in this spectral region have been achieved by phase-locking a QCL to a cavity-stabilized NIR laser through a nonlinear process using a frequency comb, leading to fairly complex setups [9,18].

An alternative method to an optical cavity enabling a significant reduction of the frequency noise of a laser was demonstrated in the NIR with the use of a much simpler setup based on an optical delay line [19–21]. The interference fringes occurring in an imbalanced Michelson or Mach-Zehnder interferometer act as a frequency discriminator that converts frequency fluctuations of the laser into intensity fluctuations, which are detected by a photodiode at the interferometer output. In the interferometer, part of the light is delayed in one path by propagating through a time delay before being recombined with the other part of the light that propagates through a much shorter path. The magnitude of the discrimination factor (in V/Hz) is approximately given by $2\pi\tau V_{pk}$, where τ is the imbalanced interferometer time delay and V_{pk} is the amplitude of the error signal [19]. The most standard configuration makes use of a frequency-shifter acousto-optic modulator (AOM) in one arm to produce a self-heterodyne beat signal at the interferometer output. This beat signal is demodulated at the shifting frequency to stabilize the laser emission frequency to the delay line, by applying a feedback signal either directly to the laser driver, or to another AOM, resulting in a high feedback locking bandwidth. High laser noise reduction can thus be achieved and a resulting linewidth at the sub-hertz level has been demonstrated in the NIR using a 500 m fiber length in a Michelson interferometer [21].

As the resulting frequency discrimination factor scales linearly with the pathlength difference between the two interferometer arms, long delay lines lead to a high discriminator factor and, thus, to a high frequency noise sensitivity. In the NIR, long delays of hundreds of meters to a few kilometers are easily achievable using low-loss single-mode optical fibers. Hence, very low FN-PSD was demonstrated for a 1.5-μm laser stabilized to a km-scale fiber delay, comparable to the residual noise achieved by stabilization to an ultra-low expansion (ULE) high-finesse optical cavity in a large range of Fourier frequencies [20]. Only at low offset frequencies (typ. below 100 Hz), the laser stabilized to the delay line was affected by higher

frequency noise and drift resulting from acoustic/mechanical noise and thermal drift of the interferometer as compared to a ULE cavity that is usually better protected against such disturbances by being mounted in a more advanced protective enclosure.

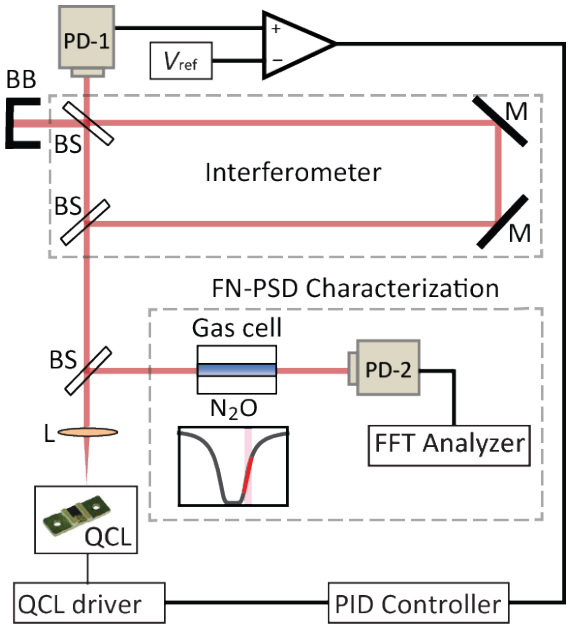

Fig. 4.2: Experimental setup for QCL frequency noise reduction using a delay line; L, lens; BS, beam splitter; M, mirror; PD, photodetector; BB, beam blocker, PID, proportional-integral-derivative servo controller; FFT, fast Fourier transform. The linear range of a N_2O transition in a gas cell (red part of the absorption line) is used to measure the frequency noise of the laser with a frequency-to-voltage conversion factor of 27.9 V/GHz.

In this Letter, we demonstrate a significant frequency noise reduction achieved for the first time to the best of our knowledge for a MIR QCL by stabilization to an optical delay line. However, AOMs are much less common in the MIR range than in the NIR and furthermore require a high radio-frequency power resulting in an elevated power dissipation and the need for a water cooling that can induce excess noise in the interferometer. Therefore, a self-heterodyne configuration as used with NIR lasers is not convenient at MIR wavelengths. Hence, our first proof-of-principle demonstration reported here is based on a simpler self-homodyne scheme that does not need an AOM. Consequently, this scheme is much more

sensitive to $1/f$ flicker noise arising from laser intensity noise and detector noise that may limit the achieved frequency noise of the stabilized laser. Furthermore, the poor availability of low-loss single-mode optical fibers in the MIR prevents the use of a fibered delay line. Hence, we restricted the experimental setup to a short free-space pathlength difference of around 1 m acting as frequency-to-amplitude noise converter in this first proof of principle.

With this scheme, we nevertheless achieved a QCL FN-PSD reduction by almost 40 dB over a large range of Fourier frequencies and a narrowing of the corresponding linewidth below 10 kHz at 1-s integration time, as compared to almost 500 kHz for the free-running laser. A scheme of the experimental setup is shown in Fig. 4.2. A DFB-QCL emitting at ~7.8 µm (from Alpes Lasers, Switzerland) and driven by a home-made low-noise current source is coupled to a Mach-Zehnder interferometer with a pathlength difference of ~90 cm. The laser is operated at a temperature of 20°C and an average current of ~435 mA located approximately in the middle of its operation range at this temperature. At this operation point, its current-tuning coefficient was assessed to be 0.29 GHz/mA. This value was spectroscopically obtained from the position of several N_2O absorption lines observed in a large current scan through a low-pressure gas cell and their comparison to the Hitran database [22]. A 2nd order fit of the QCL frequency versus current was performed to extract the tuning coefficient at the operating point. The beat signal at the output of the interferometer is detected with a Mercury-Cadmium-Telluride (MCT) photodiode (Vigo Systems, model PVMI-4TE-8) and is compared to a stable reference voltage V_{ref} to generate an error signal for the laser frequency stabilization. The interference fringes observed when scanning the QCL frequency (via a current scan) are displayed in Fig. 4.3. A high contrast of the interference of about 90% is achieved here with an optimized alignment of the interferometer, which is important to get a high discrimination factor that lowers the noise floor of the setup as discussed later. The measured slope

D_{fringe} = 7.9 V/GHz in the center of a fringe is in good agreement with the calculated value $2\pi\tau V_{pk}$ = 8.3 V/GHz assessed from the applied pathlength difference of ~88 cm and the observed fringe amplitude of 0.45 V. The reference voltage is adjusted so that the zero-crossing point of the resulting error signal lies in the middle of a fringe, in the linear range. A proportional-integral-derivative (PID) servo-controller (Vescent D2-125) amplifies the error signal and produces a feedback signal that is applied to the current driver of the QCL. A feedback bandwidth larger than 100 kHz is typically needed to achieve a substantial reduction of the QCL frequency noise and linewidth according to the crossing point of the FN-PSD of the free-running laser with the β-separation line [23]. The impact of acoustic and mechanical noise on the interferometer was reduced by enclosing the whole experimental setup in a closed wooden box whose walls are covered by a foam layer. Some foam was additionally placed underneath the optical breadboard of the interferometer.

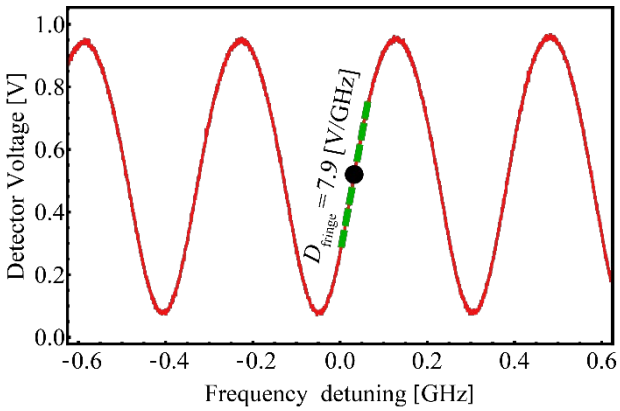

Fig. 4.3: Interference fringes detected at the output of the interferometer when scanning the QCL current. The locking point indicated by a black dot is located in the linear range of a fringe with a slope D_{fringe}. The frequency axis of the graph was obtained using the measured tuning coefficient of the QCL of -0.29 GHz/mA.

Before the interferometer, a beamsplitter directs part of the laser output beam through a 10-cm-long sealed gas cell filled with a low-pressure (2 mbar) of pure N_2O that is followed by a photodiode. This setup is used to independently characterize the frequency noise of the laser (absolute out-

of-loop measurement). The laser is tuned to the flank of a strong N_2O absorption line at 1276.4 cm^{-1}, which acts as a frequency discriminator with a typical conversion coefficient D_{gas} = 27.9 V/GHz measured in the setup (see Fig. 4.2). The voltage noise of the detector signal is measured with a fast Fourier transform (FFT) analyzer (Rhode-Schwarz FSWP-26) and is converted into laser frequency noise using the measured frequency discriminator, both for the free-running and locked laser. The frequency noise of the free-running QCL was also assessed from the error signal using the slope of the fringe (D_{fringe}) around the locking point displayed in Fig. 4.3 for cross-check. The two distinct measurements of the FN-PSD of the free-running QCL displayed in Fig. 4.4 are in good agreement, which proves their proper scaling with the discriminators slopes D_{gas} or D_{fringe}, respectively.

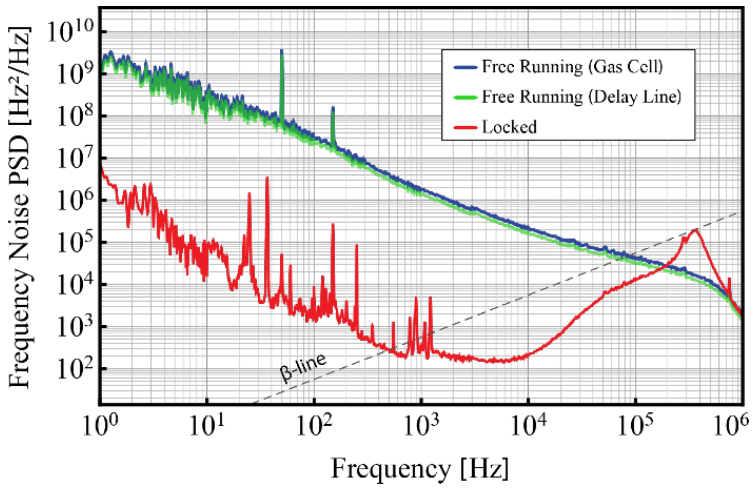

Fig. 4.4: Frequency noise PSD of the QCL in free-running (blue and green curves measured in two different ways) and locked (red) modes. The servo bump of the locked laser indicates a locking bandwith of ~400 kHz. The grey dashed line corresponds to the β-separation line used to calculate the corresponding laser linewidth [23].

Results of the stabilization to the delay line show a significant noise reduction (by almost 40 dB) at Fourier frequencies lower than 10 kHz. A locking bandwidth slightly lower than 400 kHz is assessed from the servo bump in the FN-PSD. However, the locked laser is affected by a fairly large $1/f$ noise at low frequencies. This is a consequence of the self-homodyne

scheme implemented here, as the beat signal detected around DC is sensitive to $1/f$ noise originating from different sources such as laser intensity noise and detector noise. The narrow noise peaks occurring at frequencies of 50 Hz and odd harmonics in the spectrum of the locked laser are of electronic origin, while the series of broader noise features below 1 kHz result from acoustic and mechanical noise in the interferometer, which is transferred to the laser by the feedback.

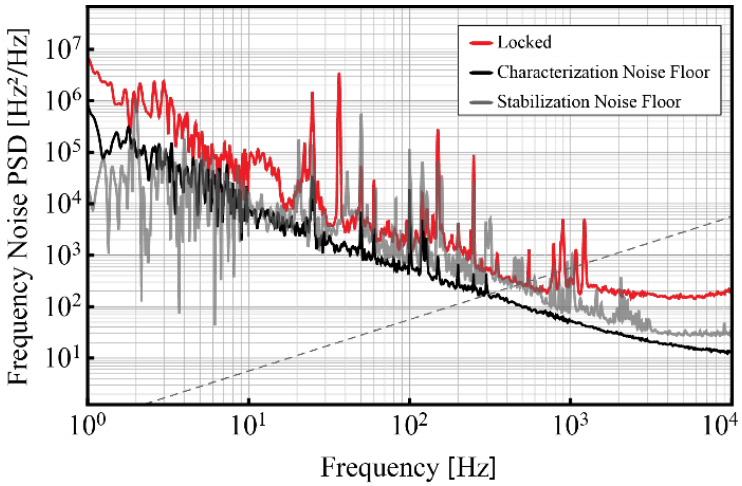

Fig. 4.5: Comparison of the frequency noise PSD of the locked laser with the noise floors originating from the characterization and stabilization parts of the experimental setup.

In order to identify the present limitation in the setup, different noise floors have been measured (see Fig. 4.5). The noise floor of the characterization setup (frequency discriminator from the gas cell and associated detector) was assessed by recording the combination of the voltage noise of the detector (PD-2) and of the laser intensity noise without the reference gas cell. The measured voltage noise floor was converted it into an equivalent frequency noise floor by scaling with the measured frequency discriminator slope D_{gas}. One notices that the spectroscopic frequency noise characterization setup used here does not constitute a limitation at the presently achieved noise level of the QCL. Hence, this simple spectroscopic setup is suitable to characterize the frequency noise of

a laser with a linewidth around or closely below 10 kHz (provided that its intensity noise is not too large). However, there is only little margin between the measured FN-PSD of the locked QCL and the noise floor of the characterization setup, so that a steeper frequency discriminator (e.g., obtained from a sub-Doppler transition) would be needed to characterize the noise of a narrower linewidth laser, e.g., at the level of a few kilohertz or below.

The achieved frequency noise of the stabilized QCL matches the system noise floor obtained when blocking one beam in the interferometer, which sets the limit corresponding to the detector noise and laser intensity noise. The measured noise was converted into an equivalent FN-PSD by scaling with the interferometer frequency discrimination factor D_{fringe} = 7.9 V/GHz (see Fig. 4.3). The associated $1/f$ noise currently limits the achieved frequency noise of the locked QCL at Fourier frequencies in the range of around 20 Hz to 1 kHz. At lower frequencies, the drift of the interferometer is likely responsible for the observed laser frequency noise that is no longer limited by the detector or intensity noise.

The laser linewidth estimated from the measured FN-PSD using the β-separation line approximation [23] is 7.8 kHz at 1-s integration time, which is 60 times narrower than the linewidth of the free-running laser (Fig. 4.6). This reduction factor is even larger than 100 at shorter integration times of 10 ms and below. The achieved linewidth narrowing is much higher than with other simple approaches previously reported for frequency noise reduction in QCLs [10,11], while being obtained with a fairly simple setup consisting only of a few standard optical components (two gold-coated mirrors and two polarization-independent beam splitters in the interferometer). This simple arrangement does not involve any vacuum chamber, temperature stabilization of the setup or active anti-vibration platform.

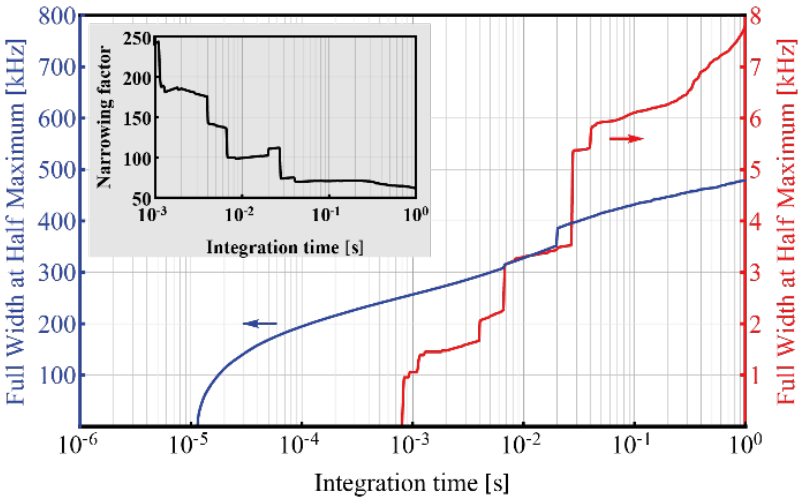

Fig. 4.6: Full width at half maximum (FWHM) linewidth of the QCL calculated from the frequency noise spectrum based on the β-separation line approximation [23] as a function of the integration time (inverse of the lower cut-off frequency for the FN-PSD integration) in free-running regime (blue) and for the QCL stabilized to the delay line (red). Inset: linewidth narrowing factor as a function of the integration time.

In conclusion, we have reported a first proof-of-principle demonstration of QCL frequency noise reduction using a free-space delay line. The achieved results are presently limited by the implemented self-homodyne scheme and by the fact that a fairly short imbalance pathlength (less than 1 m) is used in this experiment. Next steps to improve the stabilization will consist on one hand in increasing the pathlength difference to enhance the sensitivity to the laser frequency noise and decrease the stabilization noise floor, which can be achieved for instance with the use of a multipass cell to keep the setup compact. On the other hand, we will implement an absolute lock of the delay line to a molecular transition to combine the linewidth reduction brought by the stabilization to the delay line with the absolute frequency stability of the molecular reference.

Funding

Swiss National Science Foundation (SNSF) (200020_178864), European Space Agency (ESA).

References

[1] A. L. Schawlow and C. H. Townes, Phys. Rev. 112, 1940 (1958).

[2] S. Bartalini, S. Borri, P. Cancio, A. Castrillo, I. Galli, G. Giusfredi, D. Mazzotti, L. Gianfrani, and P. De Natale, Phys. Rev. Lett. 104, 083904 (2010).

[3] L. Tombez, S. Schilt, J. Di Francesco, P. Thomann, and D. Hofstetter, Opt. Express 20, 6851 (2012).

[4] S. Schilt, L. Tombez, C. Tardy, A. Bismuto, S. Blaser, R. Maulini, R. Terazzi, M. Rochat, and T. Südmeyer, Appl. Phys. B 119, 189 (2015).

[5] L. Tombez, S. Schilt, J. Francesco, T. Führer, B. Rein, T. Walther, G. Domenico, D. Hofstetter, and P. Thomann, Appl. Phys. B 109, 407 (2012).

[6] L. Tombez, J. Di Francesco, S. Schilt, G. Di Domenico, J. Faist, P. Thomann, and D. Hofstetter, Opt. Lett. 36, 3109 (2011).

[7] S. Bartalini, S. Borri, I. Galli, G. Giusfredi, D. Mazzotti, T. Edamura, N. Akikusa, M. Yamanishi, and P. De Natale, Opt. Express 19, 17996 (2011).

[8] S. Schilt, L. Tombez, G. D. Domenico, and D. Hofstetter, in The Wonder of Nanotechnology: Quantum Optoelectronic Devices and Applications (SPIE, 2013).

[9] B. Argence, B. Chanteau, O. Lopez, D. Nicolodi, M. Abgrall, C. Chardonnet, C. Daussy, B. Darquié, Y. Le Coq, and A. Amy-Klein, Nat. Photonics 9, 456 (2015).

[10] L. Tombez, S. Schilt, D. Hofstetter, and T. Südmeyer, Opt. Lett. 38, 5079 (2013).

[11] I. Sergachev, R. Maulini, A. Bismuto, S. Blaser, T. Gresch, Y. Bidaux, A. Müller, S. Schilt, and T. Südmeyer, Opt. Lett. 39, 6411 (2014).

[12] J. Alnis, A. Matveev, N. Kolachevsky, Th. Udem, and T. W. Hänsch, Phys. Rev. A 77, 053809 (2008).

[13] K. Numata, A. Kemery, and J. Camp, Phys. Rev. Lett. 93, 250602 (2004).

[14] T. Kessler, C. Hagemann, C. Grebing, T. Legero, U. Sterr, F. Riehle, M. J. Martin, L. Chen, and J. Ye, Nat. Photonics 6, 687 (2012).

[15] D. G. Matei, T. Legero, S. Häfner, C. Grebing, R. Weyrich, W. Zhang, L. Sonderhouse, J. M. Robinson, J. Ye, F. Riehle, and U. Sterr, Phys. Rev. Lett. 118, 263202 (2017).

[16] M. S. Taubman, T. L. Myers, B. D. Cannon, R. M. Williams, F. Capasso, C. Gmachl, D. L. Sivco, and A. Y. Cho, Opt. Lett. 27, 2164 (2002).

[17] E. Fasci, N. Coluccelli, M. Cassinerio, A. Gambetta, L. Hilico, L. Gianfrani, P. Laporta, A. Castrillo, and G. Galzerano, Opt. Lett. 39, 4946 (2014).

[18] M. G. Hansen, E. Magoulakis, Q.-F. Chen, I. Ernsting, and S. Schiller, Opt. Lett. 40, 2289 (2015).

[19] B. S. Sheard, M. B. Gray, and D. E. McClelland, Appl. Opt. 45, 8491 (2006).

[20] F. Kéfélian, H. Jiang, P. Lemonde, and G. Santarelli, Opt. Lett. 34, 914 (2009).

[21] J. Dong, Y. Hu, J. Huang, M. Ye, Q. Qu, T. Li, and L. Liu, Appl. Opt. 54, 1152 (2015).

[22] L. S. Rothman et al., J. Quant. Spectrosc. Radiat. Transf. 130, 4 (2013).

[23] G. Di Domenico, S. Schilt, and P. Thomann, Appl. Opt. 49, 4801 (2010).

4.2 Ultra-low noise microwave oscillator

Low phase noise electrical oscillators, especially at GHz carrier frequencies, can be divided into three categories. The first one includes fundamental or harmonic oscillation frequencies of purely electronic oscillators like temperature-compensated crystal oscillators (TCXO), oven-controlled crystal oscillators (OCXO), or dielectric resonator oscillators (DRO). They are compact, low power consumption and inexpensive, but they are far from the state-of–the-art technology in terms of achieved frequency noise and stability. This first category also includes much better, but more complex systems like active hydrogen masers and cryogenic sapphire oscillators (CSO). The second category contains the opto-electronic oscillators (OEO), which is an hybrid technology introduced in 1991[56] that includes a combined electronic and optical resonator. This technology has achieved high performances with a phase noise of -163 dBc/Hz at 6 kHz Fourier frequency for a 10-GHz carrier frequency[57]. As explained in the main introduction of this thesis, the higher the frequency of an oscillator, the better the expected performance as a rule of thumb. Hence, the third category includes cutting-edge technologies based on optical frequency division.

The general principle is to divide the frequency of a high-performance ultra-stable optical oscillator from the optical domain to a radio-frequency signal. There are at least three different possible schemes. The first one is to detect the heterodyne beat signal between two lasers that are frequency-stabilized onto two different modes of the same optical cavity, so that their noise is highly correlated[58]. In the ideal case of perfectly correlated lasers, their frequency difference would be equivalent to a frequency division. However, the imperfect correlation that arises from the limited stabilization bandwidths of the two lasers, as well as from additional noise introduced in the stabilization loops, results in degraded performance (frequency noise and stability) of the obtained signal. One possibility to mitigate the impact

of these non-correlated contributions is to use two optical modes of the reference cavity as far as possible from each other. Lasers locked to these two modes can be linked using a frequency comb, either from a mode-locked laser or generated with an electro-optic modulator. In this second case, the process referred to as electro-optical frequency division (eOFD) was introduced for the first time in 2014 by Jiang Li *et al*[59].

Optical frequency division using a frequency comb[10] is the method that demonstrated the world record-low phase noise and frequency instability by reaching a phase noise floor below -173 dBc/Hz and a fractional frequency stability of $6.5 \cdot 10^{-16}$ at 1-s integration time for a 12-GHz signal[42]. The principle is to use a self-referenced optical frequency comb (from a mode-locked laser) to divide the phase noise and transfer the fractional frequency stability of an optical reference to the repetition rate frequency f_{rep} of the comb (or generally to a harmonic of it at around 10 GHz). This requires the comb to be optically-locked to the optical reference, which needs a fast actuator in the comb and also benefits from a low-noise operation of the free-running comb. Other aspects are important to achieve an ultralow noise of the generated microwave signal, such as the quality of the optical reference[38], or the value of f_{rep} (higher is better or the use of optical pulse multiplier/filter is needed[60]), the photo-detection process[42,61], etc.

An alternative scheme for optical-to-microwave frequency division with a frequency comb developed in the frame of this thesis is reported in the next sections. It is based on a transfer oscillator approach[9,44]. The method is first presented in Section 4.2.1, which is a reprint of an article published in Optics Letters[44]. Then, the first proof-of-principle demonstration of optical-to-microwave frequency division realized with a Kerr comb using this transfer oscillator scheme is presented in Section 4.2.2, which is a reprint of a manuscript accepted for publication in Nature Communications[45]. This was done in a joint work with the group of Prof. Tobias Kippenberg at EPFL.

4.2.1 Ultra-low noise microwave generation with a free-running optical frequency comb transfer oscillator

Pierre Brochard[1], Stéphane Schilt[1] and Thomas Südmeyer[1]

[1]Laboratoire Temps-Fréquence, Institut de Physique, Université de Neuchâtel, CH-2000 Neuchâtel, Switzerland.

We present ultra-low noise microwave synthesis by optical to radio-frequency (RF) division realized with a free-running or RF-locked optical frequency comb (OFC) acting as a transfer oscillator. The method does not require any optical lock of the OFC and circumvents the need for a high bandwidth actuator. Instead, the OFC phase noise is electrically removed from a beat-note signal with an optical reference, leading to a broadband noise division. The phase noise of the ~15-GHz RF signal generated in this proof-of-principle demonstration is limited by a shot-noise level below -150 dBc/Hz at high Fourier frequencies and by a measurement noise floor of 60 dBc/Hz at 1-Hz offset frequency when performing 1,100 cross-correlations. The method is attractive for high repetition rate OFCs that lead to a lower shot-noise, but are generally more difficult to tightly lock. It may also simplify the noise evaluation by enabling the generation of two or more distinct ultra-low noise RF signals from different optical references using a single OFC and their direct comparison to assess their individual noise.

Optical frequency combs (OFC) from mode-locked lasers provide a direct and phase-coherent link between optical and microwave frequencies through their two degrees of freedom, the repetition rate f_{rep} and the carrier-envelope offset (CEO) frequency f_{CEO}. The most advanced applications of OFCs today are as optical-to-microwave frequency dividers. In the traditional implementation, one comb mode is tightly locked to an optical reference (ultra-stable laser) whose noise is divided down by a large factor to the radio-frequency (RF) domain [1,2]. This has enabled generating the microwave signals with the lowest phase noise to-date, below −173 dBc/Hz

for a 12-GHz carrier [3]. This is lower than for other well-established methods such as optoelectronic oscillators (OEO) [4], which achieved around 160 dBc/Hz at 10-kHz offset from a 10-GHz carrier [5]. The ultimate noise level of the RF signal corresponds essentially to the frequency-divided noise of the reference laser within the OFC locking bandwidth. Therefore, this approach requires a fast actuator for the optical lock of the OFC and is most often done with MHz-range repetition rate OFCs for their ease of development and tight stabilization. Intra-cavity electro-optic modulators (EOMs) with MHz bandwidth are most commonly used, but make the system more complex and costly, even though many comb systems today are equipped with such EOMs [6,7]. Higher f_{rep} in the GHz or multi-GHz range are attractive for low-noise RF generation, as the shot-noise limit in the generated signal resulting from the photo-detection of the comb pulse train is reduced when lowering the number of harmonics of f_{rep} detected in the photodiode bandwidth [1,8]. Methods have been proposed to multiply the repetition rate of MHz-range OFCs using fiber interleavers [8] or a set of filtering optical cavities [2], but the direct use of an OFC with a large repetition rate may simplify the overall setup and make it more compact. The price to pay is that the phase noise of GHz OFCs is generally higher, making them more challenging to properly phase-stabilize [9].

In the traditional approach of locking the OFC to an ultra-stable laser, the achieved phase noise of the generated microwave directly depends on the properties of the optical lock. Moreover, the OFC is dedicated to the RF signal generation, meaning that each low-noise RF signal to be generated requires a specific OFC. To characterize such a system, a second fully independent setup is needed for cross-comparison, which involves its own ultra-stable laser and OFC locked to it, making the evaluation setup fairly sophisticated [3]. In this Letter, we show a proof-of-principle demonstration of ultra-low noise microwave generation realized in a different approach, where the OFC used for optical-to-RF division acts as a transfer oscillator (TO). Hence, it does not require an optical lock of the comb, which can be

fully free-running or locked to an RF reference, providing numerous advantages. In our experiment, optical-to-RF division is demonstrated with an old generation Er:fiber OFC that is only equipped with a slow piezo-electrical transducer (PZT) for f_{rep} locking. The TO method circumvents the demanding optical lock and its associated bandwidth limitation in the division of the phase noise of the optical reference, leading to intrinsically broadband noise division. As the OFC is not phase-locked to the optical reference and remains fully independent, the same OFC can be used to down-convert different optical references to generate distinct RF signals. This makes the microwave signal generation setup more flexible, less complex and more cost-efficient in comparison to the standard approach. The implemented scheme is inspired by the initial work of Telle et al. in Ti:Sapphire mode-locked lasers [10] and by a method that we previously developed to characterize the CEO frequency in an OFC without directly detecting it by traditional *f*-to-2*f* interferometry [11]. It basically consists in cancelling out electrically the phase noise of the OFC in a judicious combination of signals involving the beat-note with the optical reference to be down-scaled, as outlined in Fig. 4.7(a). In contrast to our former implementation where only the noise of f_{rep} was removed to access the frequency noise of f_{CEO}, the noise of both degrees of freedom of the OFC, f_{CEO} and f_{rep}, needs to be cancelled here, such that the resulting output RF signal only contains the down-scaled phase noise of the ultra-stable laser without degradation by the OFC.

The experimental setup is detailed in Fig. 4.7(b). A beat-note signal f_{beat} between a mode ν_N of the OFC and an ultra-stable laser of frequency ν_{CW} is detected in a fast photodiode PD-2 (model DSC40S from Discovery Semiconductors Inc.). The signal centered at 14.95 GHz has a power of 80 dBm and a signal-to-noise ratio (SNR) higher than 50 dB in a 100 kHz resolution bandwidth (RBW).

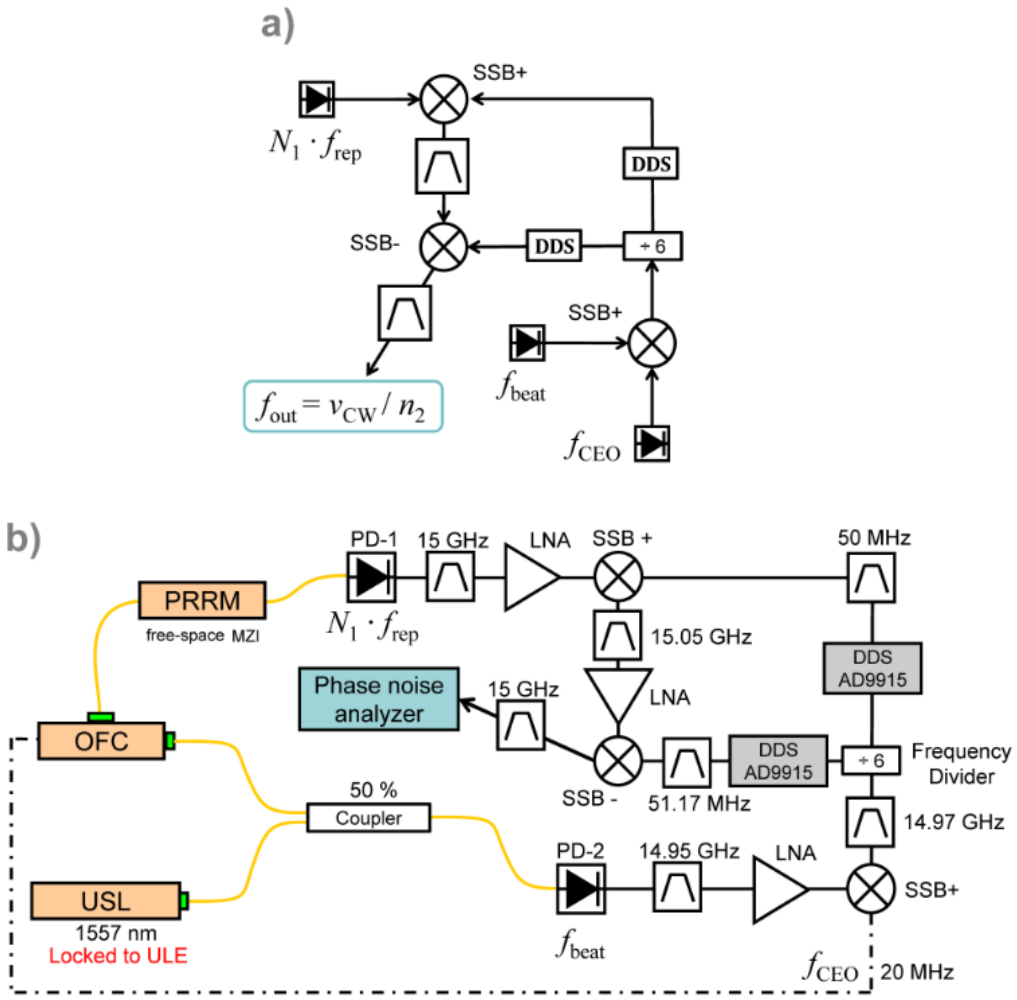

Fig. 4.7: (a) Scheme of principle of microwave synthesis by optical-to-RF division using an OFC as a transfer oscillator. PD: photodiode; SSB+/- : single sideband mixer (upper/lower sideband); DDS: direct digital synthesizer. (b) Detailed implementation of the 2-DDS scheme that improves the filtering of the generated microwave signal at 15 GHz and suppresses spurious peaks. USL: ultra-stable laser; LNA: low-noise amplifier; PRRM: Pulse repetition rate multiplier (free-space Mach-Zehnder interferometer, MZI). Yellow lines represent single-mode fibers.

The continuous-wave (CW) reference laser (model ORION, RIO Inc.) emits at 1557.4 nm and is locked to a high finesse ultra-low thermal expansion (ULE) Fabry-Pérot cavity using the Pound-Drever-Hall locking scheme [12], resulting in a linewidth of a few Hz. The OFC is an Er:fiber

comb with 250 MHz repetition rate mode-locked by nonlinear polarization rotation (FC1500 from Menlo Systems), which is significantly noisier than state-of-the-art modern fiber combs, such as based on a nonlinear amplifying loop mirror [6,13] or on difference frequency generation for passive phase stabilization [14]. The repetition rate can be locked via a slow PZT with a typical loop bandwidth lower than 1 kHz, and f_{CEO} via the pump current with a bandwidth in the range of 10 kHz. The beat-note signal f_{beat} is filtered with a narrowband RF cavity filter (3-dB bandwidth of ~70 MHz centered at 14.95 GHz) and is amplified to ~15 dBm in a set of four low-noise amplifiers (GNA 157F, RF Bay Inc.). They have a negligible contribution to the phase noise of the final RF signal as their additive phase noise is orders of magnitude lower than the noise of the ultra-stable laser present in the beat signal. The frequency of the CW laser and the comb repetition rate are tuned such that the beat frequency corresponds to $f_{beat} = \nu_N - \nu_{CW} = N \cdot f_{rep} - |f_{CEO}| - \nu_{CW}$ with a comb mode N in the order of 768,000. The sign of f_{CEO} in this expression results from its negative value that was experimentally determined. In parallel, the CEO beat is detected at 20 MHz with 40-dB SNR in 100-kHz RBW using a standard f-to-2f interferometer and is amplified to ~15 dBm. A single-sideband (SSB) mixer (model SSB 0618LXW, Marki Microwave Inc.) is used to subtract f_{CEO} from f_{beat} and produces a CEO-free beat signal $f_{beat}^{\text{CEO-free}} = N \cdot f_{rep} - \nu_{CW}$ centered at 14.97 GHz. Similar to our previous implementations [11,15], the resulting CEO-free beat signal needs to be frequency-divided by a large fractional number $n_2 = N/N1$ (where $N1$ defines the approximate output microwave frequency and we chose here $N1 = 60$ for an output signal of ~15 GHz). We replaced the combination of cascaded frequency pre-scalers that we used before and which led to a fixed integer division factor of $N2 = 12{,}800$ by a direct digital synthesizer (DDS, model AD9915, Analog Devices) to get a finer division. As the input frequency range of the DDS is limited to 2.5 GHz, the CEO-free beat frequency is first divided by a factor of 6 using a pre-scaler (FPS-6-15, RF-Bay Inc.). The DDS is adjusted to output a signal

matching its input frequency divided by a factor of ~12,800/6 ≈ 2,130, leading to a down-scaled CEO-free beat signal at 1.17 MHz. The residual OFC noise in this signal corresponding to ~60 times the phase fluctuations of f_{rep} is removed in a subsequent stage by mixing it with the 60th harmonic of f_{rep}, separately detected with another fast photodiode PD-1. This signal is band-pass filtered using a narrowband RF cavity filter (~70-MHz bandwidth centered at 15 GHz) and amplified. Even with the use of an SSB mixer, multiple peaks appear in the output signal at 15 GHz ± n ·1.17 MHz due to the high difficulty to filter out the only peak of interest (15 GHz ± n ·1.17 MHz in our case). Hence, the resulting signal is affected by strong spurious noise peaks at high Fourier frequencies (at harmonics of 1.17 MHz, see Fig. 4.8, 1-DDS grey curve). We circumvented this issue by the use of the so-called 2 DDS scheme depicted in Fig. 4.7(b). Here, the second division stage of the CEO-free beat signal at ~2.5 GHz is realized using two DDS in parallel delivering signals at 50 MHz and 51.17 MHz, respectively, such that their difference (1.17 MHz here) matches the output frequency corresponding to the targeted division factor n_2. The signal of the first DDS is mixed with 60· f_{rep} using an SSB+ mixer to produce an intermediate signal at ~15 GHz + 50 MHz where spurious components of the DDS signal can be easily filtered out using a narrowband RF filter (~70-MHz bandwidth centered at 15.05 GHz). Another SSB- mixer is used to cancel out the residual noise contribution of f_{rep} by combining the previous signal at ~15.05 GHz with the output of the second DDS (51.17 MHz). The resulting signal at 14.99883 GHz is efficiently isolated owing to the 51.17-MHz separation of spurious peaks. This output signal contains the phase noise of the ultra-stable laser electrically-divided by a factor of n_2 ≈ 12,800 without any locking bandwidth limitation as the OFC remains fully independent from the optical reference. The contribution from the OFC noise is efficiently removed by the TO setup. The implemented 2-DDS scheme leads to a clean signal without undesirable noise peaks occurring when performing the frequency division using a single DDS (see Fig. 4.8). As a first proof-of-principle demonstration of the

proposed optical-to-RF division, we characterized the phase noise of the generated signal using a cross-correlator phase noise analyzer (Rohde & Schwarz FSWP26). We performed more than two hours of measurement corresponding to 1,100 cross-correlations at 1-Hz offset frequency and up to 10^7 above 100 kHz. However, the measurement is still instrument-limited below 300 Hz. A higher number of cross-correlations might be used to lower the noise floor, but increasing it up to 10'000 at 1-Hz offset frequency would only bring an improvement of ~5 dB and would last for more than 24 h, which is still insufficient to reach the projected noise level of the optical reference (Fig. 4.9). Hence, we restricted the evaluation to this cross-correlation measurement in this proof-of-principle demonstration, but this result does not constitute an absolute assessment of the ultimate performance of the method.

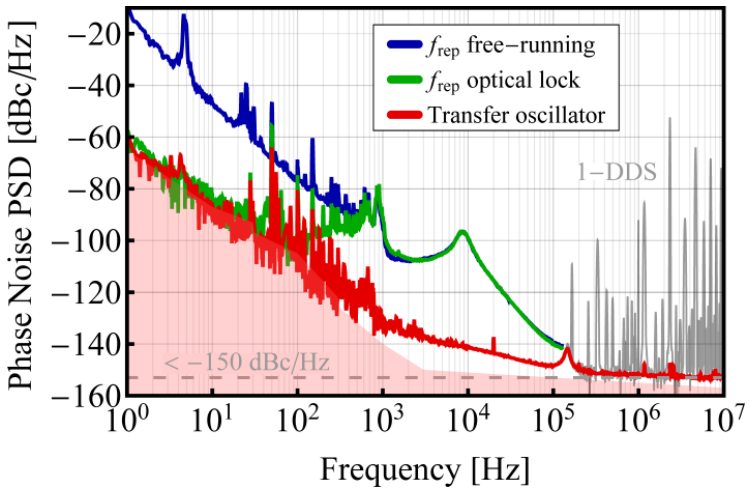

Fig. 4.8: Single sideband phase noise power spectral density (PSD) of a 15 GHz RF signal ($60 \cdot f_{rep}$) generated by different means with a self-referenced OFC: free-running f_{rep} (blue), f_{rep} optically-locked (green), OFC used as TO with the 2-DDS scheme (red). The phase noise obtained with the 1 DDS scheme is shown for comparison at high frequency (grey). The red area shows the instrumental noise floor.

We compared the phase noise of the generated RF signal to the traditional method of optically-locking the OFC in the same conditions and using the same OFC, where the optical lock was achieved with the cavity PZT. Results are displayed in Fig. 4.8. Both curves are limited to the same

level at Fourier frequencies below ~100 Hz, which matches the instrumental noise floor. From 100 Hz up to more than 100 kHz, the benefit of the TO method is clearly visible. The noise of the ultra-stable laser is not transferred to the generated microwave signal with the traditional optical lock as it is out of the limited locking bandwidth of the OFC. In contrast, the noise of the optical reference is down-scaled up to a much higher Fourier frequency using the TO method, even if some excess flicker phase noise seems to be present between 1 kHz and 100 kHz, whose origin has not yet been identified. Notably, the servo bump of the CEO stabilization that couples to the noise spectrum of the repetition rate [16] at around 10 kHz is strongly suppressed, demonstrating the high rejection of the OFC noise. In our initial measurements, we noticed an imperfect cancellation of the OFC noise, especially visible at this servo bump. The reason is that the two signals f_{beat} and $60 \cdot f_{\mathrm{rep}}$ are detected with two different photodiodes and using two distinct outputs of the OFC. With the subsequent use of several electronic devices (filters, dividers, mixers), a time delay may occur between the two signals, leading to incomplete noise compensation when they are combined. The most detrimental element was identified to be the 15.05-GHz band-pass filter in-between the two DDSs. A higher noise rejection was reached by minimizing the relative delay between these two signals by adding a 4.8-m long SMA cable at the output of the second DDS, which led to the result displayed in Fig. 4.8.

We investigated the ultimate phase noise limit arising in the 2-DDS TO setup by measuring the additive phase noise induced in the two branches of the scheme shown in Fig. 4.7(b): (i) the detection of the high harmonic of the repetition rate (upper branch) and (ii) the frequency division of the optical beat-note signal (lower branch). The results displayed in Fig. 4.9 show that the frequency division performed with the DDSs is by far not a limitation with the present projected noise of our ultra-stable laser. This could become a limitation at some Fourier frequencies if an improved optical reference with a noise reduced by at least one order of magnitude

was used. The detection of the high harmonic of f_{rep} in the other branch constitutes the main limitation at Fourier frequencies above 100 kHz. It results from the amplified shot-noise in the photo-detection of the pulse train and is similarly present in the traditional method with the optical lock of the OFC [1,8]. To reduce this high frequency noise, we used a pulse repetition rate multiplier (PRRM) composed of a 2-stage free-space in-loop Mach-Zehnder interferometer [8,17]. This increased the RF power of the 15-GHz harmonic signal detected by PD-1 by 10 dB, reaching -20 dBm for 4-mW incident optical power. This signal was further amplified by ~25 dB using a low-noise RF amplifier. As a further improvement, we minimized the amplitude to phase (AM-to-PM) noise conversion in the photo-detection. The AM-to-PM conversion factor highly depends on both the incident optical power and the photodiode bias voltage [18] and is strongly reduced at specific values of these parameters. With the used fast photodiode and Er:fiber OFC, we found a high rejection at 4-mW incident power and 9-V bias voltage. Results displayed in Fig. 4.8 and Fig. 4.9 were obtained in these conditions. Only the shot-noise of the photo-detection of the comb pulse train in PD-1 constitutes a limitation in the generated microwave signal, which lies at a level below -150 dBc/Hz in the present configuration. The shot-noise in the detection of the laser-comb beat signal in PD-2 is not limiting as this signal is subsequently divided by the larger number n_2. The shot-noise level could be further lowered by sending more optical power to the photodiode PD-1, or by adding other PRRM stages and generating the microwave signal at 16 GHz instead of 15 GHz.

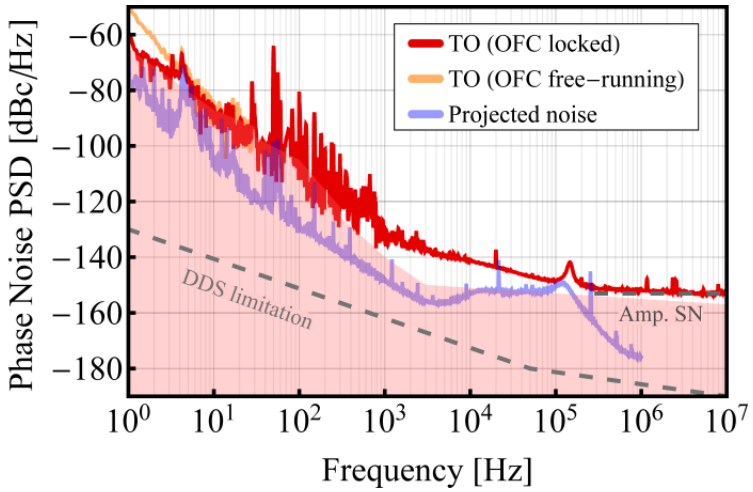

Fig. 4.9: Measured phase noise PSD of the 15-GHz signal generated by the transfer oscillator (TO) method with f_{rep} locked to an RF reference (red curve) and free-running (orange curve). In both cases, f_{CEO} is let free-running. This is in comparison to the projected noise spectrum obtained for a perfect down-scaling of the noise of the optical reference (purple). The additive phase noise floor induced in the two branches of the setup is also displayed (dashed lines): amplified shot-noise (Amp. SN) in the photo-detection of $60 \cdot f_{rep}$ and from the DDS frequency division process. The red area indicates the instrumental noise floor.

The frequency difference between the two DDSs must be precisely adjusted to fully cancel out the phase noise of the comb repetition rate. By slightly tuning one of the DDSs and minimizing the relative time delay between the two signals as previously mentioned, the point of maximum comb noise rejection was found within a tolerance of ±10 kHz on the generated 1.17-MHz signal (i.e., ~1% relative). This enables cost-efficient DDSs with a lower resolution to be used, making the method fairly easy to implement. Within this range, a proper rejection of the comb f_{rep} noise was achieved at all Fourier frequencies in the generated 15-GHz microwave signal when f_{rep} was locked to an RF reference. We also implemented the optical-to-RF division with the TO method using a free-running OFC (see Fig. 4.9). Very similar results were achieved above 5-Hz Fourier frequencies at the present level of evaluation despite the much higher noise of the comb, which demonstrates the proper noise rejection obtained by the TO method.

Only the slow drift of f_{rep} occurring below 5 Hz was more difficult to properly compensate, leading to a slightly higher resulting noise.

Besides the low-noise RF synthesis shown here, the 2 DDS TO scheme can also be used to characterize the phase noise of a free-running CW laser, even with a narrow linewidth, without a lower noise reference laser, but by employing any type of OFC (even free-running). It can also circumvent the main limitation at Fourier frequencies higher than ~10 kHz in our initial implementations of a method to analyze the noise of the free-running CEO signal in an OFC without using *f*-to-2*f* interferometry [11,15].

In conclusion, we have reported a proof-of-principle demonstration of ultra-low noise RF synthesis realized by frequency down-conversion of an optical reference using a TO frequency comb. In contrast to the traditional approach of tightly locking the OFC to the ultra-stable laser, the proposed method does not make use of any optical lock and circumvents the need for a high bandwidth actuator. Therefore, it can be implemented with any type of frequency combs. The only constraint, e.g., when using frequency combs with a higher timing jitter, is that the beat signals (CEO and optical beat) have a sufficient SNR to ensure a proper frequency division and a moderate drift such that they remain within the bandwidth of the filters (~±30 MHz is acceptable with the present filters). It is particularly attractive with the use of high repetition rate combs, e.g., produced from mode-locked diode-pumped solid-state lasers [9] or from micro-resonators [19]. In this proof-of-principle demonstration, the ultimate noise of the generated RF signal could not be assessed as it was limited by the instrumental noise floor below ~500 Hz. However, the results were compared to the standard method of locking the OFC to the optical reference using the same OFC, demonstrating its benefits.

Funding

Swiss Commission for Technology and Innovation (CTI) (17137.1 PFMN-NM)

References

[1] T. M. Fortier, M. S. Kirchner, F. Quinlan, J. Taylor, J. C. Bergquist, T. Rosenband, N. Lemke, A. Ludlow, Y. Jiang, C. W. Oates, and S. A. Diddams, Nat. Photonics 5, 425 (2011).

[2] S. A. Diddams, M. Kirchner, T. Fortier, D. Braje, A. M. Weiner, and L. Hollberg, Opt. Express 17, 3331 (2009).

[3] X. Xie, R. Bouchand, D. Nicolodi, M. Giunta, W. Hänsel, M. Lezius, A. Joshi, S. Datta, C. Alexandre, M. Lours, P.-A. Tremblin, G. Santarelli, R. Holzwarth, and Y. L. Coq, Nat. Photonics 11, 44 (2017).

[4] X. S. Yao and L. Maleki, JOSA B 13(8), 1725 (1996).

[5] D. Eliyahu, D. Seidel, and L. Maleki, in Proc. IEEE Int. Freq. Control Symp., 811 (2008).

[6] N. Kuse, C.-C. Lee, J. Jiang, C. Mohr, T. R. Schibli, and M. E. Fermann, Opt. Express 23, 24342 (2015).

[7] W. Hänsel, M. Giunta, K. Beha, M. Lezius, M. Fischer, and R. Holzwarth, in Advanced Solid State Lasers (2015), Paper ATh4A.2

[8] A. Haboucha, W. Zhang, T. Li, M. Lours, A. N. Luiten, Y. L. Coq, and G. Santarelli, Opt. Lett. 36, 3654 (2011).

[9] S. Hakobyan, V. J. Wittwer, P. Brochard, K. Gürel, S. Schilt, A. S. Mayer, U. Keller, and T. Südmeyer, Opt. Express 25, 20437 (2017).

[10] H. R. Telle, B. Lipphardt, and J. Stenger, Appl. Phys. B 74, 1 (2002).

[11] P. Brochard, S. Schilt, V. J. Wittwer, and T. Südmeyer, Opt. Lett. 40, 5522 (2015).

[12] R. W. P. Drever, J. L. Hall, F. V. Kowalski, J. Hough, G. M. Ford, A. J. Munley, and H. Ward, Appl. Phys. B 31, 97 (1983).

[13] W. Hänsel, H. Hoogland, M. Giunta, S. Schmid, T. Steinmetz, R. Doubek, P. Mayer, S. Dobner, C. Cleff, M. Fischer, and R. Holzwarth, Appl. Phys. B 123, 41 (2017).

[14] D. Fehrenbacher, P. Sulzer, A. Liehl, T. Kälberer, C. Riek, D. V. Seletskiy, and A. Leitenstorfer, Optica 2, 917 (2015).

[15] P. Brochard, N. Jornod, S. Schilt, V. J. Wittwer, S. Hakobyan, D. Waldburger, S. M. Link, C. G. E. Alfieri, M. Golling, L. Devenoges, J. Morel, U. Keller, and T. Südmeyer, Opt. Lett. 41, 3165 (2016).

[16] V. Dolgovskiy, N. Bucalovic, P. Thomann, C. Schori, G. Di Domenico, and S. Schilt, J. Opt. Soc. Am. B 29(10), 2944 (2012).

[17] L. Wang, J. Huang, L. Liu, and T. Li, Opt. Express 25, 12161 (2017).

[18] R. Bouchand, D. Nicolodi, X. Xie, C. Alexandre, and Y. Le Coq, Opt. Express 25(11), 12268 (2017).

[19] T. J. Kippenberg, R. Holzwarth, and S. A. Diddams, Science 332(6029), 555 (2011).

4.2.2 Ultralow-noise photonic microwave synthesis using a soliton microcomb-based transfer oscillator

Erwan Lucas[1,], Pierre Brochard[2,*], Romain Bouchand[1], Stéphane Schilt[2], Thomas Südmeyer[2] and Tobias J. Kippenberg[1]*

[1]Institute of Physics, École Polytechnique Fédérale de Lausanne (EPFL), CH-1015 Lausanne, Switzerland.

[2]Laboratoire Temps-Fréquence, Institut de Physique, Université de Neuchâtel, CH-2000 Neuchâtel, Switzerland.

The synthesis of low-noise microwave signals is of both scientific and technological relevance for timing, metrology, communications and radio-astronomy. Today, microwave signals with the lowest reported phase noise are produced by optical frequency-division using mode-locked laser frequency combs [1-4]. However, this technique typically places stringent demands on the comb stabilisation. Moreover, previously-employed combs have repetition rates of few hundreds of megahertz, while the targeted frequencies lie around 10 GHz, requiring pulse interleaving methods. Here, a microresonator-based Kerr frequency comb [5] (soliton microcomb) with a repetition rate of 14 GHz is generated with an ultra-stable pump laser and used to derive an ultralow-noise microwave reference signal, with an absolute phase noise level below -60 dBc/Hz at 1 Hz offset frequency and -135 dBc/Hz at 10 kHz. This is achieved using a novel transfer oscillator approach [6], where the free-running microcomb noise is cancelled via a combination of electronic division and mixing. The presented method opens new prospects for ultralow-noise microwave and sub-terahertz signal generators using modulated laser techniques [7].

The synthesis of microwave signals via photonic systems, such as dual frequency lasers [8], optoelectronic oscillators [9], Brillouin oscillators [10], or electro-optical dividers [11], hold promise for their ability to synthesise

[*] Authors contributed equally to this work

low-noise or widely tunable microwave signals with compact form factor. An additional approach is based on optical frequency division, which makes use of a self-referenced fs-laser comb optically-locked to an ultra-stable laser (USL) with a typical linewidth at the Hz-level [1-4]. If the comb line of index N is tightly phase-locked to the USL (after subtraction of the carrier envelope offset (CEO) frequency f_{CEO}), the comb repetition rate f_{rep} is directly phase-stabilised to the ultra-stable frequency ν_{usl} by frequency division: $f_{rep} = (\nu_{usl} - f_{CEO})/N$. Importantly, owing to the carrier frequency division from optics to microwaves, the absolute phase noise power spectral density is reduced by a factor $N^2 \sim 10^8$.

This method has been mostly implemented using fibre-based fs-lasers with repetition rates of a few hundred megahertz. A fast actuator (e.g., an intra-cavity electro-optic modulator [12]) is required to achieve a tight optical lock of the comb tooth to the optical reference and perform the frequency division over a wide bandwidth. Moreover, a high harmonic of the comb repetition rate must be used to synthesise a microwave signal beyond 10 GHz. Consequently, repetition rate multipliers are typically employed to reduce the impact of shot-noise in the photo-detection of the pulse train, such as optical filtering cavities [13] or fibre interleavers [14], which increases the system complexity. Therefore, the use of frequency combs directly operating at ~10 GHz repetition rates would be highly beneficial, but their optical lock and self-referencing are challenging.

Soliton-based Kerr combs (i.e., microcombs) generated via four-wave mixing in an optical microresonator [15], which naturally produce multi-GHz comb spectra [16-19], are natural candidate in this context. Pumping a cavity resonance with a continuous-wave laser can initiate and sustain a circulating dissipative Kerr soliton [16] (DKS) that is intrinsically phase-coherent with the input pump laser. The resulting comb coupled out of the micro-cavity is inherently perfectly phase-locked to the pump laser. Direct soliton generation from an ultra-stable pump laser holds potential for compact and powerful optical-to-microwave dividers. Although self-

referenced optical microcombs and clocks have been demonstrated [20-22], optical frequency division for low-noise microwave generation using such devices has not been demonstrated so far, mainly due to the complex crosstalk occurring between their two degrees of freedom [21,23] and the limited performance of the available actuators [19,24].

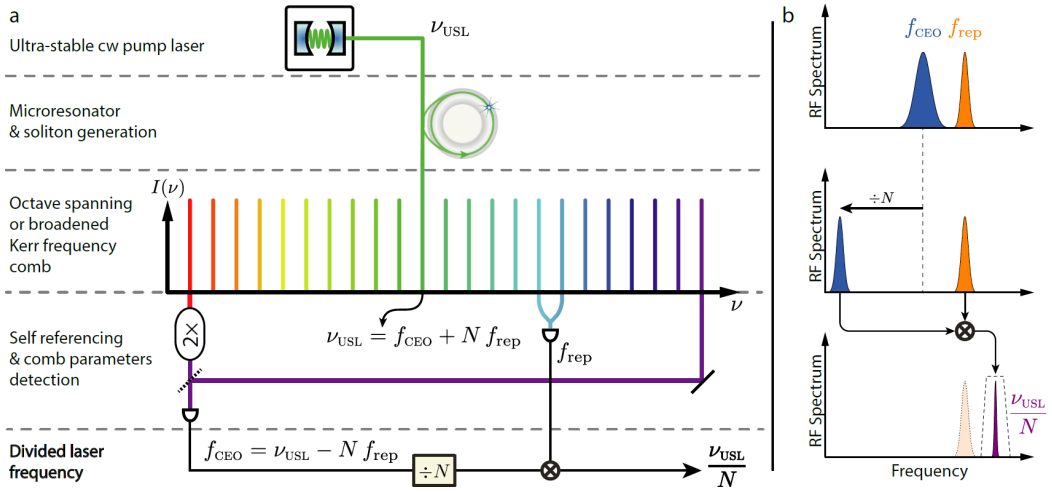

Fig. 4.10: Principle of operation of the Kerr comb-based transfer oscillator for optical-to-microwave frequency division. (a) Schematic illustration of the transfer oscillator applied to a Kerr comb (or electro-optic combs equivalently). (b) Schematic representation of the signal evolution along the electronic division chain leading to the low-noise output signal. The two comb parameters f_{CEO} and f_{rep} are detected. Both parameters can be free-running and fluctuate. The carrier envelope offset (CEO) frequency is electronically divided by a large number N that corresponds to the tooth number of the ultra-stable pump ν_{usl}. After this step, the frequency fluctuations of the divided CEO $f_{CEO}/N = f_{rep} + \nu_{usl}/N$ are dominated by the repetition rate fluctuations. These are removed by mixing f_{CEO}/N with f_{rep} to obtain the division result ν_{usl}/N. A narrow-band filtering is used to reject spurs.

Here, we demonstrate the generation of an ultralow-noise microwave signal using a microcomb-based transfer oscillator method to realise optical-to-microwave frequency division. The transfer oscillator method [6,25] bypasses the need for tight optical phase-locking of the frequency comb to the optical reference. Instead, it relies on an adequate manipulation and combination of signals to cancel the comb phase noise and to provide a broadband electronic division of the USL frequency to the microwave domain. The frequency division by a large factor N is performed

electronically, thus removing the need for high locking bandwidth actuators. In this work, the USL is used to pump the microresonator and inherently constitutes a tooth of the resulting frequency comb. We show how to extend the transfer oscillator technique to exploit this salient feature of microcombs (or equivalently of electro-optic combs [26]). In this first proof-of-principle demonstration, we achieved a measured single-sideband phase noise of -110 dBc/Hz at 200 Hz offset from the 14.09 GHz carrier, which is 15 dB below the lowest phase noise microresonator-based photonic oscillator reported so far [27], demonstrating the potential of this approach.

The working principle of our method is illustrated in Fig. 4.10. A microresonator pumped by a sub-Hz-linewidth USL at frequency ν_{usl} generates a soliton-Kerr comb with a GHz-range repetition rate f_{rep} that is set by the resonator free spectral range (FSR). The reference laser is part of the frequency comb (line N) such that its frequency can be written as $\nu_{usl} = f_{CEO} + N f_{rep}$. The detection of the CEO frequency (for example via f-to-2f interferometry [28,29] or with an auxiliary self-referenced comb as in the present work) is followed by electronic division by means of a combination of frequency pre-scalers and direct digital synthesisers (DDS). The final step consists of mixing the divided CEO signal with the repetition rate, which yields

$$f_{\text{signal}} = \frac{f_{\text{CEO}}}{N} + f_{\text{rep}} = \frac{\nu_{\text{usl}}}{N} \tag{24}$$

Importantly, this process can be carried out with a free-running Kerr comb and circumvents the need for a high-bandwidth optical lock.

The soliton-Kerr comb is generated by pumping a crystalline magnesium fluoride (MgF_2) microresonator with an FSR of 14.09 GHz using a 1553 nm diode laser. After soliton generation, the pump laser is phase-locked to a sub-Hz-linewidth USL (Menlo Systems ORS1500) at a frequency detuning of ~1.7 GHz (green box in Fig. 4.11, a detailed description is provided in the supplementary information (SI) [45]). To ensure the long-term stable operation of the Kerr comb and prevent the decay of the soliton, the

microresonator resonance is slowly locked to the pump laser with an effective-detuning stabilisation, achieved via a sideband Pound-Drever-Hall (PDH) lock [30], which feedbacks on the input pump power as well as on an LED shining on the crystal for thermal actuation of the resonance (purple box in Fig. 4.11 , see details in the SI[45]). The detuning setpoint was carefully optimised in order to minimise the noise of the Kerr comb repetition rate f_{rep}^{K} at offset frequencies beyond ~100 Hz (see the Methods section and Fig. 4.10). However, the residual thermal drift of the resonator degrades the performance at lower offset frequencies.

The used crystalline MgF_2 micro-comb features a relatively narrow spectrum that prevents a direct detection of its CEO frequency (Fig. 4.11). The self-referencing of Kerr combs remains highly demanding due to the high repetition rate, low optical power, and fairly long pulse duration (225 fs here) resulting in a low peak intensity that makes the spectral broadening for *f*-to-2*f* interferometry challenging [21,31]. Therefore, we implemented an indirect detection scheme using an auxiliary self-referenced fibre-laser frequency comb [32] with a repetition rate f_{rep}^{aux} =251.7 MHz in this first proof of concept. The relative CEO frequency Δf_{CEO} between the two combs can be retrieved from their beatnote, as schematised in Fig. 4.11, provided that their repetition rates are harmonically phase-locked, i.e., $f_{rep}^{K} = M f_{rep}^{aux}$ (superscripts 'K' and 'aux' refer to the Kerr and auxiliary comb, respectively). In such case, the repetition rate noise contributions compensate each other in the beat signal between the two combs, which thus only contains the relative noise between the two CEO frequencies Δf_{CEO} (see Fig. 4.11). The Kerr comb CEO frequency is obtained by subtracting the CEO frequency of the auxiliary comb f_{CEO}^{aux} detected with an *f*-to-2*f* interferometer (see Fig. 4.11) and corresponds to $f_{CEO}^{K} = \Delta f_{CEO} - f_{CEO}^{aux} = \nu_{pump} - N f_{rep}^{K}$.

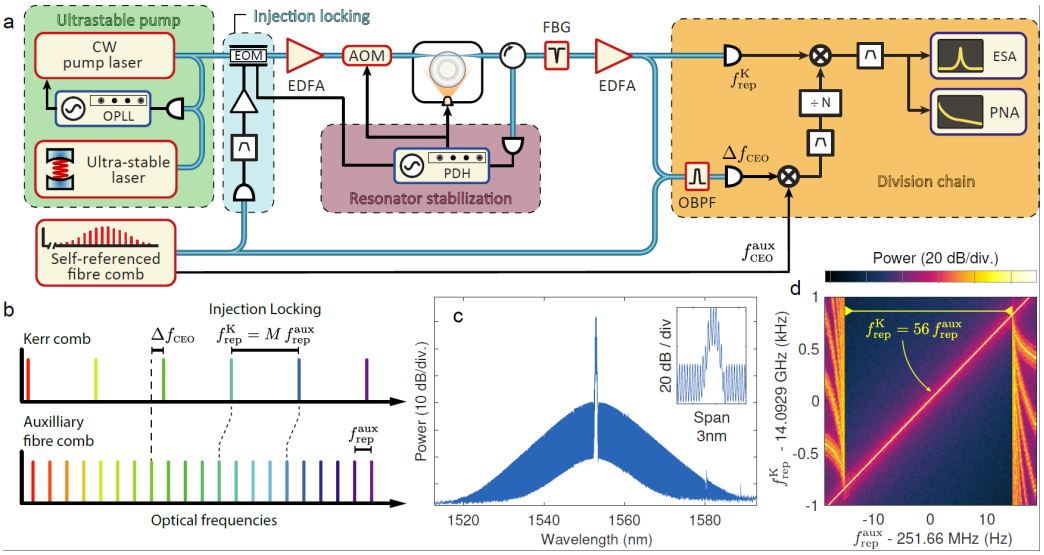

Fig. 4.11: Simplified experimental setup and principle of operation with the auxiliary comb (a) Setup for Kerr comb-based optical frequency division. The details of each highlighted block can be found in the supplementary information. EDFA, Er-doped fibre amplifier; AOM, Acousto-optic modulator; EOM, Electro-optic modulator; FBG, Fibre Bragg grating for pump rejection; OBPF, Optical band-pass filter; OPLL, Optical phase lock loop; PDH, Pound-Drever-Hall lock; DDS, Direct digital synthesiser; PNA, Phase noise analyser; ESA, Electrical spectrum analyser. (b) The harmonic relation of the repetition rate of both combs is ensured via injection locking for M = 56. The heterodyne beat between the two combs thus yields the difference of their carrier-envelope offset frequency (Δf_{CEO}). (c) Optical spectrum of the soliton-based Kerr comb. The inset shows the phase modulated sidebands around the pump laser tone that ensure the injection-locking. (d) Radio-frequency (RF) spectrogram showing the injection-locking effect between the Kerr comb repetition rate f_{rep}^{K} and the 56th harmonic of the auxiliary comb repetition rate f_{rep}^{aux}, obtained by changing the frequency of faux rep (harmonic power ~ 11 dBm applied to the EOM).

The mutual phase-locking of the comb repetition rates is achieved via soliton injection-locking [33]. The harmonic M=56 of the repetition rate of the auxiliary comb (at 14.093 GHz) is detected, filtered and amplified to phase-modulate the pump light (blue box in Fig. 4.11). This frequency is very close to the native Kerr line spacing, which gets injection-locked to this drive signal. Therefore, both repetition rates are strongly correlated over a bandwidth of ~2 kHz.

The Kerr comb CEO signal, indirectly obtained as previously described, is detected at low frequency (MHz-range) and filtered to match the bandwidth of the injection locking of the repetition rates (not represented in Fig. 4.11, see SI[45]). After up-mixing to 15 GHz, it is frequency-divided by a large pre-determined factor $N \approx 13{,}698$ and is subtracted to the separately-detected repetition rate f_{rep}^{K} to obtain the frequency-divided signal of the ultra-stable pump laser: $\nu_{pump}/N = f_{CEO}^{K}/N + f_{rep}^{K}$ (orange box in Fig. 4.11). The overall division of the Kerr comb CEO signal by the factor N is realised with a frequency pre-scaler followed by two parallel DDS, which offers improved filtering capabilities in the electronic division [6]. This second stage division with the DDS allows for a precise non-integer frequency division factor and leads to a clean single-tone output signal corresponding to the frequency-divided USL (see Fig. 4.11). The detailed description of the frequency division chain is provided in the SI[45]. The overall division factor N was straightforwardly determined experimentally, without prior knowledge of the optical frequency of the ultra-stable pump laser, by measuring the frequency change of the generated microwave signal corresponding to a small variation (140 Hz) of the Kerr comb repetition rate for different programmed division factors N (see Fig. 4.11). This simple measurement also provides an accurate determination of an optical comb line index N that can be useful for absolute optical frequency measurements.

The phase noise of the generated ultralow-noise 14.09 GHz signal was measured with a cross-correlator phase noise analyser (Fig. 4.12). It reaches -110 dBc/Hz at 200 Hz Fourier frequency, 15 dB below the lowest phase noise microresonator-based photonics oscillator [27] at 10 GHz. The phase noise is below -135 dBc/Hz at 10 kHz and -150 dBc/Hz at around 1 MHz, showing that the intrinsic good short-term purity of the soliton Kerr comb is preserved. The calculated shot-noise predicts a noise floor at -152 dBc/Hz (thermal noise floor ~-170 dBc/Hz). At 1 Hz offset, the measurement is limited by the instrumental noise floor even with 3000 cross correlations.

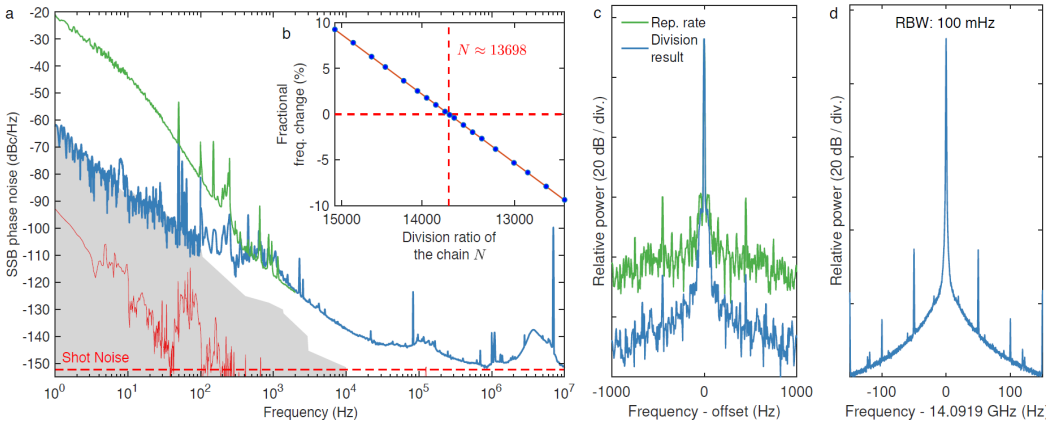

Fig. 4.12: Experimental result of the signal generated by optical-to-microwave division (a) Absolute single-sideband (SSB) phase noise of the 14.09 GHz signal generated by optical-to-microwave division of the USL via the Kerr comb transfer oscillator (blue) and obtained directly from the Kerr comb repetition rate (green) for comparison. The sensitivity limit of the phase noise analyser (Rohde & Schwarz FSWP, 3000 cross correlations applied at 1 Hz) is indicated by the grey shaded area. The red line is the limit inferred from the optical phase noise of the USL, assuming an ideal noiseless division. (b) Precise determination of the optimal division factor N corresponding to the zero crossing of the linear fit (solid line) of the measured relative frequency change of the generated RF signal for a small variation of the repetition rate (dots). (c) Comparison between the RF spectra of the Kerr comb repetition rate and the optical-to-microwave frequency division result. The resolution bandwidth (RBW) is 5 Hz. (d) RF spectrum of the frequency-divided output signal, the RBW is 100 mHz. The data was acquired with the IQ demodulation mode of the spectrum analyser.

Nevertheless, the transfer oscillator offers an improvement by at least 40 dB compared to the direct detection of the Kerr comb repetition rate (despite the resonator being stabilised to the USL), showing its ability to cancel the residual thermal drifts of the Kerr cavity. The technical limitations of the measurement, at low offset frequency, make it difficult to directly compare the method with state-of-the-art optical frequency-division using mode-locked lasers. Nevertheless, at high Fourier frequencies, our results surpass some of the first demonstrations of optical frequency division [3], even if no optimisation has been performed on the photodetection side. Over the past 10 years, the development of mode-locked lasers, as well as the improvement of photodetection noise [34,35], led to a reduction of the noise of the generated microwaves by 30 to 40 dB

in some frequency bands [2]. We believe that the transfer oscillator method can follow a similar path, as in particular, the high repetition rates of the Kerr combs should make the photodetection optimisation less stringent.

In summary, we have reported the first optical-to-microwave frequency division using a Kerr comb as transfer oscillator. This demonstrates the potential of this method in microwave photonics and enlarges its previously reported implementation with low repetition rate mode-locked lasers. The approach presented here can be further implemented with electro-optic combs, where self-referencing and feedback control were recently achieved [26,36]. Although this proof-of-principle experiment required an auxiliary comb to obtain the CEO frequency of the Kerr comb, directly self-referenced microcombs are technologically feasible in silicon nitride (Si_3N_4) photonic-chips [37]. While octave-spanning comb spectra have been achieved using dispersion control [7,22], these implementations used THz repetition rates to cover such a large spectral range, which made photodetection of the repetition rate practically impossible. Nonetheless, the residual phase noise of these combs has been shown to be suitable for frequency division [38]. Recent improvements of integrated resonators have enabled soliton microcombs with K- and X-band (20 and 10 GHz) repetition rates in integrated resonators [39]. However, the achieved spectral spans, although wider than in the crystalline case, are far from covering one octave. Pulsed pumping [40,41] appears as a promising approach to enable octave spanning microcombs with detectable microwave repetition rates. This approach uses synchronous pumping of the microresonator with picosecond pulses to generate a soliton with a much shorter duration and a spectrum that can cover an octave, similar to enhancement cavities [42]. It can be seen as a hybrid between an electro-optic (EO) comb and a microcomb, with the advantage that the spectral enlargement of the EO comb is performed in cavity and is therefore directly filtered. Crucially, even if the free-running phase noise of these integrated microcombs is typically higher than in the

crystalline platform used in this work [39,43,44], the additional noise is cancelled over a broad frequency range via the transfer oscillator method that constitutes a powerful tool for low-noise frequency division without the need for a very low-noise comb. The free-running comb operation and the maturity of RF components, which can be suitably integrated, promise robust device operation. Furthermore, improvements in resonator actuation, using micro-heaters [19], piezoelectrical transducers [45,46], or the electro-optic effect [47,48], allow direct soliton generation with the stable laser via resonator tuning, alleviating the need for an optical phase-lock loop and greatly simplifying the detuning stabilisation. If a lower stability level is acceptable, simpler and more compact low-noise lasers can be employed [49-51] instead of the USL. We believe that the presented transfer oscillator method holds promising potential for ultralow-noise high-frequency generators with a new generation of compact photonic-based systems [52] for radar applications [53], high frequency telecommunications [54] and time-frequency metrology [3].

Methods

Operating conditions. The pump power after the EOM is ~10 mW and is amplified to ~250 mW with an EDFA. The power level after the AOM (see Fig. 4.11) is set to ~210 mW. After comb generation and residual pump rejection with a fibre Bragg grating, the comb power of ~1 mW is amplified to ≳5 mW. The largest part of this power (90%) is sent onto a high power handling photodiode (Discovery Semiconductors DSC40S, generating a photocurrent of 5.12 mA and a microwave power of ~-7.4 dBm), while the remaining fraction is used for the intercomb beatnote detection. The shot noise level is estimated for a CW laser detection, based on the photocurrent and microwave power. The 56th harmonic of the auxiliary comb repetition rate f_{rep}^{aux} at 14.09 GHz is detected, selected using a narrow band-pass filter and amplified to ~19 dBm. This signal drives the phase modulator and creates an estimated phase deviation of ~1.4 rad. The injection-locking

range of the Kerr comb repetition rate [33] spans ≳2 kHz and the locking bandwidth is ~2 kHz.

Resonator characteristics. The MgF_2 whispering gallery mode resonator was fabricated via precision diamond turning and hand polishing on a lathe. The intrinsic linewidth of the pumped mode is ~80 kHz (intrinsic quality factor of 2.4×10^9). The evanescent coupling to the resonance is achieved via a tapered optical fibre. The fibre is operated in contact with the resonator to dampen its vibrations. Careful adjustment of the fibre position is required to maximise the coupling rate and increase the out-coupled comb power. The loaded resonance linewidth is estimated at ~2.4 MHz. The detuning setpoint was chosen to minimise the noise of the Kerr comb repetition rate, as described in the next section.

Soliton noise minimisation. The laser-resonator detuning $\delta=\nu_{cav}-\nu_{laser}$ is known to have a major impact on the noise and stability of Kerr frequency combs. This parameter not only sets the soliton pulse duration [55], but was also shown to modify the repetition rate frequency through the Raman self-frequency shift [56,57] $\Omega_{Raman}(\delta)$ and the soliton recoil Ω_{recoil} corresponding to dispersive wave emission [55,58]. Indeed, these two effects lead to an overall shift of the spectral centre of the soliton (i.e., the soliton spectral maximum relative to the pump frequency) $\Omega=\Omega_{Raman}+\Omega_{recoil}$, which induces in turn a change in the group velocity of the pulse and therefore of the repetition rate according to [59]

$$f_{\mathrm{rep}}^{\mathrm{K}} = \frac{1}{2\pi}\left(D_1 + \frac{D_2}{D_1}\,\Omega(\delta)\right), \tag{25}$$

where $D_1/2\pi$ = 14.09 GHz is the resonator FSR and $D_2/2\pi$ = 1.96 kHz is the group velocity dispersion (GVD) parameter at the pump frequency [60]. Thus, residual laser-resonator detuning noise can degrade the spectral purity of the repetition rate [23]. A solution to this problem was already identified by Yi et al. [58], who proposed to use the balance of dispersive-wave recoil and Raman-induced soliton-self-frequency shift to enhance the repetition-rate stability of a silica wedge-based Kerr comb. A similar

concept is applied here to minimise the repetition rate noise of the crystalline MgF_2 microresonator-based comb. Importantly, in MgF_2, the Raman self frequency shift can be neglected, due to the very narrow gain bandwidth, and the soliton shift is dominated by the soliton recoil $\Omega \approx \Omega_{recoil}$.

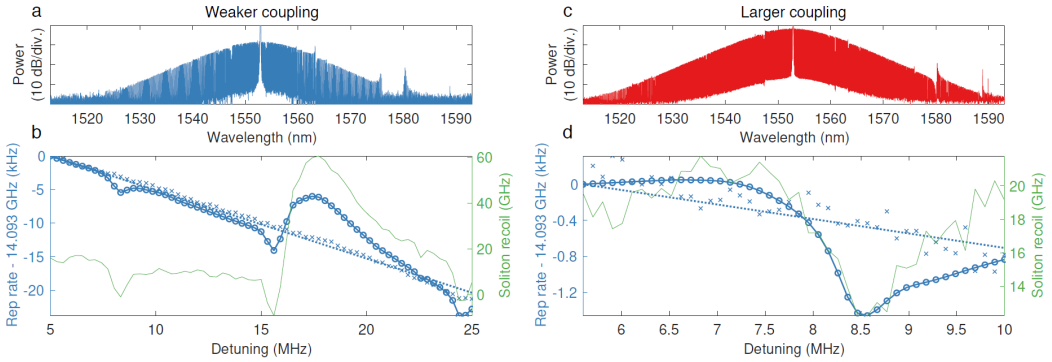

Fig. 4.13: Optimisation of f_{rep}^{K} phase noise (a) Soliton spectrum for lower coupling case (Detuning 10 MHz). (b) Evolution of the repetition rate (blue, solid) and of the soliton recoil ($\Omega/2\pi$) retrieved by fitting the optical spectrum (green), in the lower coupling case. The blue crosses and dashed line show the residual repetition rate change after subtraction of the recoil induced shift (using eq. (24)). (c) Soliton spectrum for larger coupling case (Detuning 10 MHz). (d) Evolution of the repetition rate (blue, solid) and of the soliton recoil ($\Omega/2\pi$) retrieved by fitting the optical spectrum (green), in the larger coupling case. The blue dashed line shows the residual repetition rate change after subtraction of the recoil induced shift (using eq. (24)).

We measured the variation in repetition rate of the soliton comb as a function of detuning in two coupling conditions (weak and large coupling). The coupling rate was modified by changing the position of the tapered fibre along the resonator. The detuning was scanned (forward and backward) by changing the PDH modulation frequency, while the phase lock loop offset frequency was adapted accordingly to keep the total frequency offset between the USL and the microresonator resonance constant. At each detuning point, the optical spectrum was acquired and the repetition rate frequency f_{rep}^{K} was counted. The results are displayed in Fig. 4.13. The phase modulation at the cavity FSR used for injection-locking was disabled in this measurement.

The weak coupling of the resonator allows for a relatively wide detuning range to be accessed (5 to 25 MHz, see Fig. 4.13). Over this span, the repetition rate changes in total by 22 kHz, but not linearly. The non-monotonic evolution of f_{rep}^{K} (δ) is caused by the soliton recoil induced by dispersive waves through avoided mode crossings [55,58,61]. The soliton shift $\Omega/2\pi$ is extracted by fitting the optical spectrum with a sech² function and the associated repetition rate variation can be estimated using eq. (24). Interestingly, after subtracting this contribution, the residual shift of the repetition rate follows a linear trend with a slope of ~-1 kHz/MHz. This significant variation is independent from any recoil-associated effect and could originate from more complex forms of avoided modal crossings, or third order dispersion, although we observed that the value of this slope changes with the coupling as detailed below.

Increasing the coupling rate of the resonator (see Fig. 4.13) shrinks the accessible detuning range (5.5 to 10 MHz) and radically changes the dependence of f_{rep}^{K} with δ. The overall variation is reduced to ~1.4 kHz and is dominated by solitonic recoil. Once this contribution is subtracted, the residual slope is on the order of ~-160 Hz/MHz, which is very close to the value expected from the nonlinear self-steepening effect [62].

Quiet operation point. More notably, under this larger coupling condition, the relation f_{rep}^{K} (δ) exhibits a stationary point around δ = 7 MHz, where the coupling of pump-laser frequency noise into the soliton repetition rate is expected to be minimal since $\partial f_{rep}^{K} / \partial\delta \approx 0$. To verify this prediction, the phase noise of the detected soliton pulse train was measured at different detuning points. The pump laser was phase-modulated by a low frequency tone at 9 kHz to provide a reference point. Furthermore, instead of phase-locking the pump laser to the USL, the PDH feedback was applied to the pump laser current in these measurements, and the resonator was slowly stabilised to the USL via power and thermal feedback. The larger laser noise obtained in this case helps visualising its impact on the repetition rate frequency and could be calibrated via a heterodyne measurement with

the USL. The results are displayed in Fig. 4.14 . At the operating point 2, where the slope of f_{rep}^{K} (δ) is maximum, the noise of f_{rep}^{K} follows the same features as the laser noise. Rescaling the laser noise to match the 9 kHz modulation peaks indicates that the optical noise is reduced by 56 dB. Conversely the point 1, where the slope of f_{rep}^{K} (δ) is minimum, corresponds to the lowest optical-to-RF noise transduction (dip in Fig.4.14-a), with a conversion coefficient below -100 dB. As expected, this point yields the lowest achieved phase noise, and it appears that the laser phase noise is no longer the overall limiting factor of the Kerr comb repetition rate noise.

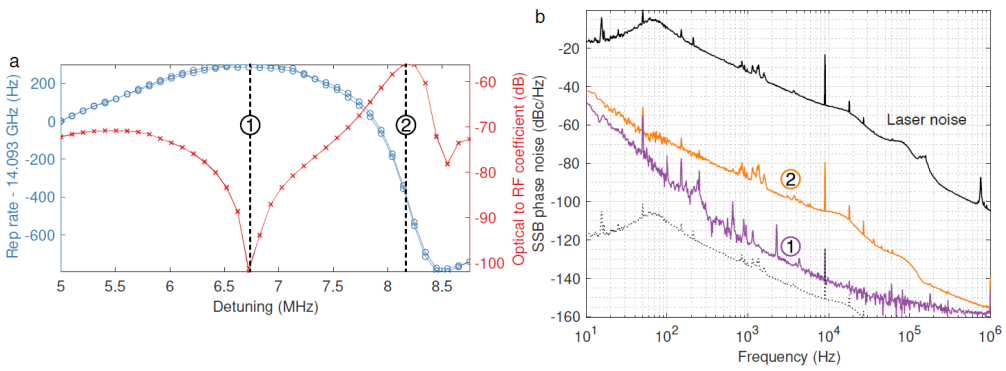

Fig. 4.14: 'Quiet' operating point (a) Evolution of the repetition rate with the detuning (blue) and associated optical phase modulation to RF phase modulation conversion coefficient calibrated with the 9 kHz phase modulation tone on the laser (red). (b) Phase noise spectra of the soliton repetition rate at the two operating points highlighted in (a). The solid black line shows the laser noise (PDH-stabilised to the microcavity). The dashed black line shows the noise of the laser scaled by −100 dB to match the 9 kHz phase calibration tone.

Noise limitations in microcombs. In a nonlinear resonator, the free spectral range $D_1/2\pi$ depends on the circulating optical power. Therefore, the relative intensity noise (RIN) of the pump laser (power P_{in}) eventually induces timing jitter of the repetition rate, according to eq.(24). Assuming a laser on resonance, the self phase modulation induced shift follows [63]

$$\frac{\delta D_1(\omega)}{2\pi} = \underbrace{\left(\frac{D_1}{2\pi}\frac{4\eta\, c\, n_2}{\kappa V_{eff} n_0^2}\right)}_{\alpha} \delta P_{in}(\omega) \tag{26}$$

where $\kappa/2\pi \approx 1.35$ MHz is the cavity energy decay rate, $\eta = \kappa_{ex}/\kappa \approx 0.94$ is the coupling impedance of the resonator (κ_{ex} is the coupling rate), $V_{\text{eff}} \approx 2.32\times10^{-12}$ m^3 is the mode volume, $n_2 = 9\times10^{-21}$ m^2/W is the (Kerr) nonlinear index and $n_0 = 1.37$ is the refractive index. These values yield a conversion coefficient $a \approx 3.8$. We measured the relative intensity noise $S_{\text{RIN}}(f)$ of the pump laser (Fig. 4.15) and the associated induced phase noise was estimated using

$$S^{\phi}_{D_1/2\pi}(f) = \left(\frac{\alpha}{f}P_{\text{in}}\right)^2 S_{\text{RIN}}(f) \tag{27}$$

for the measured input pump power of $P_{in} \approx 212$ mW. The results are displayed in Fig. 4.15. The estimated level matches remarkably the repetition rate phase noise at offsets between 500 Hz and 100 kHz (blue and green curves in Fig. 4.15), suggesting that the pump laser RIN is limiting the performances in this range. The phase noise reaches ~-143 dBc/Hz at 10 kHz, which outperforms any other microresonator-based approach [10,11,27,58,64].

At lower offest frequencies (50 – 500 Hz), the thermal fluctuations and drift of the resonator, which are beyond the power stabilisation bandwidth, are the limiting factor [27,65]. At higher offset frequencies, two noise bumps appear related to the characteristic double resonant response (S and C) of the resonator in the soliton regime [66]. In these resonant features, the transduction of the pump laser noise is enhanced [23]. Beyond 100 kHz offset, the contributions of various factors are more difficult to identify. We observed nonetheless a correlation between the microwave RIN (Fig. 4.15) and the phase noise, which suggests that amplitude-to-phase noise conversion is occurring in the photodiode [67], with a conversion of ~-25 dB (grey curve in Fig. 4.15), which is in agreement with reported values for similar photodiodes [34]. We report here the microwave amplitude noise, as our measurement device offered a better sensitivity in this configuration, but our observations showed that this amplitude noise matches well the optical RIN (measured at DC with a diplexer).

Finally, the continuous-wave shot-noise floor is expected to be at -159 dBc/Hz (photocurrent of 6.85 mA, microwave power of -3.8 dBm). However, we noticed that the phase noise floor of our measurement stands 4.1 dB below this value (at frequency offsets above 20 MHz), while the amplitude noise floor is 6.3 dB above. This imbalance between amplitude and phase needs further investigation and could be related to shot noise correlations in the detection of optical pulses [68,70].

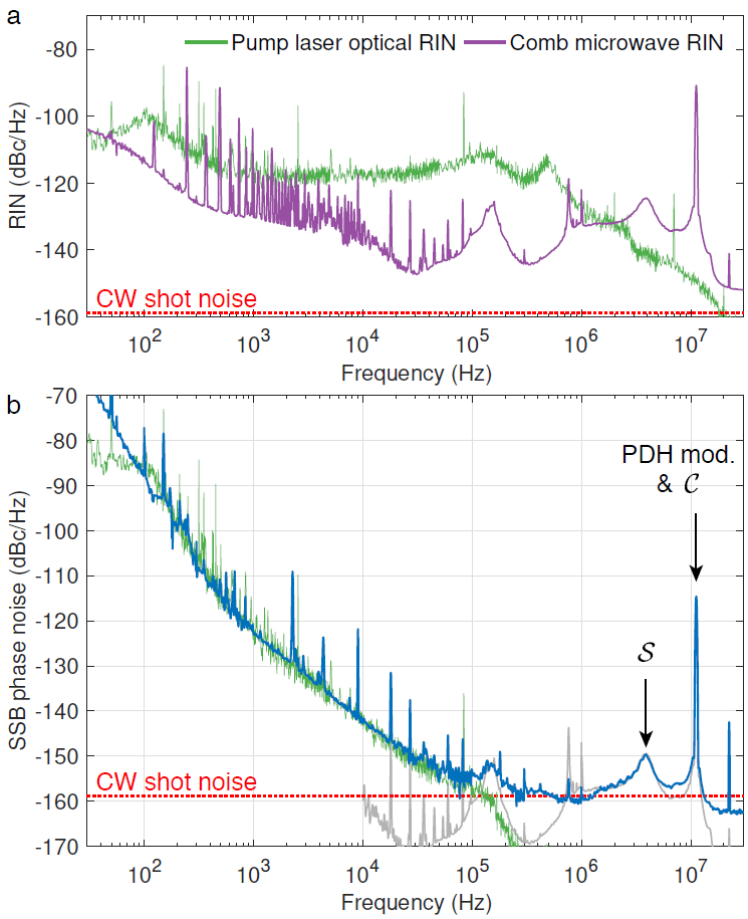

Fig. 4.15: Pump laser RIN and estimated limitation on the phase noise (a) Optical RIN of the pump laser (green) and microwave amplitude noise of the soliton repetition rate (purple). (b) Phase noise spectrum of the repetition rate in the 'quiet' point (blue) and estimated limitation from the pump laser RIN (green). The grey curve corresponds to the estimated AM-to-PM conversion in the photodiode (microwave amplitude noise scaled by −25 dB).

Data availability statement

The data and code used to produce the results of this manuscript will be available on Zenodo upon publication.

Authors contributions

E.L. and P.B. designed the experimental setup and performed the experiments with assistance of R.B. and S.S. E.L. analysed the data and wrote the manuscript, with input from other authors. T.S. and T.J.K. supervised the project.

Acknowledgments

The authors thank M. H. Anderson for the proofreading the manuscript. This publication was supported by the Swiss National Science Foundation (SNF) under grant agreement 161573, as well as Contract W31P4Q-14-C-0050 (PULSE) from the Defense Advanced Research Projects Agency (DARPA), Defense Sciences Office (DSO). This material is based upon work supported by the Air Force Office of Scientific Research, Air Force Material Command, USAF under Award No. FA9550-15-1-0099. E.L. acknowledges support from the European Space Technology Centre, with ESA Contract No. 4000118777/16/NL/GM.

References

[1] T. M. T. M. Fortier, M. S. Kirchner, F. Quinlan, J. Taylor, J. C. Bergquist, T. Rosenband, N. Lemke, A. Ludlow, Y. Jiang, C. W. Oates, and S. a. Diddams, Nature Photonics 5, 425 (2011).

[2] X. Xie, R. Bouchand, D. Nicolodi, M. Giunta, W. Hänsel, M. Lezius, A. Joshi, S. Datta, C. Alexandre, M. Lours, P.-A.

Tremblin, G. Santarelli, R. Holzwarth, and Y. Le Coq, Nature Photonics 11, 44 (2017).

[3] J. Millo, M. Abgrall, M. Lours, E. M. L. English, H. Jiang, J. Guéna, A. Clairon, M. E. Tobar, S. Bize, Y. Le Coq, and G. Santarelli, Applied Physics Letters 94, 141105 (2009).

[4] E. Portuondo-campa, G. Buchs, S. Kundermann, L. Balet, and S. Lecomte, Optics Express 23, 32441 (2015).

[5] T. J. Kippenberg, A. L. Gaeta, M. Lipson, and M. L. Gorodetsky, Science 361 (2018).

[6] P. Brochard, S. Schilt, and T. Südmeyer, Optics Letters 43, 4651 (2018).

[7] M. H. P. Pfeiffer, C. Herkommer, J. Liu, H. Guo, M. Karpov, E. Lucas, M. Zervas, and T. J. Kippenberg, Optica 4, 684 (2017).

[8] G. Pillet, L. Morvan, M. Brunel, F. Bretenaker, D. Dolfi, M. Vallet, J.-P. Huignard, and A. Le Floch, Journal of Lightwave Technology 26, 2764 (2008).

[9] L. Maleki, Nature Photonics 5, 728 (2011).

[10] J. Li, H. Lee, and K. J. Vahala, Nature Communications 4, 2097 (2013).

[11] J. Li, X. Yi, H. Lee, S. a. Diddams, and K. J. Vahala, Science 345, 309 (2014).

[12] D. D. Hudson, K. W. Holman, R. J. Jones, S. T. Cundiff, J. Ye, and D. J. Jones, Optics Letters 30, 2948 (2005).

[13] S. A. Diddams, M. Kirchner, T. Fortier, D. Braje, A. M. Weiner, and L. Hollberg, Optics Express 17, 3331 (2009).

[14] A. Haboucha, W. Zhang, T. Li, M. Lours, A. N. Luiten, Y. Le Coq, and G. Santarelli, Optics letters 36, 3654 (2011).

[15] A. L. Gaeta, M. Lipson, and T. J. Kippenberg, Nature Photonics 13, 158 (2019).

[16] T. Herr, V. Brasch, J. D. Jost, C. Y. Wang, N. M. Kondratiev, M. L. Gorodetsky, and T. J. Kippenberg, Nature Photonics 8, 145 (2013).

[17] X. Yi, Q.-F. Yang, K. Y. Yang, M.-G. Suh, and K. Vahala, Optica 2, 1078 (2015).

[18] V. Brasch, M. Geiselmann, T. Herr, G. Lihachev, M. H. P. Pfeiffer, M. L. Gorodetsky, and T. J. Kippenberg, Science 351, 357 (2015).

[19] C. Joshi, J. K. Jang, K. Luke, X. Ji, S. A. Miller, A. Klenner, Y. Okawachi, M. Lipson, and A. L. Gaeta, Optics Letters 41, 2565 (2016).

[20] J. D. Jost, T. Herr, C. Lecaplain, V. Brasch, M. H. P. Pfeiffer, and T. J. Kippenberg, Optica 2, 706 (2015).

[21] P. Del'Haye, A. Coillet, T. Fortier, K. Beha, D. C. Cole, K. Y. Yang, H. Lee, K. J. Vahala, S. B. Papp, and S. A. Diddams, Nature Photonics 10, 516 (2016).

[22] Z. L. Newman, V. Maurice, T. Drake, J. R. Stone, T. C. Briles, D. T. Spencer, C. Fredrick, Q. Li, D. Westly, B. R. Ilic, B. Shen, M.-G. Suh, K. Y. Yang, C. Johnson, D. M. S. Johnson, L. Hollberg, K. J. Vahala, K. Srinivasan, S. A. Diddams, J. Kitching, S. B. Papp, and M. T. Hummon, Optica 6, 680 (2019).

[23] J. R. Stone, T. C. Briles, T. E. Drake, D. T. Spencer, D. R. Carlson, S. A. Diddams, and S. B. Papp, Physical Review Letters 121, 063902 (2018).

[24] S. B. Papp, P. Del'Haye, and S. A. Diddams, Physical Review X 3, 031003 (2013).

[25] H. R. Telle, B. Lipphardt, and J. Stenger, Applied Physics B 74, 1 (2002).

[26] K. Beha, D. C. Cole, P. Del'Haye, A. Coillet, S. A. Diddams, and S. B. Papp, Optica 4, 406 (2017).

[27] W. Liang, D. Eliyahu, V. S. Ilchenko, A. A. Savchenkov, A. B. Matsko, D. Seidel, and L. Maleki, Nature Communications 6, 7957 (2015).

[28] H. Telle, G. Steinmeyer, A. Dunlop, J. Stenger, D. Sutter, and U. Keller, Applied Physics B 69, 327 (1999).

[29] D. J. Jones, S. A. Diddams, J. K. Ranka, A. Stentz, R. S. Windeler, J. L. Hall, and S. T. Cundiff, Science 288, 635 (2000).

[30] J. I. Thorpe, K. Numata, and J. Livas, Optics Express 16, 15980 (2008).

[31] E. S. Lamb, D. R. Carlson, D. D. Hickstein, J. R. Stone, S. A. Diddams, and S. B. Papp, Physical Review Applied 9, 024030 (2018).

[32] H. Tian, N. Raabe, Y. Song, G. Steinmeyer, and M. Hu, Optics Letters 43, 3108 (2018).

[33] W. Weng, E. Lucas, G. Lihachev, V. E. Lobanov, H. Guo, M. L. Gorodetsky, and T. J. Kippenberg, Physical Review Letters 122, 13902 (2019).

[34] R. Bouchand, D. Nicolodi, X. Xie, C. Alexandre, and Y. Le Coq, Optics Express 25, 12268 (2017).

[35] E. Ivanov, J. McFerran, S. Diddams, and L. Hollberg, in Proceedings of the 2005 IEEE International Frequency Control Symposium and Exposition, 2005. (IEEE, 2005) pp. 932–936.

[36] D. R. Carlson, D. D. Hickstein, W. Zhang, A. J. Metcalf, F. Quinlan, S. A. Diddams, and S. B. Papp, Science 361, 1358 LP (2018).

[37] V. Brasch, E. Lucas, J. D. Jost, M. Geiselmann, and T. J. Kippenberg, Light: Science & Applications 6, e16202 (2017).

[38] T. E. Drake, T. C. Briles, D. T. Spencer, J. R. Stone, D. R. Carlson, D. D. Hickstein, Q. Li, D. Westly, K. Srinivasan, S. A. Diddams, and S. B. Papp, , 1 (2018), arXiv:1811.00581.

[39] J. Liu, E. Lucas, A. S. Raja, J. He, J. Riemensberger, R. N. Wang, M. Karpov, H. Guo, R. Bouchand, and T. J. Kippenberg, (2019), arXiv:1901.10372.

[40] E. Obrzud, S. Lecomte, and T. Herr, Nature Photonics 11, 600 (2017).

[41] M. Anderson, N. G. Pavlov, J. D. Jost, G. Lihachev, J. Liu, T. Morais, M. Zervas, M. L. Gorodetsky, and T. J. Kippenberg, Optics Letters 43, 2106 (2018).

[42] N. Lilienfein, C. Hofer, M. Högner, T. Saule, M. Trubetskov, V. Pervak, E. Fill, C. Riek, A. Leitenstorfer, J. Limpert, F. Krausz, and I. Pupeza, Nature Photonics (2019), 10.1038/s41566-018-0341-y.

[43] G. Huang, E. Lucas, J. Liu, A. S. Raja, G. Lihachev, M. L. Gorodetsky, N. J. Engelsen, and T. J. Kippenberg, (2019), arXiv:1901.07112.

[44] T. E. Drake, J. R. Stone, T. C. Briles, and S. B. Papp, 1 (2019), arXiv:1903.00431.12

[45] W. Liang, V. S. Ilchenko, A. A. Savchenkov, E. Dale, D. Eliyahu, A. B. Matsko, and L. Maleki, Optica 4, 114 (2017).

[46] H. Tian, B. Dong, M. Zervas, T. J. Kippenberg, and S. A. Bhave, in Conference on Lasers and Electro-Optics, OSA Technical Digest (online) (Optical Society of America, San Jose, California, 2018) p. SW4B.3.

[47] Y. HE, Q.-F. Yang, J. Ling, R. Luo, H. Liang, M. Li, B. Shen, H. Wang, K. Vahala, and Q. Lin, (2018), arXiv:1812.09610.

[48] K. Alexander, J. P. George, J. Verbist, K. Neyts, B. Kuyken, D. Van Thourhout, and J. Beeckman, Nature Communications 9, 3444 (2018).

[49] F. Kéfélian, H. Jiang, P. Lemonde, and G. Santarelli, Optics Letters 34, 914 (2009).

[50] W. Liang, V. S. Ilchenko, D. Eliyahu, a. a. Savchenkov, a. B. Matsko, D. Seidel, and L. Maleki, Nature Communications 6, 7371 (2015).

[51] S. Gundavarapu, G. M. Brodnik, M. Puckett, T. Huffman, D. Bose, R. Behunin, J. Wu, T. Qiu, C. Pinho, N. Chauhan, J. Nohava, P. T. Rakich, K. D. Nelson, M. Salit, and D. J. Blumenthal, Nature Photonics 13, 60 (2019).

[52] D. Marpaung, J. Yao, and J. Capmany, Nature Photonics 13, 80 (2019).

[53] P. Ghelfi, F. Laghezza, F. Scotti, G. Serafino, A. Capria, S. Pinna, D. Onori, C. Porzi, M. Scaffardi, A. Malacarne, V. Vercesi, E. Lazzeri, F. Berizzi, and A. Bogoni, Nature 507, 341 (2014).

[54] S. Koenig, D. Lopez-Diaz, J. Antes, F. Boes, R. Henneberger, A. Leuther, A. Tessmann, R. Schmogrow, D. Hillerkuss, R. Palmer, T. Zwick, C. Koos, W. Freude, O. Ambacher, J. Leuthold, and I. Kallfass, Nature Photonics 7, 977 (2013).

[55] E. Lucas, H. Guo, J. D. Jost, M. Karpov, and T. J. Kippenberg, Physical Review A 95, 43822 (2017).

[56] M. Karpov, H. Guo, A. Kordts, V. Brasch, M. H. P. Pfeiffer, M. Zervas, M. Geiselmann, and T. J. Kippenberg, Physical Review Letters 116, 103902 (2016).

[57] X. Yi, Q.-F. Yang, K. Y. Yang, and K. Vahala, Optics Letters 41, 3419 (2016).

[58] X. Yi, Q.-F. Yang, X. Zhang, K. Y. Yang, X. Li, and K. Vahala, Nature Communications 8, 14869 (2017).

[59] A. B. Matsko and L. Maleki, Optics express 21, 28862 (2013).

[60] T. Herr, K. Hartinger, J. Riemensberger, C. Y. Wang, E. Gavartin, R. Holzwarth, M. L. Gorodetsky, and T. J. Kippenberg, Nature Photonics 6, 480 (2012).

[61] Q.-F. Yang, X. Yi, K. Y. Yang, and K. Vahala, Optica 3, 1132 (2016).

[62] C. Bao, Y. Xuan, C. Wang, J. A. Jaramillo-Villegas, D. E. Leaird, M. Qi, and A. M. Weiner, Optics Letters 42, 759 (2017).

[63] D. J. Wilson, K. Schneider, S. Hoenl, M. Anderson, T. J. Kippenberg, and P. Seidler, 2, 1 (2018), arXiv:1808.03554.

[64] W. Liang, A. A. Savchenkov, V. S. Ilchenko, D. Eliyahu, A. B. Matsko, and L. Maleki, IEEE Photonics Journal 9, 1 (2017).

[65] M. L. Gorodetsky and I. S. Grudinin, Journal of the Optical Society of America B 21, 697 (2004).

[66] H. Guo, M. Karpov, E. Lucas, A. Kordts, M. H. Pfeiffer, V. Brasch, G. Lihachev, V. E. Lobanov, M. L. Gorodetsky, and T. J. Kippenberg, Nature Physics 13, 94 (2017).

[67] W. Zhang, T. Li, M. Lours, S. Seidelin, G. Santarelli, and Y. Le Coq, Applied Physics B 106, 301 (2011).

[68] T. M. Niebauer, R. Schilling, K. Danzmann, A. Rüdiger, and W. Winkler, Physical Review A 43, 5022 (1991).

[69] F. Quinlan, T. Fortier, H. Jiang, and S. Diddams, Journal of the Optical Society of America B 30, 1775 (2013).

[70] F. Quinlan, T. M. Fortier, H. Jiang, A. Hati, C. Nelson, Y. Fu, J. C. Campbell, and S. A. Diddams, Nature Photonics 7, 290 (2013).

[71] M. Giunta, W. Hänsel, M. Lessing, M. Lezius, M. Fischer, X. Xie, R. Bouchand, D. Nicolodi, P.-A. Tremblin, G. Santarelli, A. Joshi, S. Datta, Y. Le Coq, and R. Holzwarth, in Conference on Lasers and Electro-Optics, OSA Technical Digest (online) (Optical Society of America, San Jose, California, 2018) p. SM2L.5.

Chapter 5

Conclusion

During this 4-year doctoral study, I focused my work on alternative approaches for low noise optical and microwave oscillators and on their characterization, especially in terms of phase/frequency noise and frequency stability. I learnt about the different statistical tools that give useful representations and figures characterizing the noise properties of oscillators. I studied the theoretical relationship between the phase noise of an oscillator and its power spectrum. By revisiting an old mathematical expression of this link introduced by D. Middleton in the 70's[20–22,62], I developed a simple guideline enabling a fairly straightforward computation of the power spectrum corresponding to an arbitrary phase noise. This approach provides a qualitative and intuitive understanding of the power spectrum corresponding to different regimes of phase noise and was validated by various types of experimental signals with different phase noise levels.

On the experimental point of view, I worked mainly on two complementary aspects towards compact low-noise optical and microwave oscillators. I modified the concept of the transfer oscillator[9] to indirectly

characterize the noise properties and modulation response of the offset frequency in a comb spectrum without the need of the commonly used *f*-to-2*f* interferometer that is challenging to implement with high repetition rate mode-locked lasers and other new technologies of frequency comb sources such as semiconductor mode-locked lasers or quantum cascade laser combs. The developed method enabled a full noise characterization of novel comb sources at various wavelengths and comb mode spacings, including the first reported noise analysis in a mid-infrared QCL comb. These results showed a similar anti-correlation between the noise of the mode spacing and offset frequency in very different comb sources, such as a 25-GHz diode-pumped solid-state laser at 1.5 μm[28] and a QCL-comb emitting at ~8 μm[63].

This principle was then modified and improved to perform the electrical division with a finer resolution and was applied to develop a new approach for an optical frequency divider system that does not require an optical lock of the frequency comb to the optical reference[44]. A main advantage of the developed transfer oscillator method is that the frequency comb that performs the frequency division is not stabilized to the optical reference and can be even stay fully free-running. This results in the possibility to generate several ultra-low noise microwave signals from different optical references using a single comb, but also in the possibility to use simpler and more compact mode-locked lasers with high repetition rates directly in the GHz range, which is beneficial for the photo-detection noise floor, but these lasers are more challenging to be tightly locked. This transfer oscillator was then applied to realize the first frequency division with a micro-resonator Kerr-comb in a joint experiment with Prof. Kippenberg's group at EPFL[64].

Finally, an optical delay-line approach was studied as an alternative for a narrow linewidth laser with a potential for a compact footprint. This method was applied to reduce the linewidth of a mid-infrared QCL below 10 kHz using only a meter-scale free-space delay-line. But much lower noise

can be achieved with a long fiber delay of hundreds of meters in the near-infrared, with the potential to reach a Hz-level linewidth.

The developed delay-line optical reference and transfer oscillator frequency dividers are two key building blocks for future compact ultra-low noise microwave generators for current or new applications.

Bibliography

1. Weiss, R. Nobel Lecture: LIGO and the discovery of gravitational waves I. *Rev. Mod. Phys.* **90**, (2018).
2. Marti, G. E. *et al.* Imaging Optical Frequencies with 100uHz Precision and 1.1um Resolution. *Phys Rev Lett* **120**, 103201 (2018).
3. Hänsch, T. W. Nobel Lecture: Passion for precision. *Rev. Mod. Phys.* **78**, 1297–1309 (2006).
4. Hall, J. L. Nobel Lecture: Defining and measuring optical frequencies. *Rev. Mod. Phys.* **78**, 1279–1295 (2006).
5. Diddams, S. A. The evolving optical frequency comb [Invited]. *J. Opt. Soc. Am. B* **27**, B51–B62 (2010).
6. Schilt, S. & Südmeyer, T. Carrier-Envelope Offset Stabilized Ultrafast Diode-Pumped Solid-State Lasers. *Appl. Sci.* **5**, 787–816 (2015).
7. Telle, H. R. *et al.* Carrier-envelope offset phase control: A novel concept for absolute optical frequency measurement and ultrashort pulse generation. *Appl. Phys. B* **69**, 327–332 (1999).
8. Jornod, N. *et al.* Carrier-envelope offset frequency stabilization of a gigahertz semiconductor disk laser. *Optica* **4**, 1482–1487 (2017).

9. Telle, H. R., Lipphardt, B. & Stenger, J. Kerr-lens, mode-locked lasers as transfer oscillators for optical frequency measurements. *Appl. Phys. B Lasers Opt.* **74**, 1–6 (2002).

10. Fortier, T. M. *et al.* Generation of ultrastable microwaves via optical frequency division. *Nat. Photonics* **5**, 425–429 (2011).

11. Chen, Y. T. Use of single-mode optical fiber in the stabilization of laser frequency. *Appl. Opt.* **28**, 2017–2021 (1989).

12. Kéfélian, F., Jiang, H., Lemonde, P. & Santarelli, G. Ultralow-frequency-noise stabilization of a laser by locking to an optical fiber-delay line. *Opt. Lett.* **34**, 914–916 (2009).

13. Dong, J. *et al.* Subhertz linewidth laser by locking to a fiber delay line. *Appl. Opt.* **54**, 1152–1158 (2015).

14. Li, D., Qian, C., Li, Y. & Zhao, J. Efficient laser noise reduction method via actively stabilized optical delay line. *Opt. Express* **25**, 9071 (2017).

15. Riehle, F. *Frequency Standards: Basics and Applications*. (2004).

16. Allan, D. W. Statistics of atomic frequency standards. *Proc. IEEE* **54**, 221–230 (1966).

17. Schawlow, A. L. & Townes, C. H. Infrared and Optical Masers. *Phys. Rev.* **112**, 1940 (1958).

18. Di Domenico, G., Schilt, S. & Thomann, P. Simple approach to the relation between laser frequency noise and laser line shape. *Appl. Opt.* **49**, 4801–4807 (2010).

19. Elliott, D. S., Roy, R. & Smith, S. J. Extracavity laser band-shape and bandwidth modification. *Phys. Rev. A* **26**, 12 (1982).

20. Middleton, D. The distribution of energy in randomly modulated waves. *Lond. Edinb. Dublin Philos. Mag. J. Sci.* **42**, 689–707 (1951).

21. Middleton, D. *An Introduction to Statistical Communication Theory:An IEEE Press Classic Reissue*. (Wiley-IEEE Press, 1996).

22. Brochard, P., Sudmeyer, T. & Schilt, S. Power spectrum computation for an arbitrary phase noise using Middleton's convolution series: implementation guideline and experimental illustration. *IEEE Trans. Ultrason. Ferroelectr. Freq. Control* **64**, 1766–1775 (2017).

23. Godone, A., Micalizio, S. & Levi, F. RF spectrum of a carrier with a random phase modulation of arbitrary slope. *Metrologia* **45**, 313 (2008).

24. Kippenberg, T. J., Gaeta, A. L., Lipson, M. & Gorodetsky, M. L. Dissipative Kerr solitons in optical microresonators. *Science* **361**, eaan8083 (2018).

25. Hugi, A., Villares, G., Blaser, S., Liu, H. C. & Faist, J. Mid-infrared frequency comb based on a quantum cascade laser. *Nature* **492**, 229–233 (2012).

26. Brochard, P., Schilt, S., Wittwer, V. J. & Südmeyer, T. Characterizing the carrier-envelope offset in an optical frequency comb without traditional f-to-2f interferometry. *Opt. Lett.* **40**, 5522–5525 (2015).

27. Brochard, P. *et al.* First investigation of the noise and modulation properties of the carrier-envelope offset in a modelocked semiconductor laser. *Opt. Lett.* **41**, 3165–3168 (2016).

28. Brochard, P. *et al.* Frequency Noise Characterization of a 25-GHz Diode-Pumped Mode-Locked Laser With Indirect Carrier-Envelope Offset Noise Assessment. *IEEE Photonics J.* **10**, 1–10 (2018).

29. Faist, J. *et al.* Quantum Cascade Laser. *Science* **264**, 553–556 (1994).

30. Piccardo, M. *et al.* Time-dependent population inversion gratings in laser frequency combs. *Optica* **5**, 475 (2018).

31. Walker, D. R., Udem, Th., Gohle, Ch., Stein, B. & Hänsch, T. W. Frequency dependence of the fixed point in a fluctuating frequency comb. *Appl. Phys. B* **89**, 535–538 (2007).

32. Newbury, N. R. & Swann, W. C. Low-noise fiber-laser frequency combs (Invited). *J. Opt. Soc. Am. B* **24**, 1756–1770 (2007).

33. Paschotta, R., Schlatter, A., Zeller, S. C., Telle, H. R. & Keller, U. Optical phase noise and carrier-envelope offset noise of mode-locked lasers. *Appl. Phys. B* **82**, 265–273 (2006).

34. Tombez, L., Schilt, S., Di Francesco, J., Thomann, P. & Hofstetter, D. Temperature dependence of the frequency noise in a mid-IR DFB quantum cascade laser from cryogenic to room temperature. *Opt. Express* **20**, 6851–6859 (2012).

35. Schilt, S. *et al.* An experimental study of noise in mid-infrared quantum cascade lasers of different designs. *Appl. Phys. B* **119**, 189–201 (2015).

36. Dolgovskiy, V. *et al.* Cross-influence between the two servo loops of a fully stabilized Er: fiber optical frequency comb. *J. Opt. Soc. Am. B* **29**, 2944–2957 (2012).

37. Schilt, S. *et al.* Frequency discriminators for the characterization of narrow-spectrum heterodyne beat signals: Application to the measurement of a sub-hertz carrier-envelope-offset beat in an optical frequency comb. *Rev. Sci. Instrum.* **82**, 123116 (2011).

38. Matei, D. G. *et al.* 1.5 μm Lasers with Sub-10 mHz Linewidth. *Phys. Rev. Lett.* **118**, 263202 (2017).

39. Kessler, T. *et al.* A sub-40 mHz linewidth laser based on a silicon single-crystal optical cavity. *Nat. Photonics* **6**, 687–692 (2012).

40. Dolgovskiy, V. *et al.* 1.5-μm Cavity-Stabilized Laser for Ultra-Stable Microwave Generation. *Proc. Joint IFCS/EFTF Conference* (2011).

41. Portuondo-Campa, E., Buchs, G., Kundermann, S., Balet, L. & Lecomte, S. Ultra-low phase-noise microwave generation using a diode-pumped solid-state laser based frequency comb and a polarization-maintaining pulse interleaver. *Opt. Express* **23**, 32441 (2015).

42. Xie, X. *et al.* Photonic microwave signals with zeptosecond-level absolute timing noise. *Nat. Photonics* **11**, 44–47 (2017).

43. Shehzad, A., Brochard, P., Matthey, R., Schilt, S. & Sudmeyer, T. 10-kHz-Linewidth Mid-Infrared Quantum Cascade Laser by Stabilization to an Optical Delay Line. *Opt. Lett.* (in press) (2019).

44. Brochard, P., Schilt, S. & Südmeyer, T. Ultra-low noise microwave generation with a free-running optical frequency comb transfer oscillator. *Opt. Lett.* **43**, 4651–4654 (2018).

45. Lucas, E. *et al.* Ultralow-Noise Photonic Microwave Synthesis using a Soliton Microcomb-based Transfer Oscillator. *ArXiv E-Prints* arXiv:1903.01213 (2019).

46. Bartalini, S. *et al.* Observing the Intrinsic Linewidth of a Quantum-Cascade Laser: Beyond the Schawlow-Townes Limit. *Phys. Rev. Lett.* **104**, 083904 (2010).

47. Fasci, E. *et al.* Narrow-linewidth quantum cascade laser at 8.6 µm. *Opt. Lett.* **39**, 4946–4949 (2014).

48. Liu, K. & Littman, M. G. Novel geometry for single-mode scanning of tunable lasers. *Opt Lett* **6**, 117–118 (1981).

49. Fleming, M. & Mooradian, A. Spectral characteristics of external-cavity controlled semiconductor lasers. *IEEE J. Quantum Electron.* **17**, 44–59 (1981).

50. Millo, J. *et al.* Ultrastable lasers based on vibration insensitive cavities. *Phys. Rev. A* **79**, (2009).

51. Millo, J. *et al.* Ultra-stable optical cavities: design and experiments at LNE-SYRTE. in *Frequency Control Symposium, 2008 IEEE International* 110–114 (IEEE, 2008).

52. Webster, S. & Gill, P. Force-insensitive optical cavity. *Opt Lett* **36**, 3572–3574 (2011).

53. Rubiola, E., Salik, E., Huang, S., Yu, N. & Maleki, L. Photonic-delay technique for phase-noise measurement of microwave oscillators. *J Opt Soc Am B* **22**, 987–997 (2005).

54. Sheard, B. S., Gray, M. B. & McClelland, D. E. High-bandwidth laser frequency stabilization to a fiber-optic delay line. *Appl. Opt.* **45**, 8491–8499 (2006).

55. Okoshi, T., Kikuchi, K. & Nakayama, A. Novel method for high resolution measurement of laser output spectrum. *Electron. Lett.* **16**, 630–631 (1980).

56. Logan, R. T., Maleki, L. & Shadaram, M. Stabilization of oscillator phase using a fiber-optic delay-line. in *Proceedings of the 45th Annual Symposium on Frequency Control 1991* 508–512 (1991). doi:10.1109/FREQ.1991.145943

57. Eliyahu, D., Seidel, D. & Maleki, L. Phase noise of a high performance OEO and an ultra low noise floor cross-correlation microwave photonic homodyne system. in *2008 IEEE International Frequency Control Symposium* 811–814 (2008). doi:10.1109/FREQ.2008.4623111

58. Chen, Q.-F., Nevsky, A. & Schiller, S. Locking the frequency of lasers to an optical cavity at the 1.6×10−17 relative instability level. *Appl. Phys. B* **107**, 679–683 (2012).

59. Li, J., Yi, X., Lee, H., Diddams, S. A. & Vahala, K. J. Electro-optical frequency division and stable microwave synthesis. *Science* **345**, 309–313 (2014).

60. Haboucha, A. *et al.* Optical-fiber pulse rate multiplier for ultralow phase-noise signal generation. *Opt. Lett.* **36**, 3654–3656 (2011).

61. Bouchand, R., Nicolodi, D., Xie, X., Alexandre, C. & Le Coq, Y. Accurate control of optoelectronic amplitude to phase noise conversion in photodetection of ultra-fast optical pulses. *Opt. Express* **25**, 12268–12281 (2017).

62. Abramson, N. Bandwidth and Spectra of Phase-and-Frequency-Modulated Waves. *IEEE Trans. Commun. Syst.* **11**, 407–414 (1963).

63. Shehzad, A. *et al.* Investigation of the noise properties of the offset frequency in a quantum cascade laser frequency comb. *UFO XII* (2019).

64. Lucas, E. *et al.* Ultralow-Noise Photonic Microwave Synthesis using a Soliton Microcomb-based Transfer Oscillator. *ArXiv E-Prints* arXiv:1903.01213 (2019).

Remerciements

Je souhaite tout d'abord exprimer ma gratitude à l'ensemble des personnes m'ayant accompagnées et soutenues durant ces 4 années de doctorat m'ayant permis d'accomplir les différents résultats présentés dans ce manuscrit.

Je tiens ainsi à remercier Thomas pour m'avoir intégré dans son laboratoire et pour la confiance et la liberté qu'il m'a accordé concernant les directions de recherche que j'ai souhaité suivre tout au long de ces années, créant un cadre de travail idéal. Ses idées et la vision qu'il a pu me transmettre durant nos différents échanges m'ont beaucoup apporté et m'aideront encore pour la suite.

Ce travail n'aurait pas pu voir le jour sans l'aide précieuse et constante de Stéphane. Toujours présent, sans pression, autant pour les bonnes que les mauvaises nouvelles, le jour comme la nuit, et avec des connaissances couvrant tous les domaines. Stéphane, bien plus qu'un collègue de travail, merci beaucoup pour tous, je te dois beaucoup !

Je tiens également à remercier le Prof. Pascal Ruello, le Dr. Giorgio Santarelli et le Dr. Rodolphe Le Targat pour avoir accepté d'être les membres externes du jury. Je les remercie notamment pour leur temps et pour les corrections et conseils apportés pour améliorer ce manuscrit ; ainsi que pour leur déplacement pour la soutenance.

Mes remerciements vont également aux indénombrables autres membres du laboratoire et de l'institut, sans lesquels ces années n'auraient pas eu la même saveur.

Mes derniers remerciements vont à ma famille pour leur soutien et support sans faille, avec une pensée toute particulière pour Laura, Paul et Alice…